The Dissertation Committee for Olga M. Paley Certifies that this is the approved version of the following dissertation:

Engineering a Novel Human Methionine Degrading Enzyme as a Broadly Effective Cancer Therapeutic

Committee:

George Georgiou, Supervisor

Brent Iverson

Hal S. Alper

Jennifer Maynard

Kenneth A Johnson

Engineering a Novel Human Methionine Degrading Enzyme as a Broadly Effective Cancer Therapeutic

by

Olga M. Paley, B.S.

Dissertation

Presented to the Faculty of the Graduate School of

The University of Texas at Austin

in Partial Fulfillment

of the Requirements

for the Degree of

Doctor of Philosophy

The University of Texas at Austin

August 2014

Acknowledgements

I would first like to acknowledge the unique opportunity provided to me by Professor Georgiou in inviting me to join his group. I am immensely thankful for his always on-point guidance and advice that often feels like it is coming from a limitless repository of knowledge. The years I have spent in the Georgiou/Iverson lab have been a time of tremendous professional and personal growth and I struggle to imagine getting the opportunity to experience carrying a potential therapeutic from initial conception to preclinical evaluation elsewhere. I thank Dr. Everett Stone for the initial idea for the project, for overseeing my training, and for being a never ending source of brilliant ideas over the years. Professor Brent Iverson has been an invaluable resource in all things chemistry as well as in a positive attitude and excitement about the research, through all successes and "opportunities for learning".

Many people have contributed their expertise to this work. Thanks to Dr. Wayne Lu for his contributions in phylogenetic analysis, engineering, and enzyme variant evaluation, Dr. Nai-Kong V. Cheung and Dr. Jian Hu for the neuroblastoma cytotoxicity and efficacy data, Kendra Garrison for PK/PD and efficacy experiments in mice and tissue culture guidance, Dr. Yan Zhang and Wupeng Yan for the crystal structures, Professor Kenneth Johnson for enzymology training and help with kinetic experiments, Shira Cramer for kinetic analyses (and exceptional moral support), Candice Lamb for experimental support along various stages of the project, Bing Tan for both training and help with many tissue culture experiments, Richard Salinas for support with all mammalian tissue culture cytometric analysis, Professor John DiGiovanni and Dr.

Achinto Saha for mouse prostate cancer model experiments, and Professor Stefano Tiziani for melabolomic analysis.

I have also been fortunate to mentor and work with extremely talented and industrious undergraduate students. I would like to deeply thank Barbara Ekerdt, Alexandra Arambula, Parth Mangrolia, Shirley Yang, and Jonathan Dau for all of their contributions and for providing me a learning opportunity in guidance.

BIGG lab members, both past and present, have all contributed in some way to my growth over the years. I would like to particularly thank the other members of the enzyme subgroup, Giulia Agnello, Dr. Nick Marshall, as well as Dr. William Kelton and Dr. Sean Carroll.

I would like to thank my parents for always prioritizing me and my education, for the sacrifices they made to give me more opportunities than they had, and for instilling in me a love of learning and of a good intellectual challenge. I would like to also thank my family of friends and loved ones without whose support this undertaking would simply not have been possible.

Finally, I thank the other members of my committee: Professor Hal Alper and Professor Jennifer Maynard, and acknowledge my funding from the National Institutes of Health and the National Science Foundation.

Engineering a Novel Human Methionine Degrading Enzyme as a Broadly Effective Cancer Therapeutic

Olga M. Paley, Ph.D.

The University of Texas at Austin, 2014

Supervisor: George Georgiou

Many cancers have long been known to display an absolute requirement for the amino acid methionine (L-Met). Studies have shown that in the absence of L-Met, sensitive neoplasms experience cell cycle arrest and perish. Without the metabolic deviations that characterize L-Met auxotrophs, normal cells are able to grow on precursors such as homocysteine and tolerate periods of L-Met starvation. The differential requirement for this amino acid between normal and tumor cells has been exploited through enzymatic serum degradation of L-Met by a bacterial methionine-γ-lyase (MGL). Though MGL was able to deplete L-Met to therapeutically useful levels in animal models and exert a significant cytotoxic effect on malignant cell lines *in vitro* and on tumor xenografts *in vivo*, the clinical implementation of this enzyme is hampered by its short serum half-life and potential for catastrophic immune response.

In the chapters that follow, we describe the engineering of a novel human methionine degrading enzyme (hMGL) that overcomes the limitations of the bacterial therapeutic. We have shown that hMGL is capable of degrading methionine at a therapeutically useful rate and inducing extensive cell killing in a variety of neoplasms. This enzyme is expected to have low immunogenicity in patients and a high therapeutic index. We have developed a high throughput screen for methionine degrading activity that we can utilize to further engineer the enzyme based on the results of additional preclinical development. We have found that hMGL is also capable of degrading cystine to operate as a dual amino acid depletion treatment that is expected to be more potent than methionine depletion alone. Due to the wide array of neoplasms sensitive to methionine and cystine starvation, the engineered enzyme holds a great deal of promise as a unique and powerful cancer therapeutic.

Table of Contents

List of Tables

List of Figures

Chapter 1: Introduction and Background

1.1 Enzymatic Depletion of Serum Amino Acids in Cancer Treatment

Many cancers exhibit significant metabolic deviations from normal cells, including a higher demand for particular amino acids, and depend on the availability of these metabolites in the serum pool for survival. The modulation of amino acid levels in serum has been investigated as a treatment strategy with a variety of human cancers (*1-4*). The clinical administration of an enzyme that catalyzes the degradation of a target amino acid efficiently and with high specificity can selectively drive malignancies to experience metabolic imbalances, inhibition of protein synthesis, irreversible cell cycle arrest, and ultimately, cell death.

Among enzyme therapies in cancer, asparaginase is one of oldest and most successful. Its inclusion has led to a > 90% cure rate for standard risk Childhood Acute Lymphoblastic Leukemia (*5*). Currently, only bacterial enzymes derived from E. coli and Erwinia chrysanthemi are available (*6*). Since bacterial asparaginase is highly immunogenic (*7*), antibody response in patients inactivates the enzyme, shortens its half-

life and induces anaphylaxis. Despite clinical success, asparaginase therapy remains limited by its immunogenicity (*4*).

1.2 L-Methionine Depletion for Cancer Therapy

Methionine depletion has long been studied as a potential treatment for cancer, as many malignant human cell lines have a substantially higher requirement for this amino acid than normal tissues (*8-15*). L-Met cannot be synthesized de novo and is essential in all cells for protein synthesis, oxidative stress protection as a precursor to glutathione, polyamine synthesis for nuclear and cell division, and as a major source of methyl groups for the methylation of DNA and other molecules (Figure 1). The abnormally high demand of malignancies has been attributed to deviations in these functions as well as defects in expression of critical enzymes in the metabolic cycle of methionine. The high rate of cell growth and division in malignant cells demands greater supplies of raw materials for protein and polyamine synthesis. Polyamines themselves have been shown to contribute to tumorigenesis and proliferation (*16-18*). Some cancers have diminished or non-existent levels of expression of methylthioadenosine phosphorylase (MTAP) which cleaves methylthioadenosine to 5-methylthioribose-1-phosphate that is further

metabolized to recycle L-Met (*19, 20*). Additionally, L-Met dependent cancer cells often express low levels of L-Met synthase or produce an enzyme with markedly lowered activity (*21-24*). L-Met synthase is responsible for recycling homocysteine back into L-Met so dependent malignant cells that are unable to utilize this precursor must instead scavenge L-Met from their environment.

The absolute requirement of neoplasms for L-Met presents an attractive opportunity for treatment. When L-Met levels decrease from the normal human serum concentration of ~ 30 µM to a threshold around ~ 5 µM L-Met dependent tumors are unable to survive (*25, 26*). Even partial depletion through nutritional deprivation has been shown to have an effect on tumor growth in both a rat model and human patients (*27-29*). However, an L-Met free diet alone is insufficient to achieve sufficiently low amino acid levels due to replenishment through protein degradation and homocysteine conversion by normal cells (levels drop by ~40% (*10*)). In an effort to overcome this limitation, enzymatic L-Met depletion has been investigated in a number of animal model studies as well as in phase I clinical trials (*30-37*).

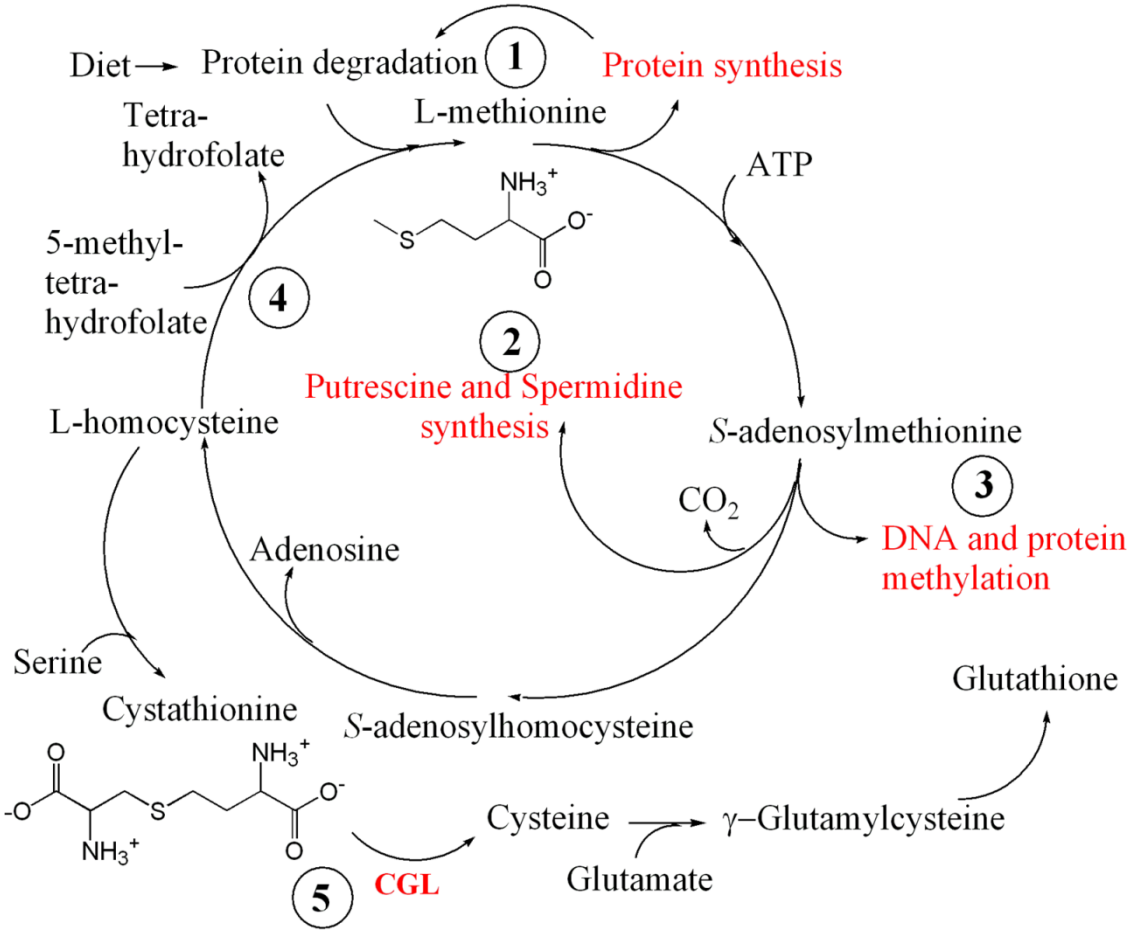

Figure 1: Overview of the role of L-Met in cell metabolism and the effects of its depletion on cancer. 1) Depletion of an essential amino acid halts protein synthesis. 2) Abrogated polyamine synthesis stalls tumorigenesis & proliferation. 3) DNA & protein methylation is halted. 4) Tumor cells are often compromised in the remethylation of L-homocysteine back to L-Met. 5) We engineered the human CGL enzyme to accept L-Met as a substrate

1.3 Methionine-γ-Lyase as a Cancer Therapeutic

L-Methionine-γ-lyase (MGL) catalyzes the α,γ-elimination of L-Met to

methanethiol, α-ketobutyrate, and ammonia (Figure 4). It is a tetrameric pyridoxal-5'-phosphate-dependent (PLP) enzyme present in many species, but absent in mammals (*38, 39*). Numerous bacterial enzymes (including MGL from *Pseudomonas putida*) have been purified and tested for L-Met degrading activity and efficacy against various cancer cell lines. The *P. putida* MGL was cloned and expressed in *E. coli* with high protein yield (~ 1 g/L) (*30, 40*) and displayed fast Michaelis-Menten kinetics including a low value of K_M (~1 mM) and a high value of k_{cat} (~50 s^{-1}) in comparison to other sources (*41, 42*).

The structure of the MGL enzyme was has been defined by crystallization (*43*). Each segment of the tetramer is composed of three regions: an extended N-terminal domain (residues 1-63) that includes two helices and three beta-strands, a large PLP (vitamin B6) binding domain (residues 64-262), and a C-terminal domain (residues 263-398). Amino acids thought to be critical for specificity have also been identified based on structure. Tyr59 and Arg61 of neighboring subunits, which are also strongly conserved in other γ-family enzymes, contact the phosphate group of PLP. These residues serve as the main anchor for the cofactor within the active site. Lys240, Asp241 and Arg61 of one partner monomer and Tyr114 and Cys116 of the other monomer form a hydrogen-bond network in the MGL active site that confers specificity to the enzyme (Figure 2).

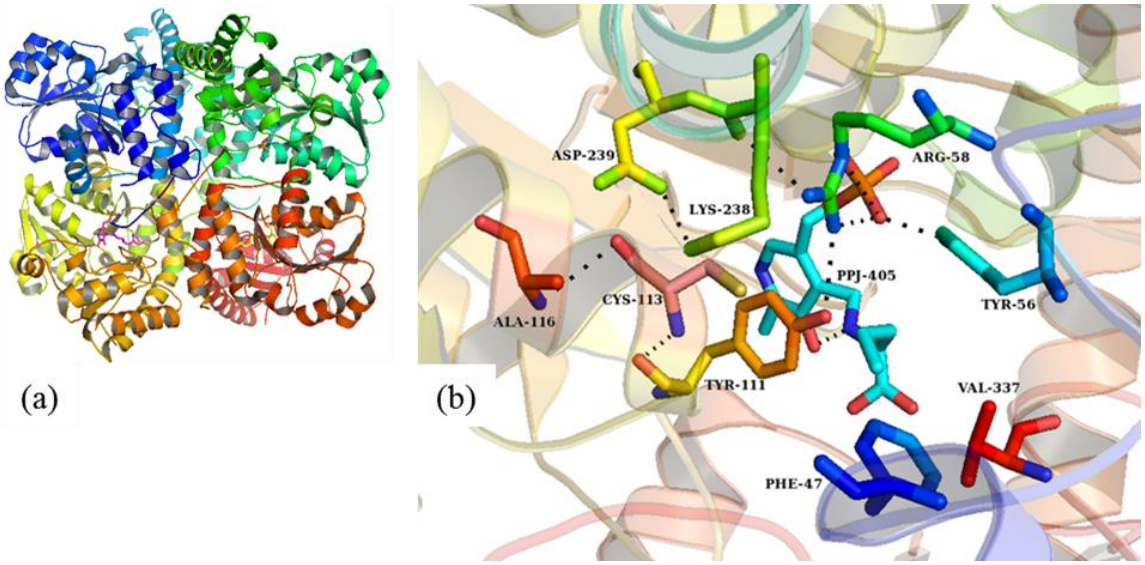

Figure 2: Structure of MGL (PDB 1E5E) tetramer (a) with PLP cofactor bound to inhibitor. (b) Active site detail showing residues discussed and hydrogen bond network

In vivo studies using MGL for L-Met depletion initially yielded promising results in animal models. Human lung, colon, kidney, brain, prostate, and melanoma neoplasms were all shown to be sensitive to recombinant MGL in a mouse xenograft model (*30*). Additionally, no toxicity was detected at effective doses (determined by absence of weight loss). However, the enzyme half-life was determined to be only ~2 hours *in vivo* and in pooled human serum (*44*).

Yang *et al*. investigated the pharmacokinetics, L-Met depletion, antigenicity, and toxicity of MGL in a non-human primate model (*36*). A 90 mg/kg dose was able to

reduce plasma L-Met to less than 0.5 μM within 30 minutes of injection and the L-Met level remained undetectable for 8 hr. Pharmacokinetic analysis showed that MGL was eliminated with a half-life of 2.5 hr. Administration of that dose every 8 hr for 2 weeks resulted in a steady-state depletion of plasma L-Met to less than 2 μM. Mild toxicity was observed through decreased food intake and slight weight loss. However, re-challenge on day 28 resulted in anaphylactic shock and death in one animal. Anti-MGL antibodies were also detected after the first challenge, and increased in concentration for the duration of treatment.

To reduce renal clearance and shield the bacterial enzyme from the primate immune system, MGL was conjugated to methoxypolyethylene glycol succinimidyl glutarate (MEGC-PEG-5000). A 90 mg/kg dose of MGLPEG was sufficient to reduce plasma L-Met to target levels and was administered every 12 hours over the course of 7 days. Anaphylactic shock was not observed upon re-challenge, but anti-MEGC-PEG-MGL antibody concentration was comparable to that elicited by unmodified MGL. Finally, although the serum longevity improved significantly by PEGylation (36 hrs vs. 2 hrs), the L-Met levels were only kept below detection for one third longer than with the unPEGylated enzyme (12 hrs vs. 8 hrs) (*45*).

Phase I clinical trials were performed on patients with advanced cancers, including: breast, lung, renal, and lymphoma, by a single injection of MGLPEG (*31, 37*). The patients experienced no significant toxicity and plasma L-Met levels were immediately dramatically reduced. However, the authors did not assess the antitumor efficacy of this treatment and to date no other clinical trials have been reported. Additionally, these studies did not provide any information regarding immunogenicity over the course of multiple injections nor enzyme half-life and duration of L-Met depletion.

MGL has also been shown to have extensive synergistic effects in combination with chemotherapeutic agents such as 5-fluorouracil and vincristine (*46*). The capacity of pMGL to reduce L-Met serum levels and lead to neoplastic cell death suggests the promise of enzyme-mediated serum amino acid depletion as a potential cancer treatment. However, pMGL is highly immunogenic and elicits a response even upon shielding by PEG. In fact, any bacterially-derived biotherapeutic runs the high risk of adverse immune response, as demonstrated by asparaginase ALL treatment described above. Additionally, the short half-life of the MGL enzyme exacerbates its immunogenicity. In order to maintain a therapeutically relevant level of L-Met in serum, the patient would have to

receive larger or more frequent doses of the enzyme subjecting them to a greater risk of a catastrophic immune response.

1.4 CYSTATHIONINE-γ-LYASE

To circumvent the significant limitations of bacterial MGLs for human therapy, we developed a human methionine-γ-lyase by protein engineering. Cystathionine-γ-lyase is the last enzyme in the mammalian trans-sulfuration pathway and aids in the conversion of L-Met to L-Cysteine (Figure 1) (*47*, *48*). In combination with a PLP cofactor, it catalyzes the α,γ-elimination of L-Cystathionine to L-Cysteine, α-ketobutyrate, and ammonia (Figure 4). CGL displays 61% amino acid similarity and extensive structural homology with the *P. putida* MGL (Figure 3) (*49*). CGL has previously been cloned, expressed in *E. coli*, and determined to convert L-Cyst with a K_M of 0.5 mM and a k_{cat} of 7.5 s^{-1} (*50*).

Structurally, CGL is a tetramer composed of two active dimers (*51*). Close contact between monomers of the tetramer are maintained by several hydrogen bonds and extensive hydrophobic interactions. Each CGL monomer consists of two domains, a larger PLP-binding domain and a smaller domain from the neighboring monomer. PLP is

anchored in position by strong hydrogen bonds between the phosphate moiety and surrounding residues from both chains: chain A (G90, L91, S209, and T211) and chain B (Y60 and R62). The cofactor is covalently bound to K212 by an internal Schiff base and is further stabilized by aromatic π-stacking interactions between its pyridine ring and the neighboring Y114.

The enzyme has been complexed and crystallized with the inhibitor DL-propargylglycine (PAG) (PDB:1E5E) and an overlay of the solved structures of CGL and MGL is presented in Figure 3. The comparison of their active sites highlights key amino acid differences that were used to guide the rational design of the first phase of engineering (Chapter 2). The structure also shows the additional α-helix at the N-terminal domain of MGL that covers the cysteine binding pocket in CGL and is thought to interact with the hydrophobic distal end of L-Met (*52*). Due to an appreciable kinetic rate, availability of crystal structures, and structural homology to the bacterial MGL, CGL was determined to be a promising candidate for protein engineering.

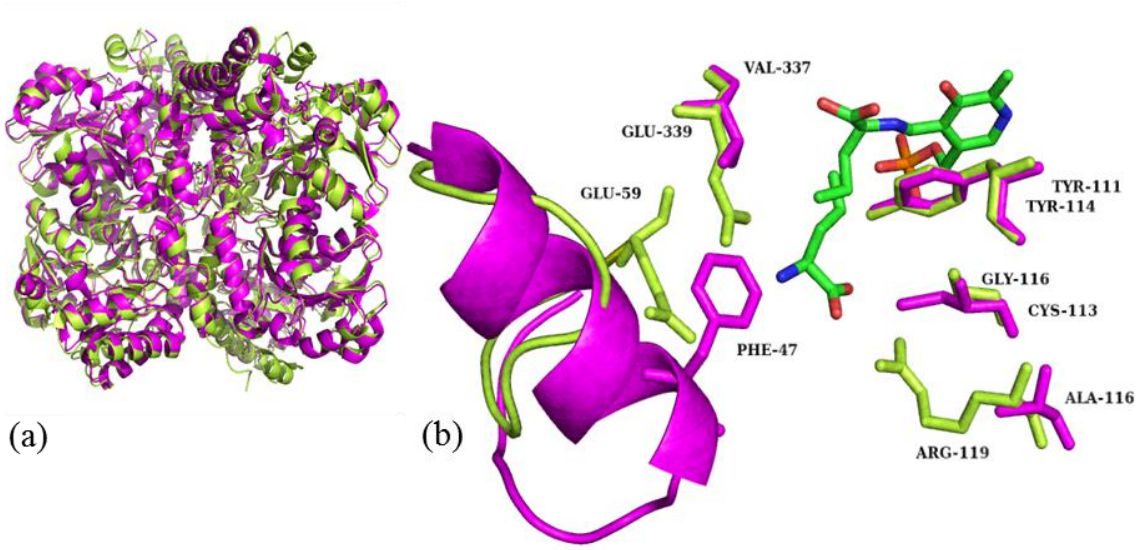

Figure 3: Overlay of two structures: MGL (PDB 1E5E) in magenta and CGL (PDB 3COG) in green. Full enzyme tetramer view (a) and active site detail with: complex of MGL with inhibitor bound to PLP, CGL complexed with an L-Cyst analog inhibitor, specific residues of CGL discussed and their corresponding amino acids in MGL, α-helical "lid" of MGL and lack thereof of CGL.

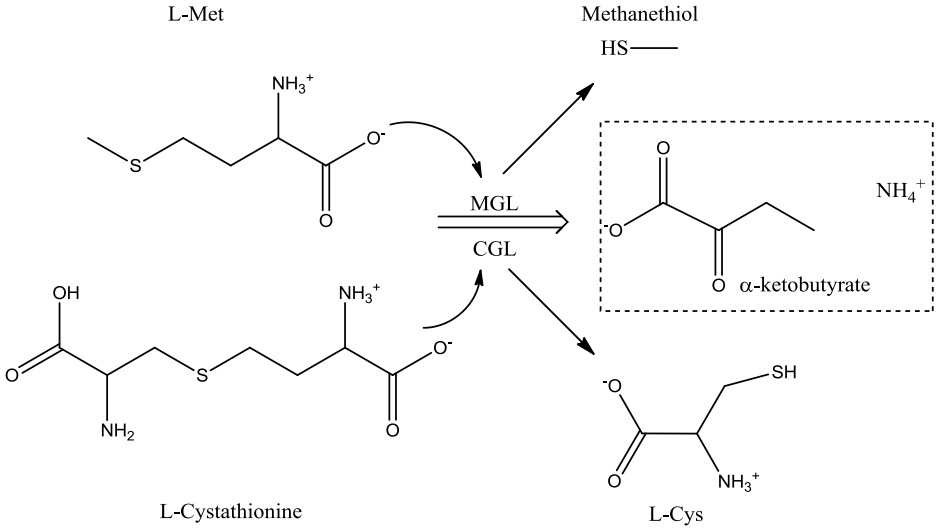

Figure 4: Reactions catalyzed by MGL and CGL with their natural substrates.

Chapter 2: *De Novo* Engineering of a Human Cystathionine-γ-Lyase for Systemic L-Methionine Depletion Cancer Therapy[1]

2.1 CHAPTER SUMMARY

It has been known for nearly a half century that human tumors, including those derived from the nervous system such as glioblastomas, medulloblastoma, and neuroblastomas are much more sensitive than normal tissues to methionine starvation. More recently, systemic L-Met depletion by administration of *Pseudomonas putida* methionine-γ-lyase (MGL) could effectively inhibit human tumors xenografted in mice. However, bacterial-derived MGLs are unstable in serum ($t_{1/2}$ =1.9 ±0.2 hr) and highly immunogenic in primates. Since the human genome does not encode a human MGL enzyme, we created *de novo* a methionine degrading enzyme by re-engineering the structurally homologous pyridoxal phosphate-dependent human enzyme cystathionine-γ-lyase (hCGL). hCGL degrades L-cystathionine but displays no promiscuous activity towards L-Met. Rational design and scanning saturation mutagenesis led to the generation of a variant containing three amino acid substitutions (hCGL-NLV) that degraded L-Met with a k_{cat}/K_M of 5.6 x 10^2 $M^{-1}s^{-1}$ and displayed a serum deactivation $t_{1/2}$

[1] Stone, E., Paley, O., Hu, J., Ekerdt, B., Cheung, N. K., and Georgiou, G. (2012) De novo engineering of a human cystathionine-gamma-lyase for systemic (L)-Methionine depletion cancer therapy, *ACS Chem Biol 7*, 1822-1829.

=78 ± 5 hr (non-PEGylated). *In vitro*, the cytotoxicity of hCGL-NLV towards 14 neuroblastoma cell lines was essentially indistinguishable from that of the *P. putida* MGL. Intravenous administration of PEGylated hCGL-NLV in mice reduced serum L-Met from 123 μM to <5 μM for over 30 hours. Importantly, treatment of neuroblastoma mouse xenografts with PEGylated hCGL-NLV resulted in near complete cessation of tumor growth. Since the mode of action of hCGL-NLV does not require breaching the blood-brain barrier we believe this enzyme may be well suited for the treatment of sensitive tumors that arise from or metastasize to the central nervous system.

2.2 INTRODUCTION

As discussed in the Introduction in Chapter 1, L-methionine (L-Met) depletion has long been studied as a potential treatment for cancer, as many malignant human cell lines and tumors have a substantially higher requirement for L-Met than normal cells and tissues (*13-15, 54, 55*). In particular, neuroblastomas, glioblastomas, and medulloblastomas are extremely sensitive to L-Met depletion (*56, 57*) and their use is so high that C11-methionine positron emission tomography (MET-PET) is used to image metastases in the brain (*58*). Depletion of any essential amino will disrupt protein synthesis, but L-Met is also required for polyamine synthesis (*59-61*) and methylation of DNA and other molecules (*62*). Most non-malignant cells can grow on homocysteine/homocystine, whereas malignant cells must scavenge L-Met directly from their extracellular environment (Chapter 1). When serum L-Met levels decrease from the

normal ~ 30 μM (*63*) to below ~ 5 μM these tumors are unable to survive (*64*). *In vivo,* a significant decrease in serum L-Met can be achieved by the systemic application of methionine-γ-lyase from *Pseudomonas putida* (pMGL) resulting in drastic retardation of tumor growth in a variety of animal models (*30, 33, 37, 46, 65-68*). However, pMGL is rapidly inactivated *in vitro* (This work) and *in vivo* (*69, 70*) and has proven to be highly immunogenic in primate models (*65*).

To circumvent the significant limitations of bacterial MGLs for human therapy, we developed a human methionine-γ-lyase by engineering methionine lyase activity into the human enzyme cystathionine-γ-lyase (CGL, Chapter 1). These enzymes are structural homologues (Figure 1a, structural alignment of hCGL and MGL from *Trichomonas*) and belong to the γ-family of pyridoxal phosphate (PLP) dependent enzymes. Although MGL and CGL are related in their reaction chemistry (Figure 1b), CGL catalyzes the α,γ-elimination of L-cystathionine to L-cysteine, α-ketobutyrate, and NH_3 but shows no detectable catalytic activity with L-Met. Using rational design and scanning saturation mutagenesis, coupled with a novel screen for methionine-γ-lyase activity, we engineered an hCGL variant containing 3 amino acid substitutions (hCGL-NLV) that displayed therapeutically significant rates of L-Met degradation.

As hCGL-NLV is an engineered human protein, it is expected to be subject to immune tolerance, and moreover, computational predictions indicate that the 3 amino acid substitutions are unlikely to generate a T cell neo-epitope. While, as with any protein therapeutic candidate, it is impossible to rule out the possibility that hCGL-NLV could

elicit antibody responses in some patients, the extensive clinical data with approved engineered antibodies (*71*, *72*) supports the notion that the introduction of a small, carefully selected number of amino acid substitutions into engineered human proteins does not generally result in an adverse immunogenicity profile.

2.3 RESULTS AND DISCUSSION

2.3.1 Construction of Synthetic Genes, Protein Expression and Purification

A synthetic hCGL gene utilizing optimal *E.coli* codons was synthesized and expressed from the T7 promoter in *E.coli* BL21(DE3). The codon-optimized gene led to very high protein yields in rich media exceeding 350 mg/L shake flask culture with >95 % of the protein present in the soluble fraction and could be purified to > 98% homogeneity (as assessed by SDS-PAGE) in a single IMAC step (Figure 1). By comparison, expression of the human hCGL gene from the same promoter was reported to yield <5 mg/L shake flask with the protein found almost exclusively in inclusion bodies (*73*).

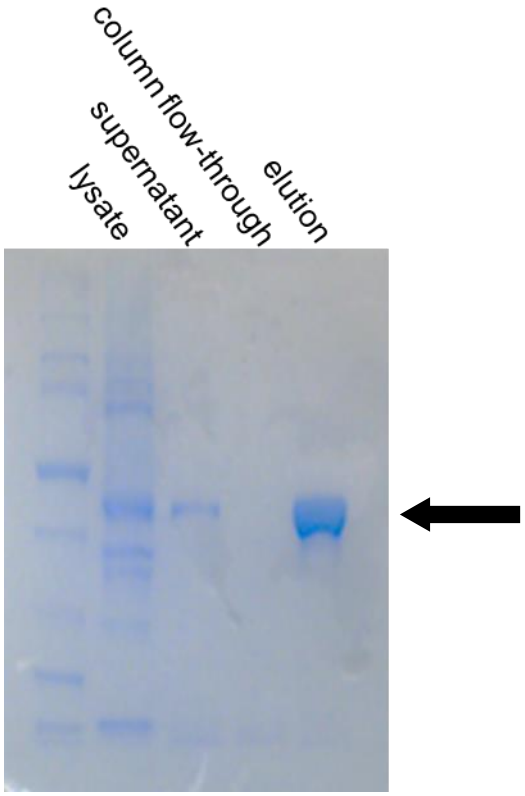

Figure 1: SDS-PAGE gel of purification of synthesized hCGL

2.3.2 Engineering

In addition to their native substrates, both hCGL and pMGL exhibit appreciable activity towards L-cysteine and DL-homocysteine (Table 1). However, L-Met is not a substrate of hCGL and likewise, pMGL has no activity with L-cystathionine as substrate, within the detection limit of our assay (Table 1). Thus, hCGL does not exhibit promiscuous activity towards substrates with a methylthioethane side chain (*74*).

Michaelis-Menten Kinetics			
	P. putida methionine-γ-lyase		
Substrate	k_{cat} (s^{-1})	K_M (mM)	k_{cat}/K_M (s^{-1} mM^{-1})
L-methionine	20 ± 0.4	0.34 ± 0.03	59 ± 6
L-cystathionine	nd	nd	nd
L-cysteine	6.5 ± 0.2	1.1 ± 0.1	6 ± 0.7
DL-homocysteine	86 ± 3	2.9 ± 0.2	30 ± 3
Substrate			
	Human cystathionine-γ-lyase		
L-methionine	nd	nd	nd
L-cystathionine	3.7 ± 0.2	0.40 ± 0.07	9 ± 2
L-cysteine	0.15 ± 0.02	0.79 ± 0.30	0.2 ± 0.1
DL-homocysteine	0.35 ± 0.02	1.7 ± 0.30	0.21 ± 0.04
Substrate	***Human cystathionine-γ-lyase-NLV***		
L-methionine	7.9 ± 0.4 ($\geq 10^6$ *)	14 ± 1.5	0.56 ± 0.07
L-cystathionine	0.54 ± 0.02	0.83 ± 0.1	0.65 ± 0.07 (-14)
L-cysteine	2.7 ± 0.1	0.84 ± 0.1	3.2 ± 0.3 (16)
DL-homocysteine	2.6 ± 0.1	0.9 ± 0.1	2.8 ± 0.3 (13)

nd = not detected, ( ) = fold change from hCGL.
* estimated from DTNB assay limits.
All reactions were performed at 37 ºC with the MBTH assay.

Table 1: Kinetic parameters of MGL, CGL, and NLV with various substrates

Structural overlays of hCGL and an MGL from *Trichomonas* revealed that in hCGL the side-chains of residues E59, R119, and E339 are important for the orientation of the cysteine terminus of its substrate, L-cystathionine, while in MGL the corresponding positions are occupied by amino acids with hydrophobic side chains, namely I55, A116, and V337 (Figure 2a).

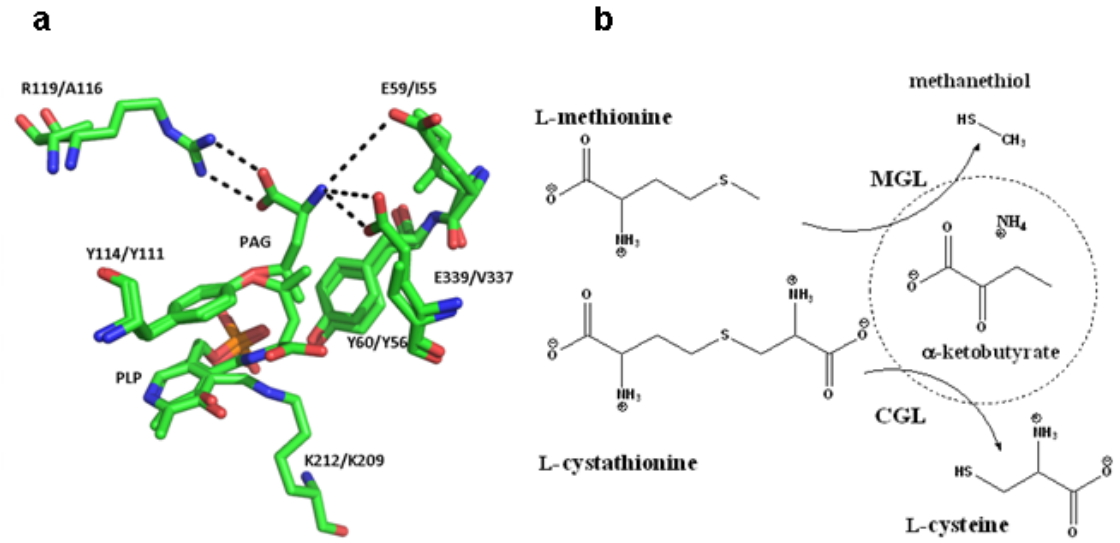

Figure 2: CGL and MGL structure and function (a) Structural overlay of human CGL and MGL from Trichomonas vaginalis (PDB 3COG:1E5E) with the inhibitor propargylglycine (PAG) bound in two different orientations. (b) Reactions catalyzed by CGL and MGL

Positions 59, 119 and 339 in hCGL were subjected to combinatorial pairwise saturation mutagenesis and the resulting clones were screened for methionine-γ-lyase activity using a novel high throughput plate assay that relies on the colorimetric detection of the α-ketobutyrate product of the reaction using 3-methylbenzothiazolin-2-one hydrazone (MBTH)(*75*). Clones expressing mutagenized hCGL were grown in microtiter well plates to mid-log phase, the cells were lysed chemically, incubated with 5 mM L-Met at pH 7.3 and 37 °C followed by MBTH and the Abs_{320} was determined spectrophotometrically.

Screening of > 2,000 colonies (2x theoretical diversity) from a saturation library (library A) at positions 119 and 339 gave 14 unique clones (Table 2, Library A) capable of producing α-ketobutyrate from L-Met. The active clones encoded hCGL with Pro or Val substitutions at position 339 with the latter resulting in higher product formation. The clone with the highest activity, hCGL(R119L, E339V), was used as a template to randomize the E59/R119L codons.

Library A			
Enzyme variant	Pos. 119	Pos. 339	Relative [α-ketobutyrate] produced
pMGL	L	V	1
	L	V	0.58
	C	V	0.29
	Q	V	0.29
	F	R	0.15
	S	V	0.11
	L	P	0.08
	V	P	0.07
	G	P	0.07
	A	Q	0.06
	M	P	0.05
	R	P	0.05
	G	V	0.05
	Q	P	0.05
	V	T	0.04
hCGL	R	E	0
MBTH assay			

Table 2: Relative activity of clones from Library A.

Screening of an additional 2,000 clones led to the isolation of 31 clones exhibiting greater α-ketobutyrate formation in the 96 well format than the hCGL(R119L, E339V) (Table 3, Library B). The respective enzymes were produced and purified by IMAC in small scale and then rank-ordered with respect to their relative 2nd order rate constants (apparent k_{cat}/K_M when [S] is << K_M) in a reaction with 0.1 mM L-Met and continuous monitoring of methanethiol formation with 5,5'-dithiobis-2-nitrobenzoic acid (Table 4). This was done to minimize possible expression effects in the screen signal. The highest apparent k_{cat}/K_M was obtained with hCGL (E59N, R119L, E339V) designated hCGL-NLV.

Library B		
Pos. E59	Pos. R119	Relative [α-ketobutyrate] produced
A	L	1.00
N	L	0.58
S	P	0.56
V	L	0.49
A	S	0.41
S	L	0.40
H	L	0.38
S	A	0.36
M	L	0.35
S	S	0.32
Q	L	0.32
A	V	0.32
A	A	0.31
V	A	0.29
S	Q	0.28
H	S	0.27
V	S	0.25
M	A	0.24
A	E	0.24
H	Q	0.23
A	H	0.22
H	A	0.20
P	Q	0.17
L	L	0.17
L	Q	0.16
T	A	0.13
F	Q	0.13
I	S	0.12
Y	A	0.11
T	S	0.06
V	Q	0.04
MBTH assay		

Table 3: Relative activity of clones from Library B

Library B Ranked			
Pos. E59	Pos. R119	Pos. E339	Relative *V/K*
N	L	V	1
A	L	V	0.87
V	L	V	0.84
S	P	V	0.73
A	S	V	0.43
DTNB assay			

Table 4: Relative *V/K* of select clones from Library B

Steady state Michaelis-Menten parameters for pMGL, hCGL, and hCGL-NLV with L-Met, L-cystathionine, L-cysteine or DL-homocysteine were determined in 100 mM phosphate buffer, pH 7.3 at 37 °C (Table 1). hCGL-NLV displayed significant methionine-γ-lyase activity as well as increased activity towards L-Cys and DL-homocysteine. However, this enzyme had approximately 15-fold lower k_{cat}/K_M for L-cystathionine, the physiological substrate of hCGL, suggesting that its methionine-γ-lyase activity is not simply a consequence of broader substrate specificity, a rather common outcome in enzyme engineering. For comparison, the kinetics of hCGL-E339V, hCGL-E339P, hCGL-R119Q-E339V, hCGL-E339V-R119L and hCGL-E59A-R119S- E339V (hCGL-ASV) for the degradation of L-Met and L-cystathionine were also determined (Table 5). Consistent with the results of the screening assay, hCGL-NLV displayed better kinetics than either the single or the double mutant enzymes above.

Kinetic comparison of select hCGL variants							
k_{cat}/K_M $mM^{-1}s^{-1}$							
[S]	hCGL	E339V	E339P	R119Q-E339V	R119L-E339V	hCGL-ASV	hCGL-NLV
L-Cysta	**2.90 ± 0.02**	**0.37 ± 0.03**	**0.09 ± 0.01**	**0.043 ± 0.016**	**0.10 ± 0.02**	**0.08 ± 0.01**	**0.034 ± 0.01**
L-Met	**n/a**	**0.005 ± 0.003**	**0.001 ± 0.0005**	**0.003 ± 0.001**	**0.013 ± 0.004**	**0.036 ± 0.003**	**0.041 ± 0.01**
Steady-State Kinetics determined at 25 °C with DTNB							

Table 5: Kinetics (k_{cat}/K_M) of hCGL, and variants E339V, E339P, R119Q-E339V, R119L-E339V, and hCGL-NLV.

2.3.3 Serum Inactivation

Of importance to therapeutic applications, (non-PEGylated) hCGL-NLV displayed substantially greater stability in pooled human serum at 37 °C relative to the *P. putida* MGL with $t_{1/2}$ deactivation of 78 ± 5 hr in contrast to 1.9 ± 0.2 hr for the bacterial enzyme (Figure 3).

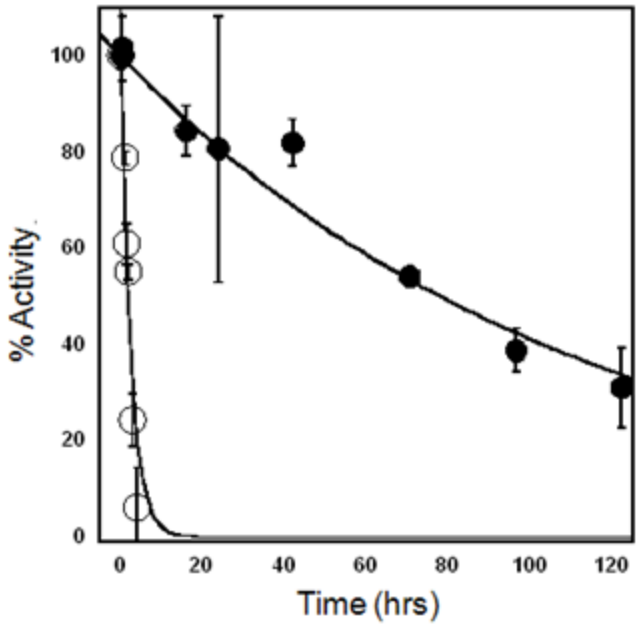

Figure 3: Stability of enzymes incubated in pooled human serum at 37 °C. (●) hCGL-NLV had a calculated $t_{1/2}$ = 78 ± 5 hr and (○) pMGL exhibited a $t_{1/2}$ = 1.9 ± 0.2 hr.

2.3.4 Promiscuity

Although hCGL-NLV has activity *in vitro* with other plasma metabolites (eg L-cystathionine, L-Cys, and L-homocysteine) it is not expected that this will greatly affect their homeostasis *in vivo*. Plasma L-Cystathionine is excreted in the urine at a rate of 38.5 μM/day and maintained in the serum at concentration of 0.24 ± 0.06 μM (*76*) at which concentrations hCGL-NLV would have the negligible turnover rate of 1.5 x 10^{-4} s^{-1} on its degradation. In humans plasma L-Cys, and L-homocysteine exist either as the free amino acids, the (mixed) disulfide form, or bound to serum proteins at concentrations around

170 μM (54% free) and 6 μM (31% free) respectively (*77*). Consistent with the existence of a protected fraction of L-Cys and L-Hcys, mice injected with pMGL were shown to have a 90 % reduction in L-Met, but only a 46 % reduction in L-Hcys and no effect on L-Cys levels(*12*). hCGL-NLV is 2–and 10-fold less active towards L-Cys and L-homocysteine respectively relative to pMGL and therefore its effect on these metabolites would be expected to be significantly lower.

2.3.5 Methionine Inhibition of hCGL

It was surprising that we could not detect any L-Met hydrolysis with hCGL at any concentration despite its smaller size compared to L-cystathionine. DL-homocysteine is also smaller than L-cystathionine yet it is degraded by hCGL, though with a 40-fold lower k_{cat}/K_M. We examined the hypothesis that DL-homocysteine is a substrate of hCGL whereas L-Met is not due to leaving group effects. Degradation of homocysteine leads to H_2S (pK_a = 7)(*78*) whereas L-Met degradation leads to methanethiol (pK_a = 10.3 (*78*)). The possibility that L-Met binds to the active site but the γ-lyase activity is disfavored by the high pK_a of methanethiol could be ruled out since we found that even 20 mM L-Met did not inhibit L-cystathionine degradation by hCGL. This observation raised the possibility that the relatively hydrophobic L-Met molecule is unable to partition into the hydrophilic active site of hCGL.

2.3.6 Hydropathy Studies

The LogP values of the active-site residues unique to hCGL were summed (Σ LogP) to yield a value = -19.7 (hydrophilic) while the Σ LogP value of the pMGL unique active-site is -2.87 (hydrophobic). These values correlate well with the LogP values of their respective substrates (L-cystathionine = -5.82, L-Met = -2.19). Consistent with this hypothesis, comparison of the active-site hydropathy values (Σ LogP) of hCGL, hCGL-E339V, hCGL-E339P, hCGL-E339Q-R119L, hCGL-E339V-R119L, hCGL-ASV and hCGL-NLV with the Log k_{cat}/K_M values (log10 value of k_{cat} divided by K_M values found from fits to the Michaelis-Menten equation) for L-Met and L-cystathionine hydrolysis revealed a positive linear relationship for the turnover of L-Met and a negative linear relationship for the turnover of L-cystathionine (Figure 4). This appears to hold true for DL-homocysteine and L-Cys as well which have intermediate hydropathy values, LogP = -2.58, and -2.79 respectively. DL-homocysteine and L-Cys are substrates that can partition into the hCGL active-site and hCGL-NLV with a more hydrophobic active site (Σ LogP = -7.64) increases the k_{cat}/K_M for these substrates 13 and 6-fold respectively. It should be noted that in previous studies , when E339 of hCGL was mutated to either Lys, Ala or Tyr the k_{cat}/K_M for L-Cys increased by 2-, 3-, and 7-fold respectively, results that are also consistent with the effect of active site hydrophobicity as a key determinant of CGL substrate specificity (*79*).

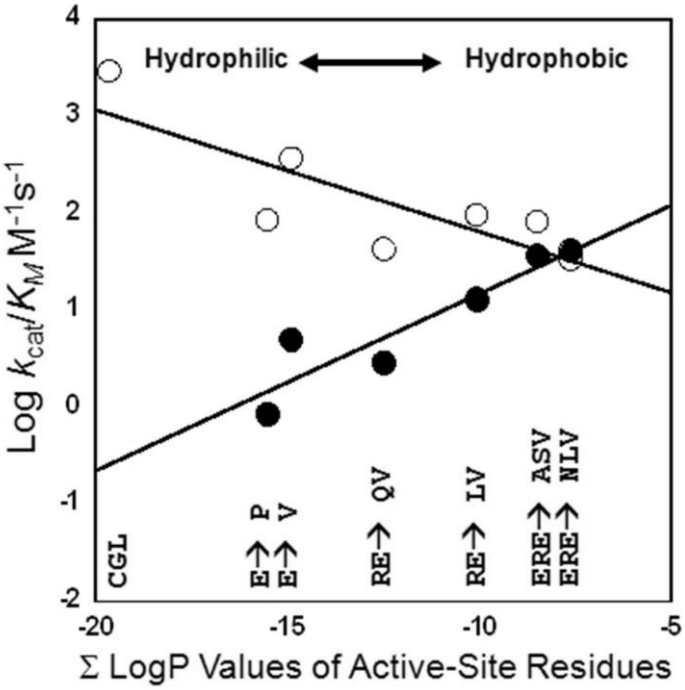

Figure 4. Plot of the sum of the calculated LogP values of residues in the active sites of hCGL, hCGL-E339P, hCGL-E339V, hCGL- R119L-E339Q, hCGL-R119L-E339V, hCGL-ASV and hCGL-NLV versus their Log k_{cat}/K_M values for the hydrolysis of L-Met (●) and L-Cystathionine (○).

2.3.7 Immunogenicity Assessment

To assess the likelihood that the three point mutations (E59N-R119L-E339V) in hCGL could generate a novel T cell epitope (i.e. generate a peptide fragment with affinity to MHC II) we compared the computationally predicted MHC(II) binding scores (consensus method) for peptides containing each mutated residue relative to the corresponding wild type sequence for 8 of the most common HLA alleles that collectively cover nearly 95% of the human population (*80*) The consensus percentile

rank (CPR) score ratios indicated no significant change in predicted MHCII binding suggesting that the E59N-R119L-E339V mutations are unlikely to introduce neo-epitopes (Table 6).

Computational comparison of T-cell epitopes in WT hCGL and the hCGL-NLV variant by IEDB consensus method			
Allele	WT:E59N	WT:R119L	WT:E339V
HLA-DRB1*01:01	1.1	1.2	1.3
HLA-DRB1*03:01	0.8	0.7	1.4
HLA-DRB1*04:01	1.6	1.2	1.2
HLA-DRB1*07:01	1.4	1.0	1.9
HLA-DRB1*08:01	1.1	1.4	1.0
HLA-DRB1*11:01	1.3	0.7	1.0
HLA-DRB1*13:01	1.0	1.0	2.1
HLA-DRB1*15:01	1.1	1.4	1.9
Average	1.2	1.1	1.5

Table 6: Computational comparison of T-Cell epitopes.

2.3.8 Pharmacological Optimization

To investigate the therapeutic efficacy of hCGL-NLV *in vivo*, the enzyme was PEGylated by conjugation to methoxy PEG succinimidyl carboxymethyl ester, MW 5,000 Da at an 80:1molar ratio (80 PEGs per subunit). Initial tests using PEG:enzyme ratios of 10:1, 20:1, 40:1, and 80:1 showed the greatest homogeneity at an 80:1 ratio (Figure 5). PEGylation has been extensively exploited to increase the hydrodynamic radius of proteins, preventing renal filtration and in turn markedly increasing circulation

persistence; note that PEGylation significantly increased the circulation $t_{1/2}$ of the structurally homologous pMGL in mice and primates (*65*). To prevent inactivation during PEGylation it was essential to pre-incubate the enzyme with 10 mM pyridoxal phosphate (PLP), to avoid conjugation of K212 to the PEG succinimidyl ester. Analytical size exclusion chromatography of the resulting PEG-hCGL-NLV gave a single homogeneous peak with an apparent MW of 1,300 KDa per tetramer, a 6-fold increase from unmodified tetramer (Figure 6). PEG-hCGL-NLV displayed L-Met degradation kinetics identical to those of the unmodified hCGL-NLV with k_{cat} = 7.8 ± 0.4 s^{-1}, K_M = 13.5 ± 1.5 mM and a $t_{1/2}$ = 39 ± 2 hrs in pooled human serum (Figure 7). The specific activity of PEG-hCGL-NLV was 10 U/mg protein at 37 ºC and pH 7.3 and had an endotoxin level of ≤ 12.5 EU/mg as assessed by Limulus Amebocyte Lysate assay (The endotoxin received by the mice was >> 2 orders of magnitude fold lower than doses showing no observed effect in mice (*81, 82*)).

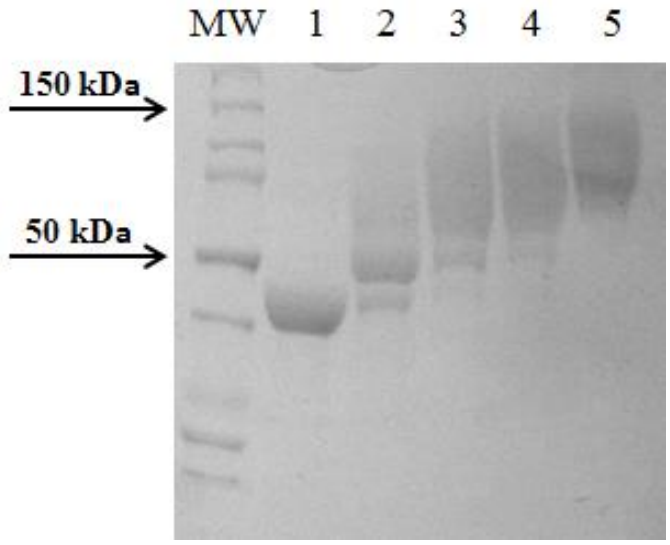

Figure 5: SDS-PAGE gel of PEGylation. hCGL-NLV (Lane 1), Lanes 2-5: hCGL-NLV after PEGylation with 10, 20, 40, & 80 fold molar excess of methoxy PEG succinimidyl carboxymethyl ester.

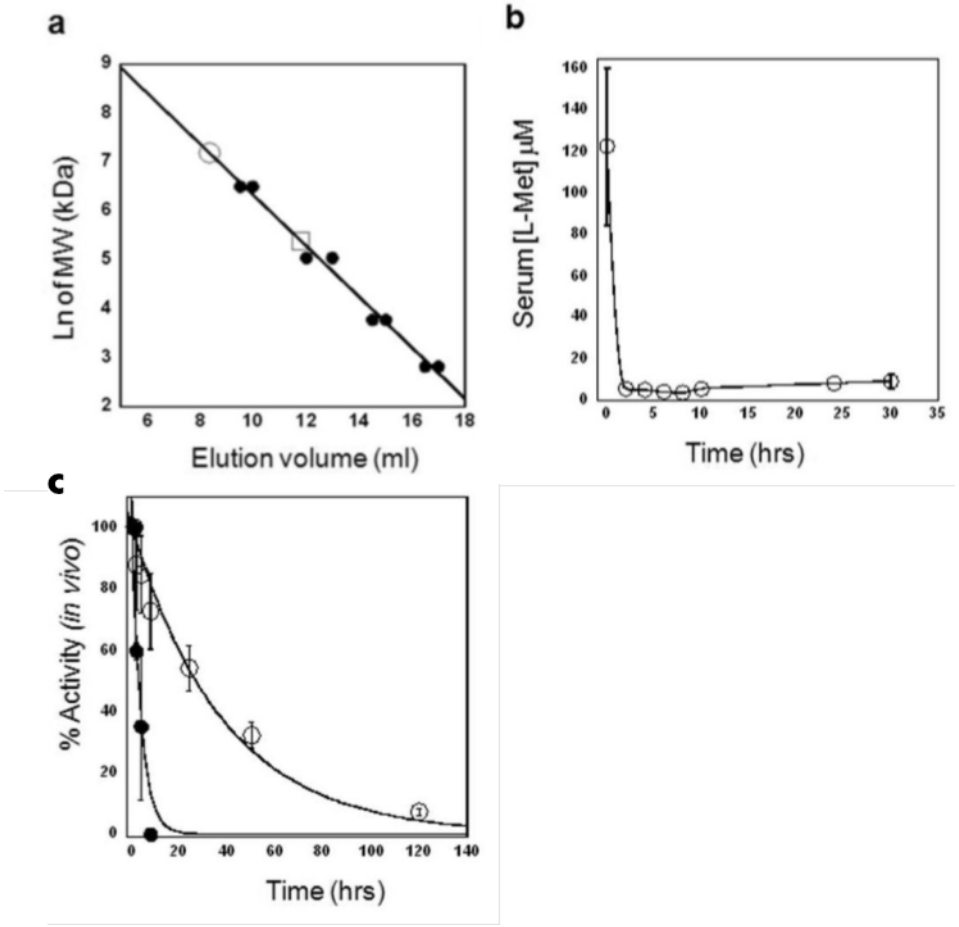

Figure 6: (a) Analytical size exclusion chromatography of MW standards (●), hCGL-NLV (□) and PEGylated hCGL-NLV (○). **(b) Pharmacodynamics of PEG-hCGL-NLV in balb/c mice maintained on a Met(-)Hcyss(-)Chl(-) diet.** Mice (n=5) were treated with 200 U PEG-hCGL-NLV administered by tail-vein injection and blood methionine level (○) was monitored by HPLC. **(c) *In vivo* activity of PEG-hCGL-NLV** (○) and unPEGylated hCGL-NLV (●) in serum as a function of time following tail-vein injection of 100U PEG-hCGL-NLV in athymic mice (n=5).

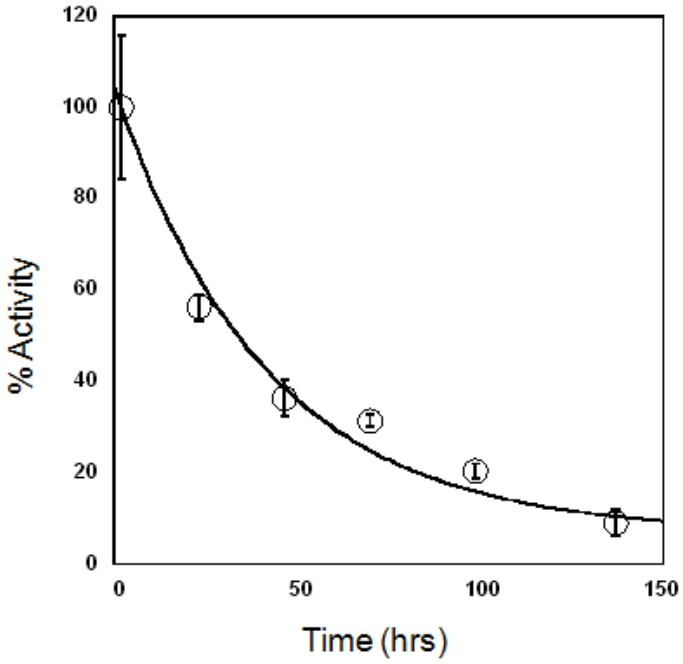

Figure 7: Stability of (o) PEG-hCGL-NLV incubated in pooled human serum at 37 °C with an apparent $t_{1/2}$ = 39 ± 2 hrs.

2.3.9 *In Vitro* Cytotoxicity & *In Vivo* Half Life of PEG-hCGL-NLV

The cytotoxicity of PEG-hCGL-NLV towards 14 neuroblastoma (NB) lines established to be L-Met dependent (*46*) was compared to that of pMGL (The myelocytomatosis viral related oncogene, neuroblastoma derived (MYCN) amplification (*83*) status, anaplastic lymphoma kinase (ALK) mutation (*84*) status, and α-thalassemia/mental-retardation-syndrome-X-linked (ATRX) mutation (*85*) status and IC_{50} values are summarized in Table 7). While PEG-hCGL-NLV has a lower k_{cat}/K_M than pMGL for L-Met, its much higher stability in serum and in growth media led to nearly

identical IC_{50} values with an average of 0.091 ± 0.043 U and 0.086 ± 0.037 U, respectively. In Balb/c mice (n=5) maintained on a L-Met(-)Homocysteine(-)Choline(-) diet, tail vein administration of 200 U PEG-hCGL-NLV led to a decrease in the serum L-Met concentration from 124 ± 37 μM (pretreatment) to 3.9 ± 0.7 μM at 8 hr post-injection. Maintaining the animals on a Met(-)Hcyss(-)Chl(-) diet during treatment is necessary due to the high metabolic rate of mice which leads to rapid replenishment of the serum L-Met pool following depletion(*46, 64*). (It is not yet known if L-Met depletion therapy in humans will necessitate that the patients are placed on L-Met-deficient diet. The serum L-Met replenishment rate in man is estimated to be roughly 2 μM/hr (est. from Ref (*37*)) compared to ~ 4 μM/hr in mice (est. from Ref (*86*)) . An L-Met deficient diet would likely augment a treatment regimen but may not be necessary with an enzyme displaying a good PK/PD profile). In mice treated with PEG-hCGL-NLV, the serum L-Met was maintained at a therapeutically relevant level for at least 30 hr (Figure 6b). This is on par with various formulations of PEGylated-pMGL which have been reported to maintain serum L-Met levels in mice at <5 μM for 8 hrs in one study (*86*) to 48 hrs in an earlier report (*69*). The PEG-hCGL-NLV activity in the blood of the injected mice decreased with a $t_{1/2}$ of 30 ± 3 hr (Figure 6c), much longer than non-PEGylated hCGL-NLV ($t_{1/2}$ = 1.8 ± 0.7 hr).

			PEG-hCGL-NLV	pMGL
Cell lines	*MYCN* amplification	*ALK or ATRX* mutations	IC50 (U) Average of 2 exp.	IC50 (U) Average of 2 exp.
BE(1)N	Amplified	Wild type	0.039± 0.009	0.042 ± 0.007
BE(2)N	Amplified	Wild type	0.076 ± 0.004	0.074 ± 0.008
BE(2)S	Amplified	Wild type	0.076 ± 0.035	0.075 ± 0.038
BE(2)C	Amplified	Wild type	0.063 ± 0.004	0.061 ± 0.005
SK-N-LD	Amplified	Wild type	0.074 ± 0.021	0.100 ± 0.050
NMB-7	Amplified	Wild type	0.067 ± 0.018	0.080 ± 0.021
SH-EP-1	Not amplified	F1174L	0.151 ± 0.054	0.174 ± 0.086
IMR32	Amplified	Wild type	0.051 ± 0.002	0.043 ± 0.005
CHP-212	Amplified	Wild type	0.175 ± 0.077	0.137 ± 0.065
SKN-MM	Not amplified	K1329*	0.161 ± 0.052	0.111 ± 0.054
LAN-1	Amplified	Wild type	0.075 ± 0.020	0.053 ± 0.006
LAI-66N	Amplified	Wild type	0.068 ± 0.003	0.088 ± 0.025
LAI-55N	Amplified	Wild type	0.073 ± 0.004	0.072 ± 0.003
LAI-5S	Amplified	Wild type	0.123 ± 0.035	0.099 ± 0.012
IC_{50} (half maximal inhibitory concentration) was expressed as mean ± SD				

Table 7: Inhibition of *in vitro* proliferation of various neuroblastoma cell lines.

2.3.10 Therapy of established NB Xenografts

Athymic mice bearing LAN-1 neuroblastoma tumor xenografts were treated with 100 Units PEG-hCGL-NLV, administered via tail vein injection once daily for 3 times a week for 4 weeks. Met(-)Hcyss(-)Chl(-) diet was fed to the animals on the days of PEG-hCGL-NLV administration. Xenografted control mice were either fed a constant normal diet or a Met(-)Hcyss(-)Chl(-) diet 3 times a week for 4 weeks using an identical schedule as in the treatment group. 24 hr after the third PEG-hCGL-NLV injection during the last (4^{th}) week of treatment, plasma methionine concentration was 6 ± 2 μM among PEG-hCGL-NLV-treated mice fed Met(-)Hcyss(-)Chl(-) diet, in contrast to 124 ± 37 μM before treatment (n=10). Mice fed Met(-)Hcyss(-)Chl(-) diet exhibited a 10 - 15%

reversible weight loss (Figure 9). While control mice on Met(-)Hcyss(-)Chl(-) diet only had no significant reduction in tumor growth, the administration of PEG-hCGL-NLV completely inhibited the growth of the LAN-1 tumors during the treatment period ($p<0.01$, Figure 8). Even three weeks after the last round of treatment with PEG-hCGL-NLV, rebound tumor volume was small (0.5 fold increase), whereas in the control groups tumor growth increased 3- and 4-fold in mice maintained on Met(-)Hcyss(-)Chl(-) or on normal diet, respectively.

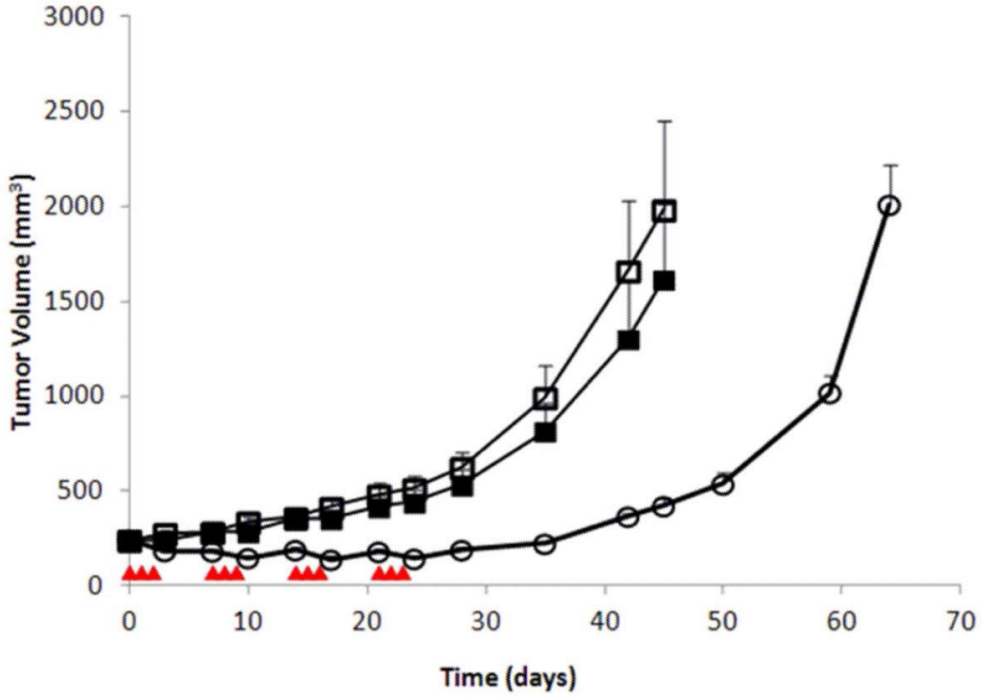

Figure 8: Evaluation of PEG-hCGL-NLV in athymic mice bearing LAN-1 xenografts. (□) Control animal group maintained on normal diet (N=10); (■) Animals maintained on Met(-)Hcyss(-)Chl(-) diet (N=10); (○) animals treated with 100 U PEG-hCGL-NLV in combination with Met(-)Hcyss(-)Chl(-) mouse feed (N=10). Treatment days are designated by (▲). Tumor growth rate was expressed as mean ± SEM (standard error of the mean) for each group. * $p<0.01$ for the PEG-hCGL-NLV treated group relative to the two untreated groups.

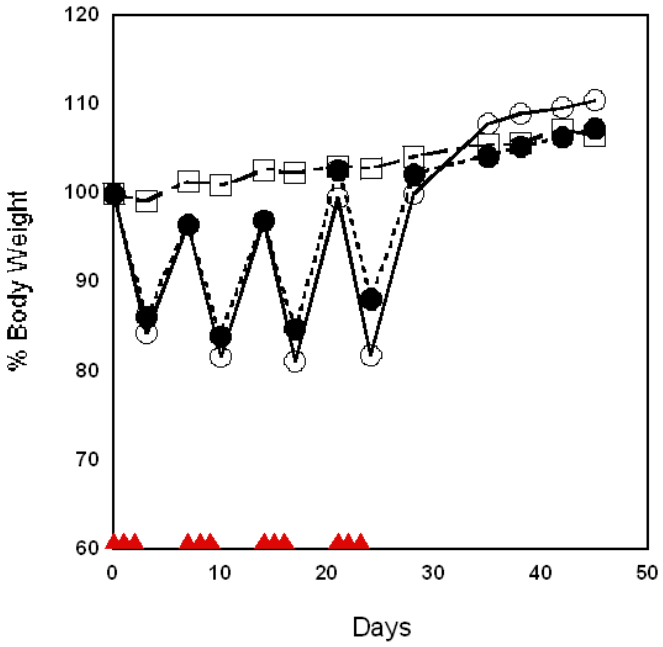

Figure 9: Toxicity as assessed by body mass. (□) Control with normal diet (N=10); (●) Met(-)Hcyss(-)Chl(-) mouse feed (N=10); (○) 100 U PEG-hCGL-NLV in combination with Met(-)Hcyss(-)Chl(-) mouse feed (N=10) (▲ treatment days with PEG-hCGL-NLV and/or Met(-)Hcyss(-)Chl(-) diet).

2.4 SUMMARY

The differential susceptibility of malignant and non-malignant cells to L-Met starvation provides a useful therapeutic window for cancer therapy. Even partial depletion solely through L-Met omission in a parenteral nutrition (TPN) regimen has been shown to result in tumor reductions in gastric cancer in both the rat model and in humans (*27, 87, 88*). However, dietary restriction alone only results in ~ 40 % decrease in serum L-Met levels (*89*). A much more significant reduction in the serum L-Met concentration,

resulting in drastic inhibition of tumor growth in a number of animal models (*12, 68, 90, 91*), has been achieved by the administration of MGLs. Humans do not encode an MGL and consequently, bacterial enzymes have been investigated as agents for L-Met depletion therapy. In particular, the *P. putida* MGL was found to display the most favorable catalytic properties, having a low K_M and a relatively high k_{cat} (*41, 42*). Administration of pMGL was shown to drastically affect the growth of human neuroblastoma, lung, colon, and brain tumors in mouse xenografts maintained on L-Met restricted diet (*30, 33, 46, 92*). Unfortunately, both in mice and in the non-human primate model, pMGL was shown to be deactivated very rapidly with a half-life of approximately 2 hr due to the loss of the PLP cofactor(*67*). Nonetheless, pMGL given at a 90 mg/kg dose every 8 hr for 2 weeks resulted in a steady-state depletion of plasma methionine to less than 2 μM in animals maintained on L-Met restricted diet. Only mild toxicities were observed, manifested as decreased appetite and slight weight loss. However, anti-MGL antibodies were detected after administration and an additional round of treatment with pMGL resulted in anaphylactic shock and death in some animals(*67*). Yang *et al.* sought to increase the pharmacokinetic half-life and reduce the immunogenicity of MGL by amine conjugation to polyethylene glycol (PEGylation). PEGylation of pMGL drastically improved circulatory persistence (≥ 36 fold) in primates and attenuated severe immunological responses (with anti-MGL antibody titers increasing upon repeated treatments), however only a marginal improvement in pharmacodynamics was observed (serum L-Met was maintained at <5 μM for 12 hrs vs 8 hrs for the unPEGylated enzyme)

(*65, 70*). PEGylation of bacterial and even of mammalian proteins appears to delay but not eliminate immune responses as evident in clinical studies of PEGylated *M. arginii* arginine deiminase (*93*) or pegloticase (*94*).

To augment the anti-neogenic potential of systemic L-Met depletion and overcome the disadvantages observed with pMGL we engineered hCGL into a pharmacologically efficacious human methionine γ-lyase. Although the overall structures of hCGL and pMGL align with a RMS deviation of 0.8 Å they only share a 61 % aa sequence similarity. Many of the differences are seen in the degree of hydrophobicity in the active sites which correlates with the relative hydrophobicities of their substrates. The hCGL-NLV is engineered from a native human enzyme and thus it is likely to be much less immunogenic than pMGL circumventing problems with adverse immune responses, including neutralizing antibodies and anaphylactic reactions observed in earlier studies. L-Met depletion may be particularly attractive for the treatment of brain tumors, a hypothesis we plan to test in future studies using orthotopic glioblastoma mouse models (*90*). The paucity of chemotherapeutics that can target tumors from across the blood-brain barrier makes systemic L-Met depletion an appealing strategy for the treatment of tumors that arise from or metastasize to the central nervous system, both significant challenges in cancer treatment.

2.5 Materials and Methods

Construction of Synthetic Genes

Overlapping oligonucleotides (IDT) comprising the coding sequence of a 6X histidine tag and human cystathionine-gamma-lyase or *p. putida* methionine-gamma-lyase were designed to be codon-optimized for expression in *E. coli*. Human CGL contains mutiple rare *E. coli* codons that can interfere with expression. Thus, in order to optimize protein expression in *E. coli*, the hCGL gene was assembled with codon optimized oligonucleotides designed with DNA-Works software (*95*). These were combined with dNTPs, buffer and DNA polymerase (Finnzymes) and allowed to react for 30 cycles of 98°C for 30 s, 61°C for 30 s, and 70°C for 1 min. A 1 µL aliquot of this mixture was then used as a template along with specific end primers (Forward `5-gatataccATGGGAGGCCATCACCACCATCATCATGGCGGGCAGGAAAAGGATGCG and Reverse `5-CTCGAATTCTCAACTGTGGCTTCCCGATGGGGGATGGGCCGCTTTCAGCGCCTGATCC in another PCR reaction to amplify the full length gene. The product was cleaned on a micro-column (Zymo), digested with NcoI and EcoRI, ligated into a pET28a vector (Novagen) and transformed into *E. coli* (MC1061).

Saturation Mutagenesis Libraries

Codons from the synthetic hCGL gene corresponding to AA positions E59, R119, and E339 were randomized using overlap extension PCR with complementary

oligonucleotides containing an NNS codon scheme (N = A,C,T,G, and S = G ,C). Library (A) was constructed by randomizing positions corresponding to R119 and E339 using the previously mentioned specific end primers and the following mutagenic oligonucleotides, R119-For- `5-gtatggtgggaccaatNNStatttccgtcaggtggcg, R119-Rev- `5-CGCCACCTGACGGAAATASNNATTGGTCCCACCATAC, E339-For `5-ctgaaactgtttaccctggca-NNSagcttgggcggctttg, E339-Rev`5-CAAAGCCGCCCAAGCTSNNTGCCAGGGTAAACAGTTTCAG, and the synthetic gene as a template. Library (B) was constructed by randomizing positions corresponding to R119 and E59 using a new template gene that had incorporated a codon for Val at position 339, specific end primers, the aforementioned R119 mutagenic primers and mutagenic oligonucleotides E59-For `5-ggccagcatagcggttttNNStatagccgtagcggc and E59-Rev `5-GCCGCTACGGCTATASNNAAAACCG-CTATGCTGGCC. Following digestion with NcoI and EcoRI restriction enzymes, the randomized genes were ligated into pET28a previously digested with NcoI and EcoRI. After ligation, plasmids were transformed into *E. coli* BL21 and transformants were screened as described above. Clones displaying activity were identified by sequencing, re-transformed into *E. coli* BL21, purified and kinetically characterized.

Construction of hCGL-E339V variant

In order to characterize the effect of an individual mutation on the ability to degrade L-Met we generated a singly mutated clone with the E339V mutation. (We only

isolated doubly mutated variants through our screens such as hCGL-R119L-E339V.) Overlap extension PCR was used to replace the mutated 119 codon for the wild-type sequence. The hCGL-R119L-E339V template and correcting primers (Forward`5-TTGCATGGATGATGTGTATGGTGGGACCAATCGTTATTTCCGTCAGGTGG and Reverse`5-GATATCTTCAGGCCGAACTCGCTCGCCACCTGACGGAAATAACGATTGGT) were combined with dNTPs, buffer and DNA polymerase (Finnzymes) and allowed to react for 30 cycles of 98°C for 30 s, 61°C for 30s, and 70°C for 1 min. A 1 μL aliquot of this mixture was then used as a template along with specific end primers (Forward `5-gatataccATGGGAGGCCATCACCACCATCATCATGGCGGGCAGGAAAAGGATGCG and Reverse `5-CTCGAATTCTCAACTGTGGCTTCCCGATGGGGGATGGGCCGCTTTCAGCGCCTGATCC) in another PCR reaction to amplify the full length gene. The product was cleaned on a micro-column (Zymo), digested with NcoI and EcoRI, ligated into a pET28a vector (Novagen) and transformed into *E. coli* (MC1061).

Protein Expression and Purification- E. coli (1 L scale)

E.coli-BL21 cells harboring plasmids with a given enzyme gene were grown in TB media containing 50 μg/ml kanamycin at 37°C to an OD_{600} of ~ 0.5 upon which time IPTG was added to a concentration of 1 mM. After an additional ~ 12 hr of incubation at 25°C, cells were collected by centrifugation, re-suspended in immobilized metal

affinity chromatography (IMAC) buffer (10 mM $NaPO_4$/10 mM imidazole/300 mM NaCl, pH 8) and lysed by a French pressure cell. The lysates were centrifuged at 14,000 x g for 30 min at 4°C, the resulting supernatant applied to a nickel IMAC column, washed with 10-20 column volumes of IMAC buffer, and eluted with IMAC elution buffer (50 mM $NaPO_4$/ 250 mM imidazole/ 300 mM NaCl, pH 8). All chromatography was performed at 4°C. Eluted enzyme was then incubated with 10 mM pyridoxal-5'-phosphate (Sigma) for 30 min to 1 hr at 25°C. Using a 10,000 MWCO centrifugal filter device (Amicon), protein was then buffer exchanged into a solution comprised of 1X Phosphate Buffered Saline (PBS), 10 % glycerol, pH 7.4. Aliquots of purified enzyme were then flash frozen in liquid nitrogen and stored at -80°C.

To determine protein concentrations, extinction coefficients, were calculated based on amino acid sequence (ε_{280} = 29,870 $M^{-1}cm^{-1}$ for hCGL, 22,330 $M^{-1}cm^{-1}$ for pMGL) (*96*). All protein concentrations were determined from the absorption at 280 nm (A_{280}) in 6 M guanidinium hydrochloride, 20 mM phosphate buffer, pH 6.5.

Protein Expression and Purification- E. coli (50 mL scale)

Cultures (50 ml) of *E.coli* expressing hCGL variants were grown in 125 ml shake flasks and induced for protein synthesis as described previously(5 ml scale purification). 5 ml aliquots were centrifuged and the resulting cell pellets were lysed with 400 μL of B-PER protein extraction reagent (Pierce, Rockford IL) and centrifuged. (50 ml scale cultures had better expression levels, and the remaining 45 ml culture pellets were frozen

for later use) The soluble fractions were then mixed with 500 μL IMAC lysis buffer and 100 μL of IMAC beads (Talon, Mountain View CA) in a 1.5 ml Eppendorf tube. After a 2 min incubation, the suspensions were centrifuged at 3000 rpm for 20 s in a table top centrifuge. The supernatants were discarded and enzyme-bound beads were washed with 4 x 1 ml lysis buffer by mixing/centrifuging and discarding the supernatant. Proteins were then eluted from the beads by addition of 300 μL of IMAC elution buffer followed by another centrifugation step. The elutions were quantified by measuring A_{280}, and purity was assessed by SDS-PAGE. This method allows purification of 12–16 proteins in ~ 2 hrs with a yield of 50 – 300 μg protein with the purity varying between 80 – 95 % as assessed by SDS-PAGE.

Kinetic Assays

Kinetic analyses were performed as described elsewhere (*75*) to measure α-ketobutyrate production by reaction with 3-methyl-2-benzothiazolone hydrazone hydrochloride (MBTH) to generate a chromophore with a λ_{max} of ~ 320 nm. Eppendorf tubes (1.5 ml) containing 220 μL of substrate in a 100 mM sodium phosphate buffer, 1 mM EDTA (pH 7.3), and 10 μM PLP were incubated at 37°C in a heat block. Reactions were started by adding 20.3 μL of enzyme solution and quenched with 26.7 μL of 50% trichloroacetic acid after a set length of time (without shaking). Reactions and blanks were then mixed with 733 μL of MBTH solution (2.2 ml: 1.6 ml of 1 M acetate buffer pH

5.0 and 0.6 ml of 0.1% MBTH in same) and incubated at 50°C for 40 minutes. After cooling, the samples were transferred to cuvettes and the A_{320} nm was determined. The assay was shown to be linear between 0 - 320 μM α-ketobutyrate with a lower detection limit of 15 μM. One unit of MGL activity was defined as the amount of enzyme that produced 1 μmol of α-ketobutyrate per minute at infinite concentration of L-methionine. We also followed enzyme reactions in a continuous assay by detection of product methane-thiol with 5,5'-Dithiobis(2-nitrobenzoic acid) (DTNB) using 96-well plates and a microtiter plate reader set at 405 nm.

96-well plate screen

Both MGL and CGL produce α-ketobutyrate from their respective substrates. The aforementioned colorimetric assay was adapted to a 96-well plate scale for screening small libraries and for ranking clones with the greatest L-Met degrading activity. Single colonies of *E. coli* BL21(DE3), containing plasmids encoding either wild-type (pMGL of hCGL control) or variant hCGL enzymes were picked into 96-well culture plates containing 75 μL of TB media/well and 50 μg/ml kanamycin. Cells were grown at 37 °C on a plate shaker to an OD_{600} of ~0.8–1, cooled to 25 °C, whereupon an additional 75 μL of media containing 50 μg/ml kanamycin, and 2 mM IPTG were added and incubation with shaking was continued for 2 hrs at 25 °C. Subsequently, 100 μL of culture/well were transferred to a fresh 96 well plate (assay plate). The assay plates were centrifuged

(10 min x 3,500 g) to pellet the cells, the media was removed, and the cells were chemically lysed by addition of 50 μL/well of B-PER protein extraction reagent (Pierce, Rockford IL) and mixing for 5 min on a plate shaker. Then 20 uL of 5 mM L-Met at pH 7.3 was added to the lysates and incubated at 37°C for approximately 12 hours. The α-keto acid reaction product is then derivatized by addition of 146 μL of MBTH solution to 54 μL of reaction and heated for 40 min at 50°C. The absorbance at 320 nm was determined spectrophotometrically using a microtiter plate reader. Variants exhibiting high absorbance values and indicative of production can thus be identified and selected for further characterization.

L-Met Inhibition of hCGL

We measured the rate of L-cystathionine (1 mM) hydrolysis by hCGL in the presence of varying concentrations of L-Met (0-20 mM). The reactions were conducted at 25°C by mixing 5 μL enzyme (20 μM) with 95 μL of a solution of 1 mM cystathionine and either 0 or 20 mM L-Met in 100 mM sodium phosphate buffer with 1 mM EDTA and 10 μM PLP at pH 7.3. Ellman's reagent was used to quantify product formation by the method previously described.

Immunogenicity Calculations

We used software from the Immune Epitope Database (IEDB) (consensus method for MHC(II) binding) (*97*) to evaluate peptides spanning 9 residues on either side of the WT or the mutated position (i.e. pos. 59,119, 339). Using the averaged consensus percentile rank (CPR) scores for the 8 most common HLA alleles as reported previously (*98*) we then calculated the ratio of the predicted CPR scores for each WT:mutant peptide for each HLA allele.

WST8 Assay for NB Cell Proliferation

In vitro proliferation of NB cell lines was assayed in 96-well plates (BD Biosciences, Bedford, MA). Twenty-four hours after seeding at a density of 3000-6000 cells/well, PEG-hCGL-NLV and pMGL were added. After 3 days of culture, PEG-hCGL-NLV and pMGL were removed and fresh medium was added for another 36 hr incubation because methioninase activity interferes with WST8 assay). WST8 (Dojindo Molecular Technologies, MA) was added to culture wells at volume ratio of 1:10. After 4-6 hr of reaction, optical density (OD) was read at 450 nm. Cell proliferation was calculated as follows: % Cell Growth = (OD_{450} of experimental well - OD_{450} of medium-only well)/(OD_{450} of control well - OD_{450} of medium-only well) × 100%. IC_{50} (half maximal inhibitory drug concentration) was calculated using SigmaPlot 8.0 (Systat Software, Inc., San Jose, CA).

In vitro half lives

In vitro half– life of PEG-hCGL-NLV activity was assayed by incubating PEG-hCGL-NLV in RPMI medium containing 10% calf serum at 37°C. Additionally purified enzymes were also added to pooled human serum (Innovative, Novi MI) at a concentration of 20 μM and incubated at 37°C. At various time points, aliquots were withdrawn and tested in triplicate for their ability to hydrolyze L-Met (10 mM). Data were plotted as observed reaction rate vs. time and fit to a single exponential equation to calculate $t_{1/2}$ values.

Serum Stability

Purified enzymes were added to pooled human serum (Innovative, Novi MI) at a concentration of 20 μM and incubated at 37°C. At various time points, aliquots were withdrawn and tested in triplicate for their ability to hydrolyze L-Met (10 mM). Data were plotted as observed reaction rate vs. time and fit to a single exponential equation to calculate $t_{1/2}$ values.

Pharmacological Optimization of hCGL Variants

Human CGL variants were conjugated to lysyl residues using methoxy PEG succinimidyl carboxymethyl ester of MW 5000 (PEG-5K) (JenKem, Inc.). Purification

was performed as described above, with inclusion of an additional on column wash step using 100 column volumes of IMAC buffer containing 0.1% Triton X114 (Sigma, MO) in order to remove endogenous endotoxin. Purified proteins were then buffer exchanged into 1X PBS using a 10,000 MWCO filtration device (Amicon). PEG-5K was added at an 80:1molar ratio to enzyme and allowed to react for one hour at 25° C in glass vials with gentle stirring. PEGylated hCGL variants were extensively buffer exchanged using a 100,000 MWCO centrifugal filter device (Amicon) into storage buffer (PBS made 10% v/v with glycerol). Aliquots of PEGylated enzyme were flash frozen in liquid nitrogen and stored at -80°C. All PEGylated enzymes were analyzed for lipopolysaccharide (LPS) content using a Limulus Amebocyte Lysate (LAL) kit (Cape Cod Incorporated).

Methionine Depletion in mouse plasma

Methionine levels were measured according to the method of Sun *et al (99)* with minor modifications. 15 µl acetonitrile was added to 5 µl plasma samples, mixed, and centrifuged at 14000 rpm for 2 min at 4°C. 10 µl supernatant was transferred to an Eppendorf tube. 5 µl OPA (o-phthaldialdehyde) solution (Sigma-Aldrich) was added, mixed, and incubated at room temperature for 90 sec. 150 µl 0.1 M sodium acetate (pH 7.2) was added. After mixing, the OPA–derivatized samples were loaded (50 µl sample volumes) immediately on a Supelcosil^{TM} LC-18 DB column (particle size 5mm, 25cm × 4.6mm, 120 Å pores) for HPLC analysis. Solution A for HPLC was prepared with tetrahydrofuran/methanol/0.1M sodium acetate (pH 7.2) at volume ratios of 5/95/900.

Solution B for HPLC was methanol. The elution gradient for HPLC was as follows: (1) 0 - 5 min: 40% solution B; (2) 5 - 10 min: 40-46% solution B; (3) 10 - 20 min: 46-48% solution B; (4) 20 - 25 min: 48-60% solution B; (5) 25 - 26 min: 60-100% solution B; (6) 26 - 30 min: 100% solution B; (7) 30 - 31 min: 100-40% solution B; and (8) 31 - 35 min: 40% solution B. At a flow rate of 1 ml/min, total running time was 35 min. Fluorescence detection by in-line spectrophotometer (Waters, Milford, MA) was set at the wavelength of 350-450 nm and Gain = 1. Amino acid standard H solution (Pierce Chemicals) was used for methionine quantification and methionine from Sigma-Aldrich was used to characterize the methionine peak.

Mouse Feed

The Met(-)Hcyss(-)Chl(-) mouse feed, purchased from Dyets (Bethlehem, PA) was methionine, choline and DL-homocystine deficient.

Hydropathy Calculations

Using structural alignments of hCGL (3COG) and pMGL (2O7C) as a guide we identified residues in the active site within 5-6 Å of a covalently bound inactivator, propargylglycine. We found that F58, L62, C116, A119, and V339 were unique to the pMGL active-site whereas in hCGL these residues correspond to E59, S63, G116, R119, and E339 respectively. By convention, the relative hydropathy of a solute is described by

the logarithm of its octanol water partition coefficient (LogP). Using ChemAxon software we calculated the LogP values of each of the aforementioned residues with their α amino and carboxy termini in the amide form (*100*). (We used this method because the LogP values are in good agreement with available experimental values and allowed us to estimate LogP values for compounds without known reference values like L-cystathionine) We also calculated the active site LogP values for three hCGL variants, hCGL-E339V, hCGL-R119L -E339V, and hCGL-E59N-R119L-E339V - (hCGL-NLV). These LogP values were summed for each enzyme to calculate an overall hydropathy value for each active site and plotted against the Log k_{cat}/K_M values for each enzymes ability to hydrolyze L-Met and L-cystathionine (This is similar to an analysis of lipase performed by Hirata et.al. (*101*)). We also calculated the LogP values for the substrates L-Met, L-homocysteine, L-Cys, and L-cystathionine.

Tumor Cell Lines

NB cell line LAN-1 was obtained from Dr. Robert Seeger (Children's Hospital of Los Angeles; Los Angeles, CA), NB cell line NMB-7 from Dr. Liao of McMaster University (Hamilton, ON, Canada). SK-N-BE(1)N, SK-N-BE(2)C, SK-N-BE(2)N, SK-N-BE(2)S, LAI-5S and SH-EP-1, 55N and 66N were kindly provided by Dr. Robert Ross, Fordham University (New York, NY). NB cell lines SK-N-LD and SK-N-MM were established at Memorial Sloan-Kettering Cancer Center (MSKCC, New York, NY). IMR-32 and CHP-212 were purchased from American Type Culture Collection

(Manassas, VA). Cells were cultured in RPMI with 10% fetal calf serum (F10) as previously described (*102*).

In vivo half-lives

hCGL-NLV and PEG-hCGL-NLV activity was assayed on sera following injection of 50 U of enzyme in nude mice. Serum samples were obtained at 1, 2, 4, 8, 24, 50, and 120 hours after injection. Half-lives of enzymatic activity was calculated by SigmaPlot using the exponential decay equation ($y = ae^{-bx}$).

Therapy of established NB Xenografts

All animal experiments were carried out according to an Institutional Animal Care and Use Committee (IACUC) approved protocol at Memorial Sloan-Kettering Cancer Center, following institutional guidelines for the proper and humane use of animals in research. Athymic female nude mice were purchased from the National Cancer Institute. Mice with 5-10 mm established tumors were randomly separated into groups of 10 mice each. In mice xenografted with LAN-1 neuroblastoma, 100 Units of PEG-hCGL-NLV was given iv three times a week for 4 weeks. 0.5 cm -1 cm tumors are generally regarded as standard for tumor therapy studies since Institutional Animal Care and Use Committee (IACUC) requirement stipulates that mice with tumor that is >15% body weight (or 2 cm maximal tumor diameter) causes undue distress and animals have

to be sacrificed. Tumor volume was calculated as $(a^2b)/2$ where a is the width of the tumor (small diameter), and b the length (large diameter), both in millimeters (*103*). All of the tumors were growing at the time when the treatment was started and all of the mice finally died of tumor when the treatment was stopped. There were no spontaneous regressions in this experiment and in this tumor model. Met(-)Hcyss(-)Chl(-) diet was fed to the animals on the days of PEG-hCGL-NLV administration. Mice were bled 24 hr after the third PEG-hCGL-NLV injection during the last week of treatment. The weight of mice was measured twice weekly and normalized to the weight at day 0 (start of experiment) and used as an index of toxicity. A 20% maximum weight loss was used as a guideline in designing PEG-hCGL-NLV dosing, and none of the mice required sacrificing because of toxicity. Tumor size was measured twice per week and expressed as mean ± SEM (standard error of the mean) for each group. Mice were sacrificed when their tumor sizes exceeded 20 mm in diameter.

Chapter 3: Augmenting hMGL Activity through Phylogenetic Analysis

3.1 Chapter Summary

Many decades of research support the cancer treatment strategy of L-Met depletion. When the serum pool of this amino acid is enzymatically degraded, many tumors are unable to survive. Normal cells, however, are generally able to withstand the absence of L-Met and the differential requirements between normal tissues and cancer present an attractive therapeutic opportunity. We have previously shown that the human CGL can be engineered into a proficient L-Met degrading enzyme with the addition of three mutations established by rational design and saturation mutagenesis (CGL-NLV k_{cat}/K_M 0.56 $s^{-1}mM^{-1}$). The resulting enzyme was able to induce cell death in a variety of neuroblastoma cell lines and retard Lan-1 neuroblastoma tumor growth in a mouse xenograft. The dosage required to achieve the efficacy result, however, was impractically high and helped define the threshold activity necessary for a viable therapeutic as 10 times faster than CGL-NLV. We describe the utility of phylogenetic analysis as a method to identify critical residues for engineering a variant with improved L-Met degradation kinetics. The resulting enzyme "Variant 9" has a k_{cat}/K_M 5.3 $s^{-1}mM^{-1}$ and a selectivity that is 9 fold higher for L-Met than for the wild-type substrate cystathionine. This second-generation enzyme also displays improved structural stability and a slow rate of

inactivation in serum. Finally, mice treated with a therapeutically useful dose of Variant 9 display significantly reduced L-Met serum levels for up to 24 hours.

3.2 INTRODUCTION

3.2.1 Phylogenetic Analysis as a Tool of Protein Engineering

We had previously engineered an enzyme with novel L-Met-degrading activity by analyzing structural overlays of a bacterial methionine-γ-lyase and the human cystathionine-γ-lyase to identify residues critical for substrate binding (Chapter 2, (*53*)). The resulting "first generation" engineered enzyme degraded L-Met with a k_{cat}/K_M of 0.56 $s^{-1}mM^{-1}$ (NLV). However, the catalytic activity of this enzyme was 100 fold slower than the k_{cat}/K_M of the *P. pseudomonas* MGL that had been used earlier for L-Met depletion in animal studies, but had the significant advantage of a 15 fold better half-life *in vivo* and *in vitro*. The improved half-life in turn translated into lower IC_{50} values *in vitro* with several cell lines. Treatment with NLV also reduced serum L-Met levels to $\leq$ 5 μM and had a significant ($p < 0.01$) effect on retardation of tumor growth of Lan-1 neuroblastoma xenografts. The mice received a dose of 500 mg/kg and were fed a L-Met-free diet on treatment days to minimize resupply of L-Met. Murine metabolism is much faster than human (*37, 57, 64*) so L-Met resupply from the diet can be expected to play a less significant role in the clinic. Nonetheless, the dose required is impractically high and

would pose a challenge in both formulation and cost as a therapeutic. We therefore set out to improve kinetics by additional engineering and set a benchmark of 10 fold higher k_{cat}/K_M against L-Met as the target catalytic proficiency activity.

The Ellington group has extensive experience engineering proteins based on phylogenetic analysis. We evaluated this approach in collaboration with Dr. Wayne Lu. Phylogenetic analysis takes advantage of the evolutionary history of two or more paralog enzymes that likely originated from a single ancestral protein. Though these paralogs may have evolved different substrate specificities, we expect them to have similar protein folds, defined amino acid conservations, and notable residue differences at key positions across sub-families (*104-106*). The human CGL shares 61% amino acid similarity and a high degree of structural homology with the *P. putida* bacterial MGL (Chapter 2). MGL and CGL both belong to the γ-family of pyridoxal phosphate (PLP) dependent enzymes and can be assumed to have shared an ancestor in their evolutionary history. We aligned the sequences of a set of both eukaryotic cystathionine-γ-lyases and bacterial methionine-γ-lyases from a variety of organisms. As shown in Figure 1, residues can fall into four different categories in the alignment: conserved across both sub-families shown in the phylogenetic tree, not conserved, conserved within each sub-family but different between them, and conserved within just one sub-family or the other. Conservation across all enzymes at a given position identifies that residue as necessary for structure or for general γ-lyase reaction activity. Alignment categories 2-4 in Figure 1 identify residues

that are specific to L-Met or cystathionine activity and represent an opportunity for targeted mutagenesis.

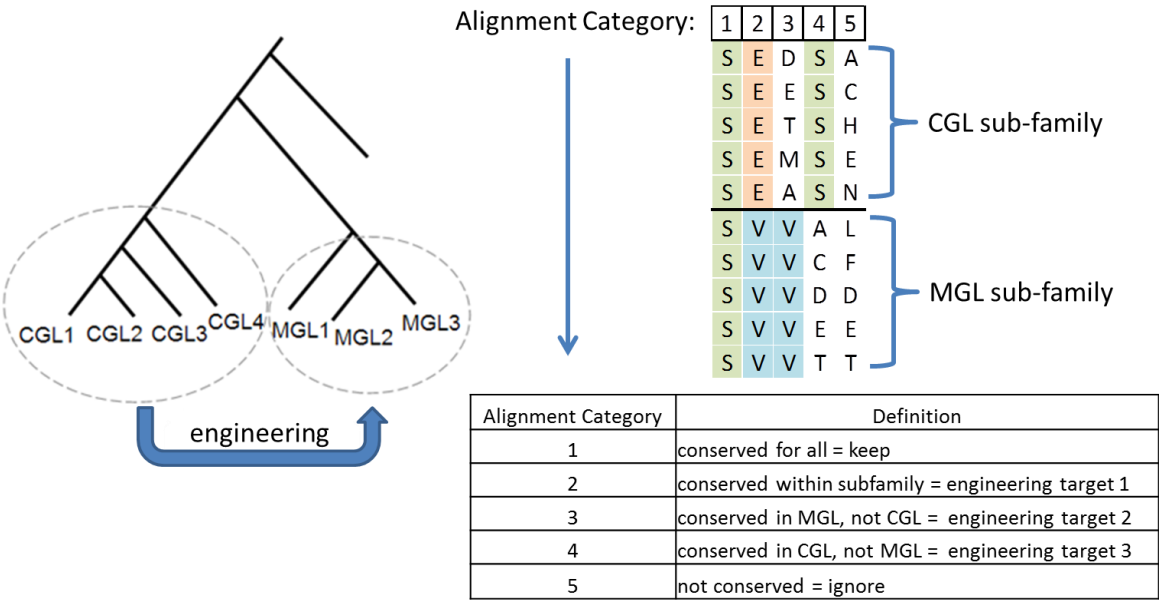

Alignment Category	Definition
1	conserved for all = keep
2	conserved within subfamily = engineering target 1
3	conserved in MGL, not CGL = engineering target 2
4	conserved in CGL, not MGL = engineering target 3
5	not conserved = ignore

Figure 1: Overview of phylogenetic analysis based on the assumption that paralog enzymes derive from the same ancestral protein; definitions of 5 possible cases of alignment.

3.2.2 Experimental Approach

The application of phylogenetic analysis to the engineering of a human L-Met-degrading enzyme consisted of four phases. In the first, a proof of concept alignment of the active site-associated C-terminal domain of the enzymes identified 11 target residues of interest. These were of the type defined as "2" in Figure 1: residues that were conserved within each sub-family yet different between them. Such differences likely

govern substrate specificity, making these positions an obvious first choice for mutagenesis. Individual clones with each respective mutation were generated by substituting the MGL residue at each position and screened by the 96 well plate method discussed in Chapter 2 and in the Methods section. Although variants were found with greater than NLV baseline activity, this simplified method of screening did not take into account potential cooperative interactions between different mutations.

To account for cooperation between residues, the second phase in the protein engineering campaign consisted of the construction of a combinatorial library on top of the NLV variant by overlap extension PCR. Each residue position was allowed to be occupied by either the wild type CGL amino acid or the MGL consensus substitution. The identity of the residues was limited to these two options in order to keep the library size small enough to be screened by hand (2^{11} = 2048 possible variants vs. 20^{11} variants in the case of a full saturation mutagenesis library). This library was screened by the 96 well plate method described previously. "Winners" from the screen were sequenced, re-transformed, expressed, purified, and tested for kinetic activity against L-Met.

In the third phase of engineering, the scope of the alignment was extended to encompass the entire sequence as well as to include the identification of residues falling into classes 2, 3 and 4 as defined in Figure 1. This resulted in 20 additional positions identified and a larger library constructed and screened by the same method as in phase I.

Finally, the fourth phase of engineering involved revisiting the previously mutated 59 and 119 positions by the same method of analysis. In the initial stages of this

project N59, L119, and V339 were selected as conferring the best L-Met degrading activity to the enzyme, but were chosen within the context of wild-type residues everywhere else in the active site. Given the changes in the active site environment caused by additional mutations, we investigated whether altering residues at these positions may enhance activity further. We generated variants with point mutations to the MGL equivalent residue at each position (I59, A119, V339 remained unchanged) and measured their Michaelis-Menten kinetics against L-Met.

3.3 RESULTS

3.2.1 Phase I: Proof of Concept

The 11 positions initially determined to be conserved within each sub-family but different between them are presented in Figure 2. Variants with the mutations T311G and I353S were identified individually for their improved activity and were subsequently combined to yield a variant with 2.3 fold improved activity against L-Met as compared to NLV (Table 1). In the cases of all three variants (T311G, I353S, and T311G + I353S) the improvement in k_{cat}/K_M stemmed from a dramatic decrease in K_M. The magnitude of k_{cat} was reduced as well, but that reduction was insufficient to negate the K_M effect. As a proof of concept experiment, this approach confirmed phylogenetic analysis as a powerful tool for further enzyme optimization.

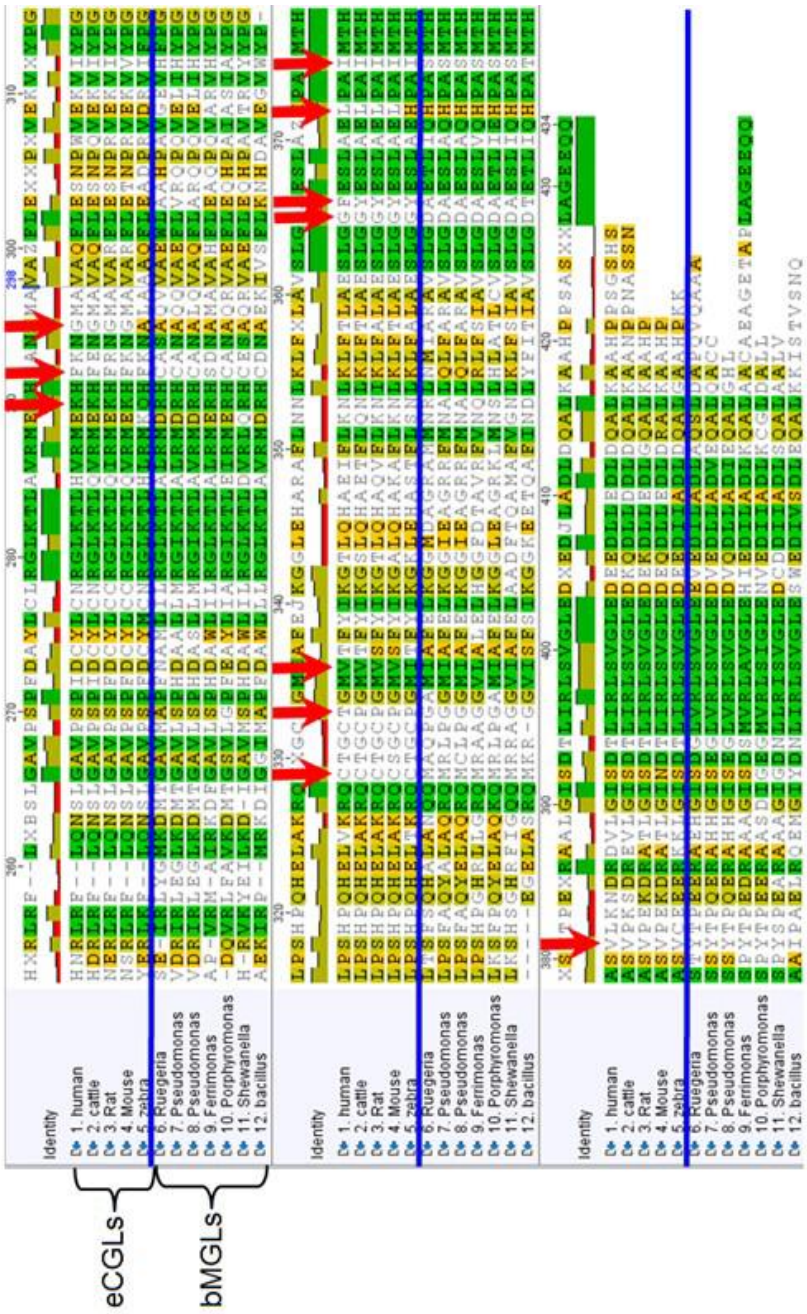

Figure 2: (W. Lu) Alignment used to identify the 11 critical positions for the proof of concept library (red arrows). All meet Alignment Condition 2 as defined by Figure 1.

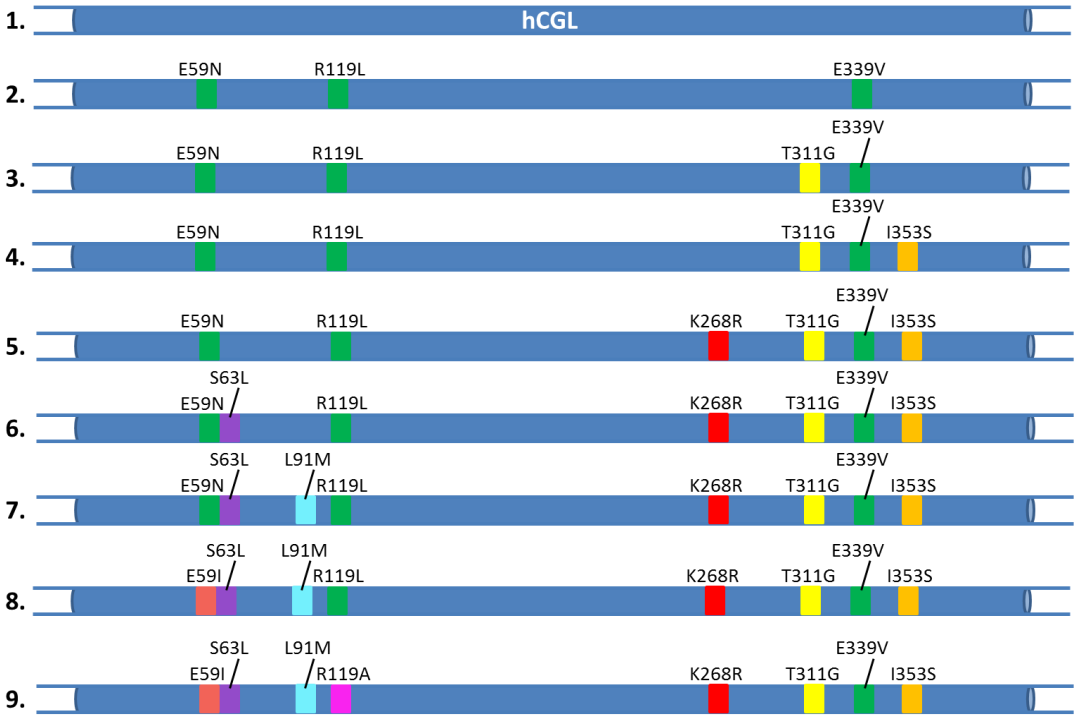

Figure 3: Identification of Variants 1-9 and their respective mutations.

Substrate:	**L-Methionine**		
Variant	k_{cat} (s^{-1})	K_M (mM)	k_{cat}/K_M ($s^{-1}mM^{-1}$)
pMGL	20 ± 0.4	0.34 ± 0.03	**59 ± 6**
1. hCGL	nd	nd	**nd**
2. NLV	7.9 ± 0.4	14 ± 1.5	**0.56 ± 0.07**
3. NLGV	3.1 ± 0.01	2.8 ± 0.1	**1.1 ± 0.1**
NLVS	4.4 ± 0.1	4.6 ± 0.2	**0.96 ± 0.06**
4. NLGVS	3.0 ± 0.1	2.4 ± 0.2	**1.3 ± 0.1**

Table 1: Kinetic parameters for reaction with L-Met for Variants 1, 2, 3 (as defined by Figure 3) and NLVS (Variant 1 NLV + I353S)

Substrate:	L-Methionine			L-Cystathionine		
Variant	k_{cat} (s^{-1})	K_M (mM)	k_{cat}/K_M ($s^{-1}mM^{-1}$)	k_{cat} (s^{-1})	K_M (mM)	k_{cat}/K_M ($s^{-1}mM^{-1}$)
pMGL	20 ± 0.4	0.34 ± 0.03	**59 ± 6**	nd	nd	**nd**
1. hCGL	nd	nd	**nd**	3.7 ± 0.2	0.4 ± 0.07	**9 ± 2**
2. NLV	7.9 ± 0.4	14 ± 1.5	**0.56 ± 0.07**	1.5 ± 0.05	0.71 ± 0.07	**2.2 ± 0.3**
3. NLGV	3.1 ± 0.01	2.8 ± 0.1	**1.1 ± 0.1**	1.7 ± 0.04	0.63 ± 0.05	**2.7 ± 0.3**
4. NLGVS	3.0 ± 0.1	2.4 ± 0.2	**1.3 ± 0.1**	1.8 ± 0.03	0.80 ± 0.04	**2.2 ± 0.1**
5. NLRGVS	6.3 ± 0.2	3.5 ± 0.3	**1.8 ± 0.2**	1.6 ± 0.02	0.77 ± 0.03	**2.1 ± 0.1**
6. NLLRGVS	9.0 ± 0.2	4.6 ± 0.4	**2.0 ± 0.2**	0.77 ± 0.02	1.3 ± 0.1	**0.61 ± 0.06**
7. NLMLRGVS	7.9 ± 0.2	2.2 ± 0.1	**3.6 ± 0.3**	1.1 ± 0.04	1.0 ± 0.1	**1.1 ± 0.2**
8. ILMLRGVS	7.3 ± 0.1	1.6 ± 0.1	**4.5 ± 0.3**	0.51 ± 0.03	0.74 ± 0.15	**0.69 ± 0.18**
9. ILMARGVS	9.8 ± 0.2	1.8 ± 0.1	**5.3 ± 0.5**	0.70 ± 0.03	1.2 ± 0.2	**0.59 ± 0.11**

Table 2: Kinetic parameters for Variants 1-9 with L-Met and cystathionine.

3.2.2 Phase II: Combinatorial Library

The 11 positions which were found to be occupied by two different amino acids in the phylogenetic analysis were introduced in a combinatorial fashion to construct a library to investigate cooperative interactions. After screening ~4000 clones, 34 were identified as having a detectable signal in the screen, the top 10 of which were chosen for subsequent purification and characterization. From these, one variant was selected for the best kinetic parameters. This variant contained both the T311G and I353S mutations identified previously as well as the additional mutation K268R (variant 5 in Table 2).

Interestingly, the small improvement in k_{cat}/K_M for this enzyme came exclusively from a doubling of $k_{cat,}$ with this variant having a slightly worse K_M than the previous.

3.2.3 Phase III: Comprehensive Alignment

The new NLRGVS variant served as the starting point for the next round of engineering. A comprehensive phylogenetic analysis was performed on the full-length eukaryotic CGLs (16 enzymes), bacterial MGLs (18), as well as a collection of bacterial CGL enzymes (8). Sixty seven positions were initially identified as potential mutagenesis targets and were further narrowed down by proximity to the active site to reduce the theoretical library to a more manageable size. The twenty positions ultimately chosen were: Q49F, P52A, G53E, H55G, S63L, L91M, A92G, T94S,D112T, G116C, W155Y, T160A, S218G, M222A, Q240K, N241D, O247L, Y317E, E349Q, and A357S. In order to rule out expression effects in a 96-well plate screen, these variants were generated individually and their respective enzymes expressed and directly purified by Ni-NTA chromatography. At low substrate concentrations, Michaelis-Menten kinetics are linear and the slope of a line through the data should be equivalent to the value of k_{cat}/K_M for the enzyme. Therefore, these variants were tested at a range of low L-Met concentrations and compared. Three of these mutations resulted in improved activity: S63L, L91M and Y317E. These three variants were further subjected to detailed kinetic analysis to determine their k_{cat} and K_M values against L-Met and Y317E was discarded as having worse kinetics. In the case of S63L (NLLRGVS), the mutation slightly elevated K_M but

significantly improved k_{cat} while the L91M mutation (NMLRGVS) improved K_M at the expense of k_{cat} (Table 3). When these two mutations were combined, the resulting variant (NLMLRGVS) exhibited the benefits of both a lowered K_M and an increased k_{cat}, resulting in an overall improvement of 6.4 fold in k_{cat}/K_M over NLV.

Substrate:	**L-Methionine**		
Variant	k_{cat} (s^{-1})	K_M (mM)	k_{cat}/K_M ($s^{-1}mM^{-1}$)
pMGL	20 ± 0.4	0.34 ± 0.03	**59 ± 6**
1. hCGL	nd	nd	**nd**
5. NLRGVS	6.3 ± 0.2	3.5 ± 0.3	**1.8 ± 0.2**
6. NLLRGVS	9.0 ± 0.2	4.6 ± 0.4	**2.0 ± 0.2**
NMLRGVS	5.8 ± 0.1	2.8 ± 0.2	**2.1 ± 0.3**
7. NLMLRGVS	7.9 ± 0.2	2.2 ± 0.1	**3.6 ± 0.2**

Table 3: Kinetics parameters with L-Met of Variants 1, 5, 6, 7 and NMLRGVS (Variant 5 NLRGVS + L91M)

3.2.4 Phase IV: Reevaluating Previous Residues

In the initial stages of this project N59, L119, and V339 were selected for the best L-Met degrading activity, but were chosen within the context of wild-type residues elsewhere in the active site. Given the changes to the active site environment introduced by additional mutations, we questioned whether different residues at these positions would yield greater activity. Sequence alignment defined the most common equivalent

MGL residue at the 59, 119, and 339 positions (Figure 4). As evident from this alignment, the 339 position residue in NLV had already been optimized. Isoleucine and alanine at positions 59 and 119, respectively, were significantly different from the asparagine and leucine previously identified in our selection, motivating the investigation of these variants. We found that these two mutations did improve k_{cat}/K_M to a small degree individually and significantly improved it when combined (Table 4). The asparagine to isoleucine substitution in particular served to lower the K_M of the enzyme by ~20%. The resulting Variant 9 had a k_{cat}/K_M of 5.3 ± 0.5 $s^{-1}mM^{-1}$, 10 fold greater than the first generation NLV enzyme (Table 2).

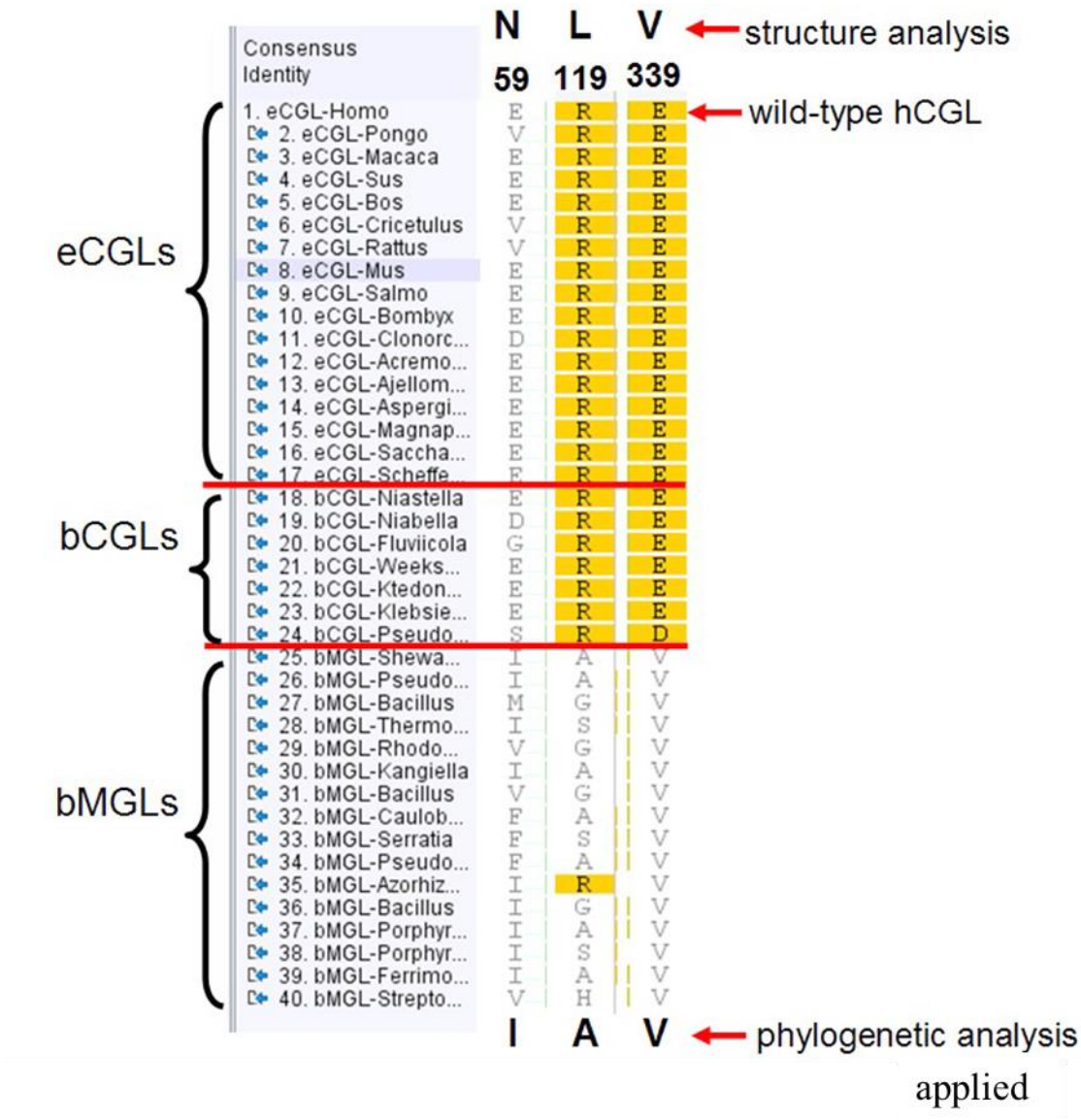

Figure 4: (W. Lu) Sequence alignment at the three positions previously identified by structural alignment and mutated in Variant 1 NLV (59, 119, 339) used to identify target residues. Bacterial CGL sequences were included to identify and rule out bacteria-specific (rather than enzyme-specific) residues.

3.2.5 Evaluating Mutation Requirement

A human enzyme was initially chosen as a scaffold for engineering due to its low immunogenicity risk. Through engineering a variant that met kinetic criteria for use, we had introduced a total of eight mutations to the parent enzyme. With each additional non-human residue we run the risk of generating immunogenic epitopes within the protein. We wanted to investigate whether we could trade an insignificant drop in activity for a significant reduction in the number of mutations. We therefore generated two revertant variants based on Variant 7 (Figure 3): M91L and R268K. Michaelis-Menten steady state kinetics confirmed that both mutations are required for activity within the desired range (Figure 5).

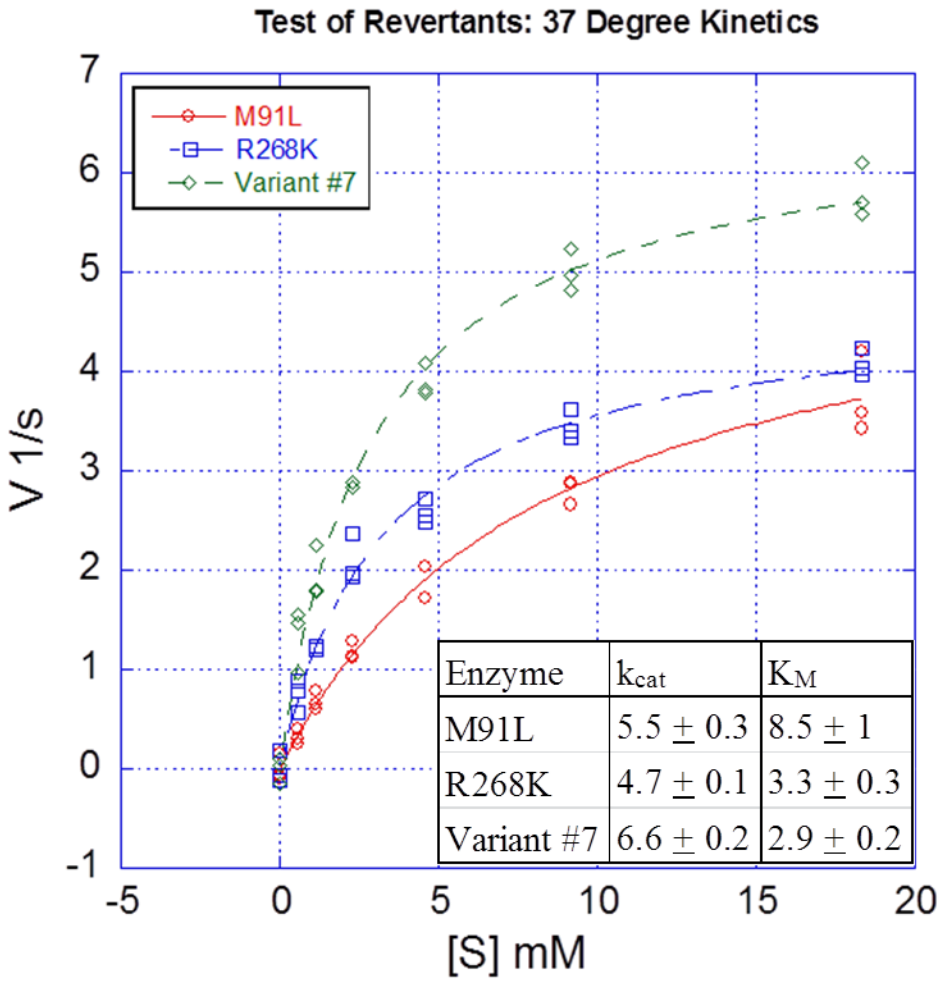

Figure 5: Michaelis-Menten kinetics for Variant 7 and its revertants at positions 91 and 268. *Note: Kinetic parameters for Variant 7 differ slightly from those previously reported in Table 2 due to experimental variability. Each set of kinetic values compared for best variant identification were determined at the same time to mitigate this effect.

Substrate:	L-Methionine		
Variant	k_{cat} (s^{-1})	K_M (mM)	k_{cat}/K_M ($s^{-1}mM^{-1}$)
pMGL	20 ± 0.4	0.34 ± 0.03	**59 ± 6**
1. hCGL	nd	nd	**nd**
7. NLMLRGVS	7.9 ± 0.2	2.2 ± 0.1	**3.6 ± 0.3**
8. ILMLRGVS	7.3 ± 0.1	1.6 ± 0.1	**4.5 ± 0.3**
NLMARGVS	8.2 ± 0.2	2.2 ± 0.3	**3.7 ± 0.5**
9. ILMARGVS	9.8 ± 0.2	1.8 ± 0.1	**5.3 ± 0.5**

Table 4: Kinetics parameters with L-Met of Variants 1, 7, 8, 9 and NLMARGVS (Variant 7 NLRGVS + L119A)

3.2.6 Enzyme Selectivity/Promiscuity

In their native form, both CGL and MGL have high activity against their "target substrates"- cystathionine and L-Met, respectively. Although CGL catalyzes the gamma elimination of cystathionine and is capable of accepting the smaller cysteine and homocysteine as substrates, it shows no detectable activity with L-Met (Chapter 2). MGL, likewise, is incapable of accepting cystathionine as a substrate. An ideal engineered enzyme therapeutic should degrade L-Met with high selectivity in relation to cystathionine to mitigate any physiological side effects during treatment. We tested the Michaelis-Menten kinetics of a selection of variants against cystathionine (Table 2 and Figure 6). Mutagenesis to alter substrate specificity initially yielded highly promiscuous variants, but the introduction of almost every additional mutation improved the L-Met to

cystathionine selectivity, as defined by the ratio of their k_{cat}/K_M values (inset Figure 6). Particularly, with the addition of the S63L mutation (Variant 6) the cystathionine lyase activity fell by 70% and the selectivity for L-Met over cystathionine increased by > 3 fold. Variant 9 ultimately had a 9 fold higher selectivity for L-L-Met over L-cystathionine. For comparison, the first generation Variant 1 NLV mutant only showed a selectivity of 0.25 resulting in an increase in selectivity of 36 fold through engineering.

Two other substrates known to be degraded by both CGL and MGL are cysteine and homocysteine (structures in Chapter 2). We measured the Michaelis-Menten kinetics for both substrates with the same collection of variants as above (Table 6) and found that the activity tracked with the evolution from a wild-type cystathionine-γ-lyase to an enzyme with methionine--γ-lyase character and a higher rate of turnover of both of these amino acids. Notably, Variant 9 k_{cat}/K_M for cysteine is ultimately higher than that of the bacterial enzyme.

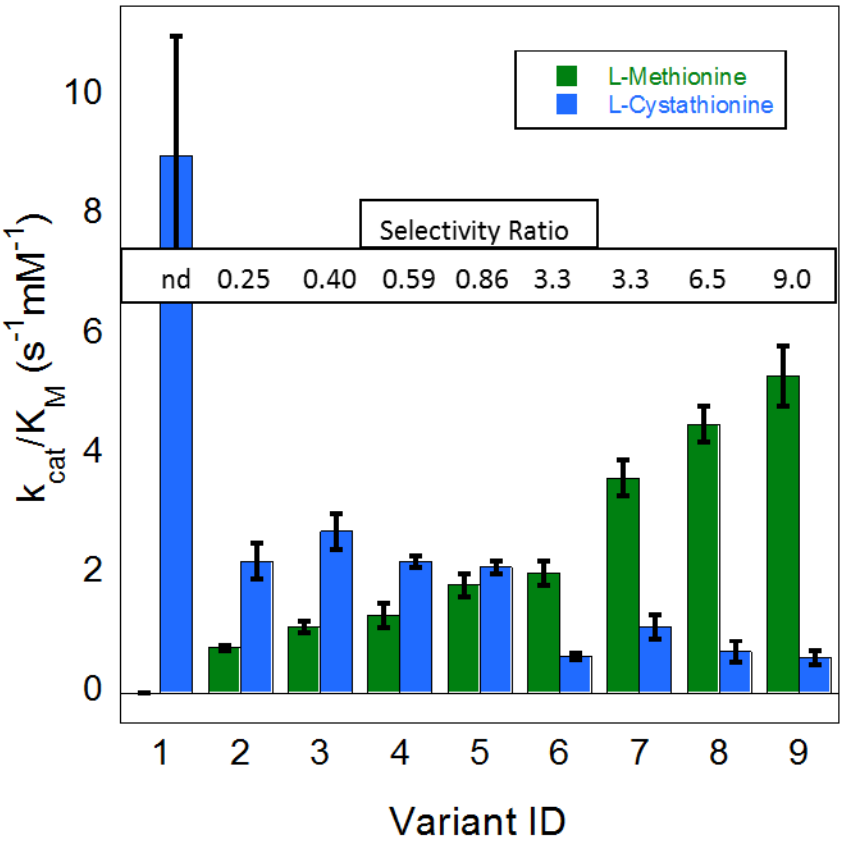

Figure 6: Activity of each significant variant with and cystathionine as defined by k_{cat}/K_M. Inset: selectivity ratio obtained by dividing the k_{cat}/K_M of L-Met activity with that of cystathionine for each variant.

Substrate:	L-Cysteine			DL-Homocysteine		
Variant	k_{cat} (s^{-1})	K_M (mM)	k_{cat}/K_M ($s^{-1}mM^{-1}$)	k_{cat} (s^{-1})	K_M (mM)	k_{cat}/K_M ($s^{-1}mM^{-1}$)
pMGL	6.5 ± 0.2	1.1 ± 0.1	**6 ± 0.7**	86 ± 3	2.9 ± 0.2	**30 ± 3**
1. hCGL	0.13 ± 0.01	0.58 ± 0.15	**0.22 ± 0.07**	0.35 ± 0.02	1.7 ± 0.3	**0.21 ± 0.04**
2. NLV	1.8 ± 0.03	0.68 ± 0.03	**2.7 ± 0.2**	7.2 ± 0.2	0.91 ± 0.11	**8 ± 1**
3. NLGV	2.5 ± 0.05	0.36 ± 0.03	**6.6 ± 0.7**	4.2 ± 0.1	0.53 ± 0.05	**8.1 ± 0.9**
4. NLGVS	2.1 ± 0.04	0.26 ± 0.02	**8.2 ± 0.7**	3.0 ± 0.9	0.49 ± 0.05	**6.1 ± 0.8**
5. NLRGVS	2.5 ± 0.06	0.34 ± 0.03	**7.3 ± 0.8**	3.0 ± 0.1	0.51 ± 0.04	**5.8 ± 0.7**
6. NLLRGVS	2.2 ± 0.03	0.49 ± 0.03	**4.4 ± 0.3**	6.8 ± 0.1	1.1 ± 0.04	**6.3 ± 0.3**
7. NLMLRGVS	2.6 ± 0.04	0.36 ± 0.02	**7.2 ± 0.6**	7.6 ± 0.1	1.0 ± 0.1	**7.4 ± 0.6**
8. ILMLRGVS	3.1 ± 0.1	0.35 ± 0.02	**8.9 ± 0.7**	7.0 ± 0.1	0.60 ± 0.04	**12 ± 1**
9. ILMARGVS	3.6 ± 0.04	0.43 ± 0.02	**8.5 ± 0.4**	10 ± 0.1	0.85 ± 0.03	**12 ± 1**

Table 6: Kinetic parameters for Variants 1-9 with cysteine and homocysteine.

3.2.7 Structure

In order to better understand the effects of specific mutations, we collaborated with the Zhang crystallography group to solve the structure of Variant 9. Important features of this structure aligned with the wild-type CGL (PDB file: 3COG) are presented in detail in Figures 7-11. The overall quaternary and tertiary structures of the engineered variant align with the parent enzyme. As discussed in Chapter 2, the introduction of N59, L119, and V339 residue mutations increases hydrophobicity of the active site substrate-binding pocket thus enabling the more hydrophobic L-Met to be a substrate for the mutant enzyme. A reduction in the number of charged side chains around the

hydrophobic methyl group of are expected to further improve L-Met docking into the correct orientation for catalytic gamma elimination, enhance the reaction rate at the exclusion of the charged cystathionine substrate, and improve selectivity (Chapter 2). The Variant 9 mutations N59I and L119A are shown in Figures 7a and 7b, confirming the orientation of these new residues and their proximity to the distal end of the substrate analog.

The mutations identified in the engineering campaign described in this chapter fall into three categories: 1st shell active site residues that are close enough to the substrate to directly interact with it (E/N59I, S63L, L91M, R/L119A, E339V), 2nd shell residues several angstroms further away from the active site (I353S), and other residues distant from the active site (T311G, K268R).

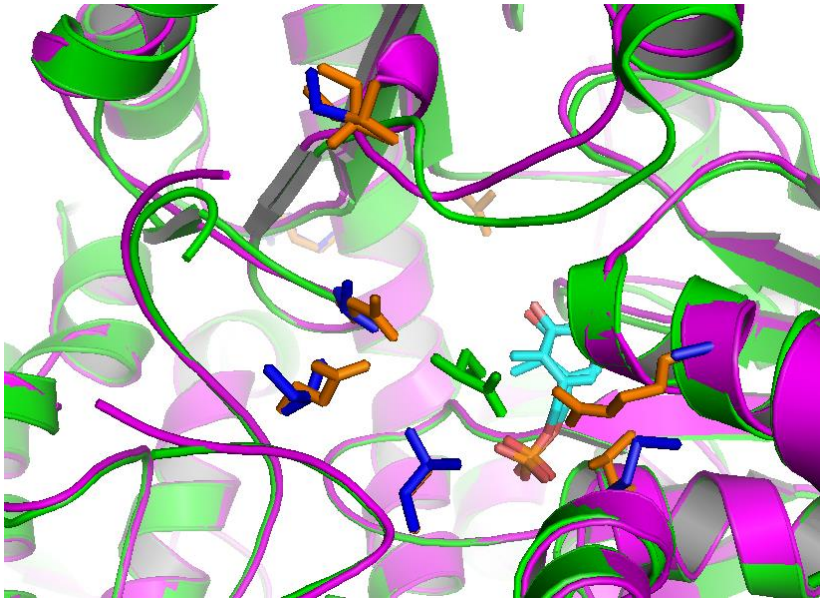

Figure 7a: Alignment of the active site of the solved structure of Variant 9 and CGL with substrate analog bound (PDB: 3COG).

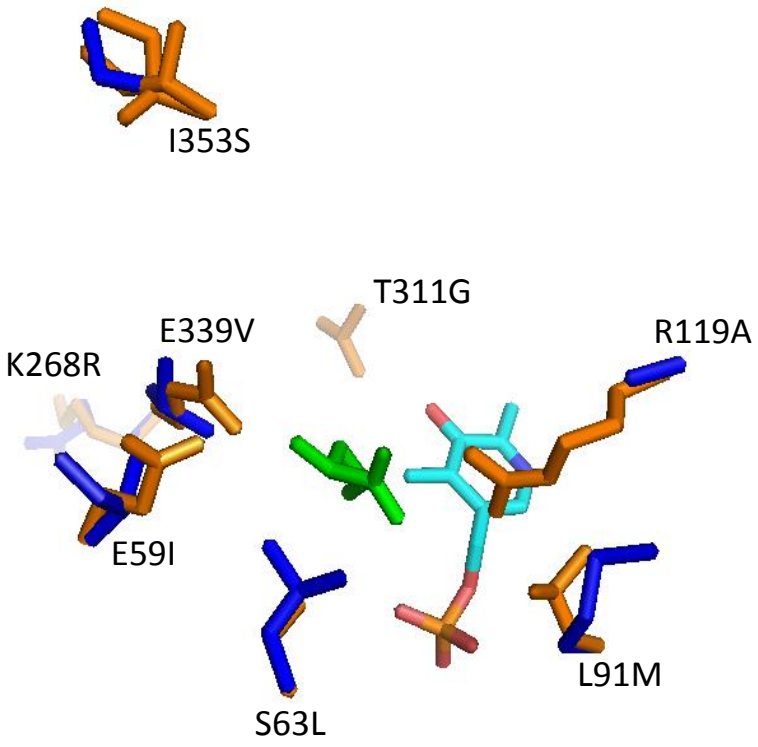

Figure 7b: Closer view of mutations around the active site.

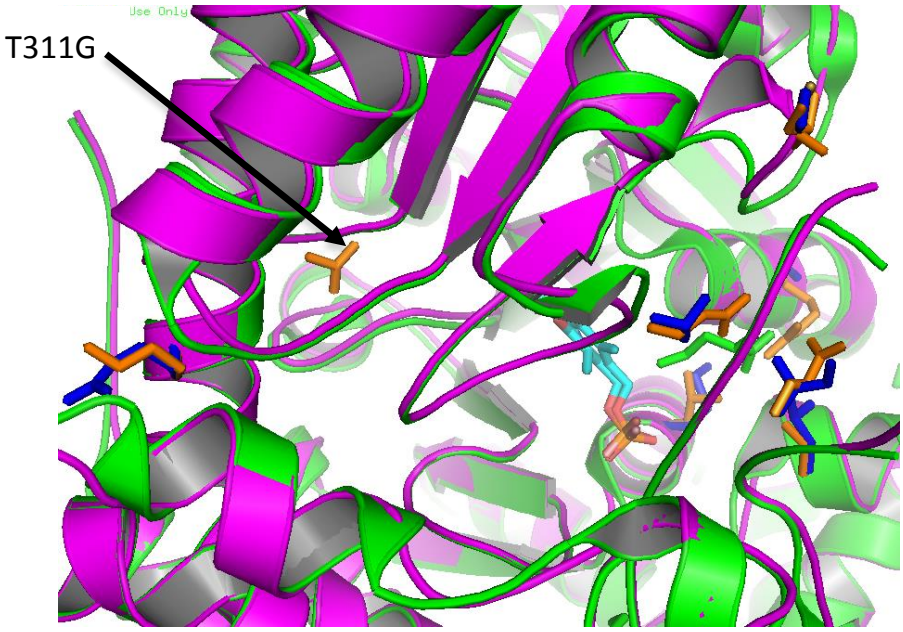

Figure 8: Additional view of mutation T311G showing its distance from the active site.

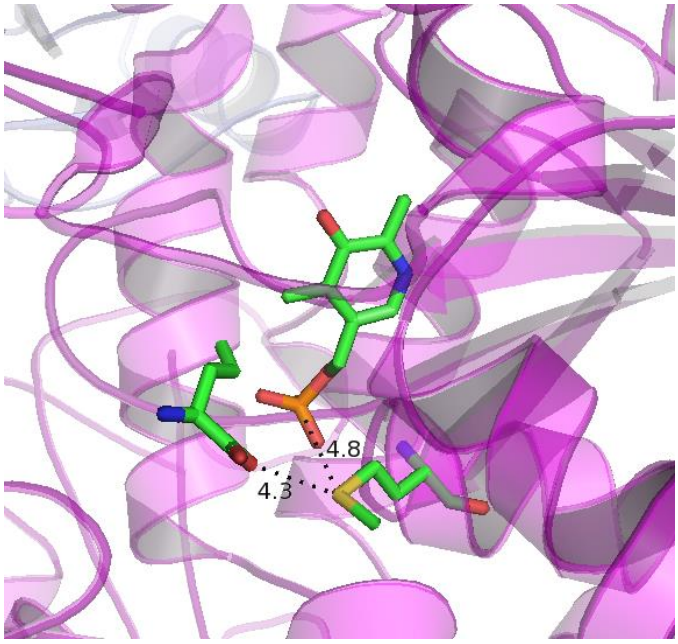

Figure 9: Variant 9 structure details of the L91M mutation and proximity of the sulfur to both PLP and the substrate analog.

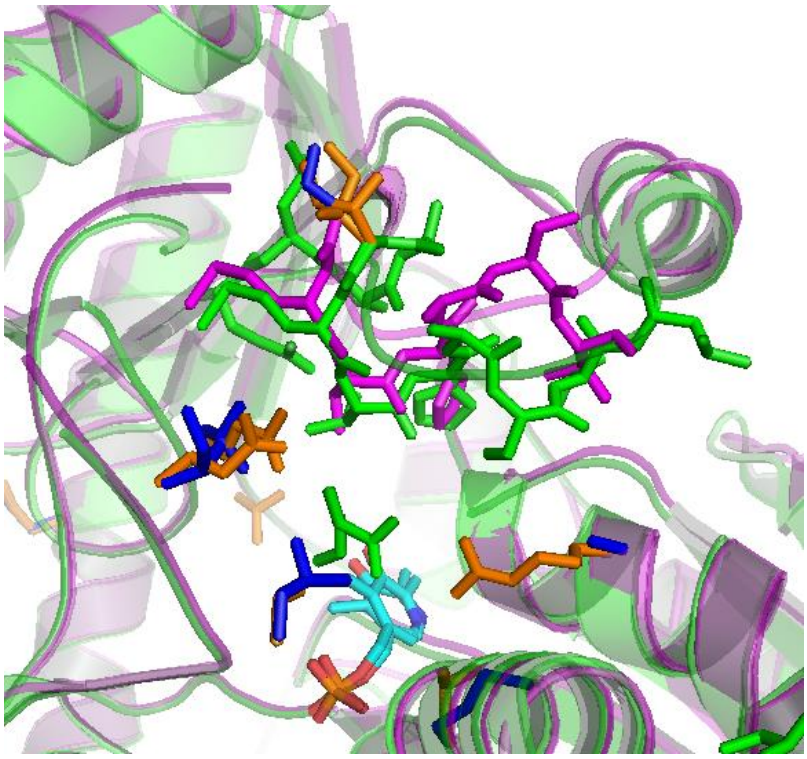

Figure 10: Alignment of CGL and Variant 9; I353S mutation in the context of the flexible loop showing conformational change.

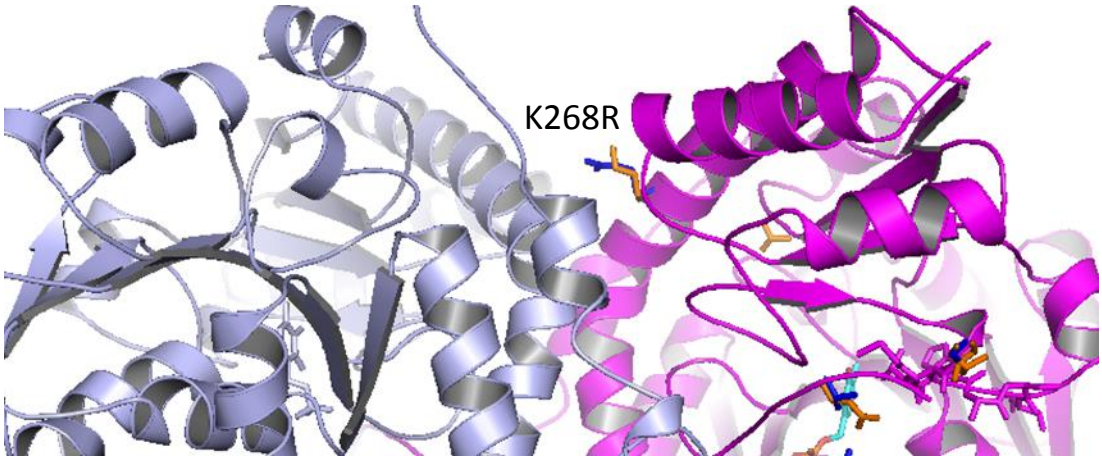

Figure 11a: General view of the K268R mutation positioned directly between two Variant 9 monomers.

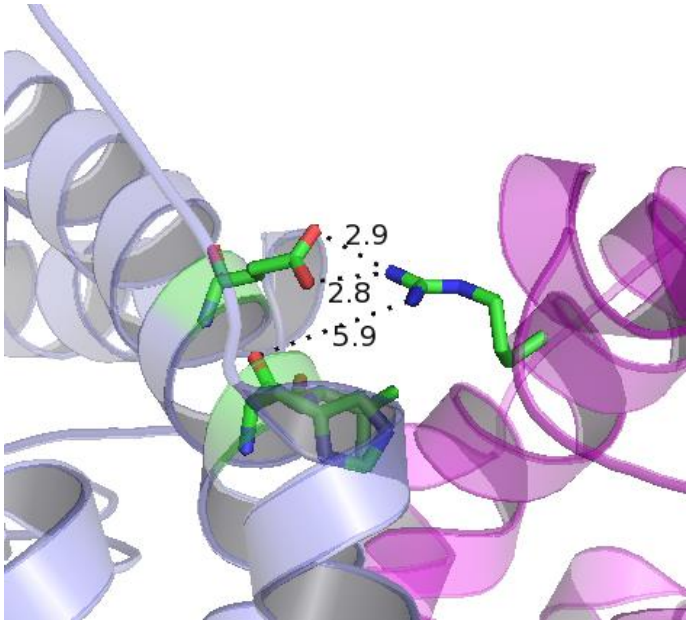

Figure 11b: Variant 9 structure details of the K268R mutation, its proximity to residues of the neighboring monomer chain, and its potential for hydrogen bonding.

3.2.8 Structural Stability

In order to ascertain that the engineering of CGL to increase catalytic activity towards L-Met did not negatively impact the structural stability of the enzyme, we determined the Tm of the most active variant isolated from the engineering campaign (Variant 9) by Circular Dichroism Spectroscopy and compared it to that of NLV (Figure 12). Variant 9 had a Tm that was 8 degrees higher than that of NLV (81°C vs. 73°C). We note that the K268R mutation introduced a guanidinium group on an extended side chain at this position that is in the correct orientation to hydrogen bond with the E267 carboxylic acid functional group and the backbone carbonyl oxygens of H263 and V264

on the neighboring chain (Figure 11b). Arginine has been previously reported to form more stable surface ionic interactions than lysine due to its capability to form a larger number of these interactions as well as its higher pKa (*107*). We therefore hypothesize that the K268R mutation and the more stable salt bridge that results increase the overall structural stability and Tm of the tetrameric enzyme.

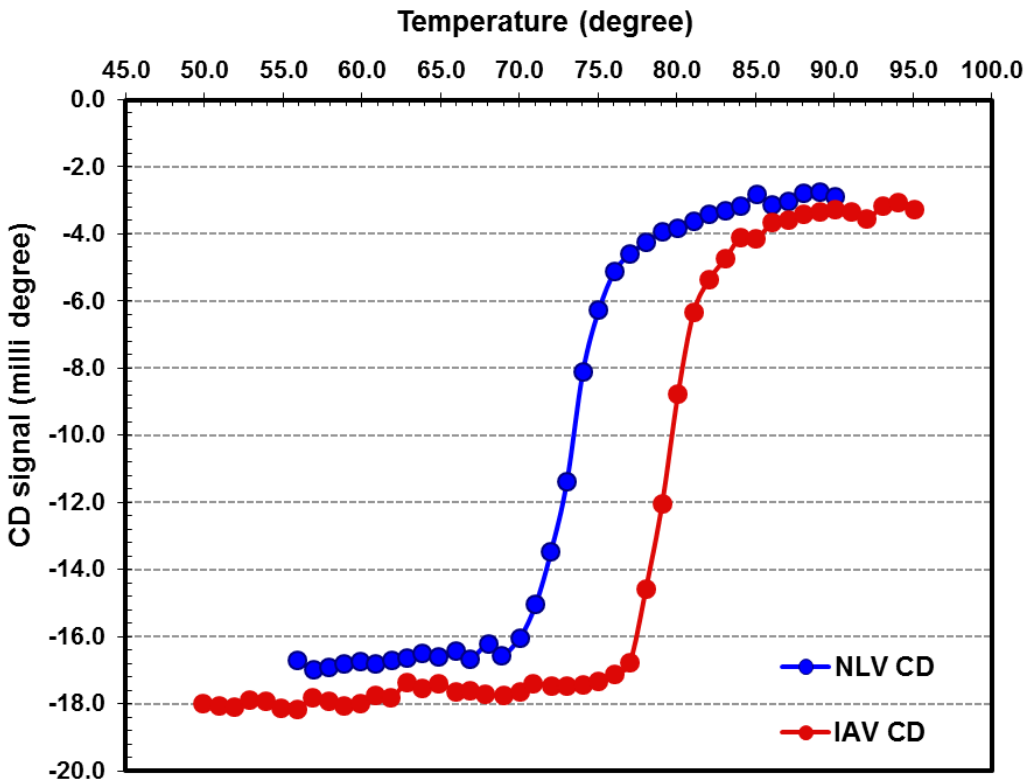

Figure 12: Melting curves of NLV and Variant 9 (labeled IAV). The calculated Tms were: NLV 73°C, Variant 9 81°C.

3.2.9 Serum Inactivation

We evaluated whether the additional mutations in Variants 7, 8, and 9 relative to the NLV variant reported in Chapter 2 impact the rate at which the enzyme become inactivated in the presence of serum. We have previously shown that supplementation of additional PLP cofactor in the pooled serum/enzyme incubation significantly extended the half-life of the NLV variant. In the first step of the gamma elimination reaction, the PLP cofactor forms an external Shiff base with the substrate. Without a covalent bond to the enzyme, the PLP-substrate and PLP-intermediate complexes have some probability of diffusing out of the active site. Since serum contains significant concentrations of potential substrates for the enzyme, we hypothesize that an important mechanism of inactivation in serum is the loss of the externally bound cofactor from the active site. Additionally, serum albumin has been implicated in binding PLP and inactivating the bacterial MGL enzyme (*108*). It stands to reason that mutagenesis of residues around the PLP cofactor within the active site may have an effect on the probability of its escape. We have previously shown that NLV-PEG half-life in the mouse was effectively the same as in pooled human serum (Chapter 2). Thus the deactivation stability of CGL variants in serum is likely to correlate well with stability *in vivo*. It was important to modify the enzyme with methoxy PEG succinimidyl carboxymethyl ester for *in vivo* experiments to increase the hydrodynamic radius and reduce renal clearance of the drug (described in the Pharmacological Optimization section of Chapter 2). We had found that unmodified enzyme had a much longer half-life and could not be used as a

physiologically representative model for the rate of inactivation *in vivo*. Consequently, purified enzyme Variants 7, 8, and 9 were modified by PEG, added to pooled human serum at 37°C, and tested for activity at various time points. The calculated half-lives were compared to previously determined $t_{1/2}$ values for NLV and NLV-PEG (Figure 13 and Table 7). The apparent half-life of the variants tested was > 100 hours, significantly longer than the 30 hours seen previously with NLVPEG.

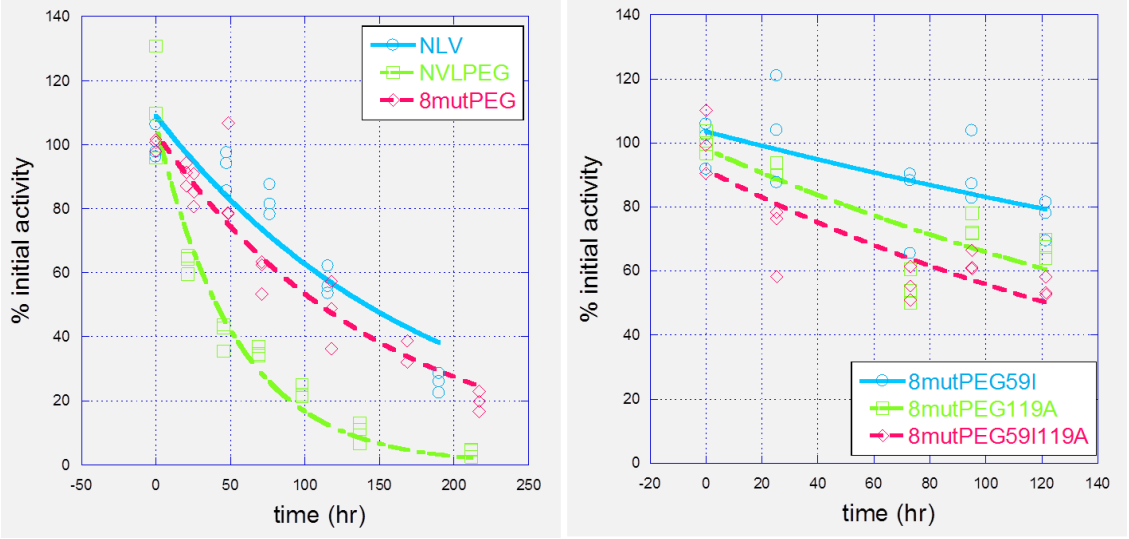

Figure 13: Serum inactivation of Variant 1 NLV with and without conjugation to PEG, PEG-modified Variant 7 (8mutPEG), Variant 7 + N59I (8mutPEG59I), Variant 7 + L119A (8mutPEG119A), and Variant 9 (8mutPEG59I119A) as measured by activity against L-Met and 100% activity defined as the rate at t = 0.

Enzyme	Half Life (hrs)
NLV	75
NLVPEG	30
8mutPEG (Variant 7)	101
8mutPEG59I119A (Variant 9)	>>100

Table 7: Calculated $t_{1/2}$ values based on fitting the curve to exponential decay equation.

3.2.10 *In Vivo* Pharmacodynamics

In order to test how well the new drug candidates reduced L-Met levels *in vivo*, we performed a small scale PK/PD experiment in mice with PEG modified Variant 7. This experiment was performed before the final phase of engineering and identification of Variants 8 and 9. The animals were dosed once at 50 mg/kg by intraperitoneal (IP) injection at time zero and groups of three mice were sacrificed at 8, 24, and 48 hours each. Throughout the experiment, the animals had access to complete feed. Blood was drawn from each sacrificed mouse and allowed to clot. The serum was then drawn off and filtered through a 3000 Da cutoff membrane. This assures that any enzyme (active or otherwise) present in the sample is separated from the filtered fraction and all possible enzyme L-Met degradation had ceased. The filtered serum was then analyzed for L-Met content by reversed-phase High-Performance Liquid Chromatography. The L-Met

concentrations obtained were compared to the depletion achieved previously with NLVPEG.

The resulting time course for both enzyme injections is compared in Figure 14. The mice previously treated with NLVPEG were also fed a full diet and received one dose of 250 mg/kg of enzyme at time zero, with L-Met levels determined at set times thereafter. At the 8 hour time point, the L-Met levels were an average of 18 μM- much higher than the ≤ 5 μM target level. By 24 hours, L-Met levels had rebounded to approximately 60% of untreated, and by 48 hours had effectively returned to normal. In addition to insufficient degradation of L-Met, an obvious concern was the extremely high dose necessary to achieve even this modest effect.

In vivo efficacy data in Chapter 2 was obtained with still a higher dose of 500 mg/kg with animals maintained on a diet restricted for L-Met, homocysteine, and choline on treatment days (Figure 6b in Chapter 2). At this dose, an average 70 kg human being would have to receive a prodigious 35 grams of enzyme per injection. This is not only impractical to administer but would be prohibitively expensive. This rationale ultimately defined the criteria used in engineering the enzyme further.

Based on the preliminary PD data, Variant 7 has sufficient activity to deplete L-Met to desirably low levels for a useful amount of time. At a dose of only one fifth of the 250 mg/kg tested previously for NLVPEG, the L-Met levels drop to < 5 μM by hour 8, recover to about 15% of untreated at hour 24, and are still only 50% of untreated by 48

hours after injection. Experiments are ongoing to determine if Variant 9 has even better *in vivo* performance.

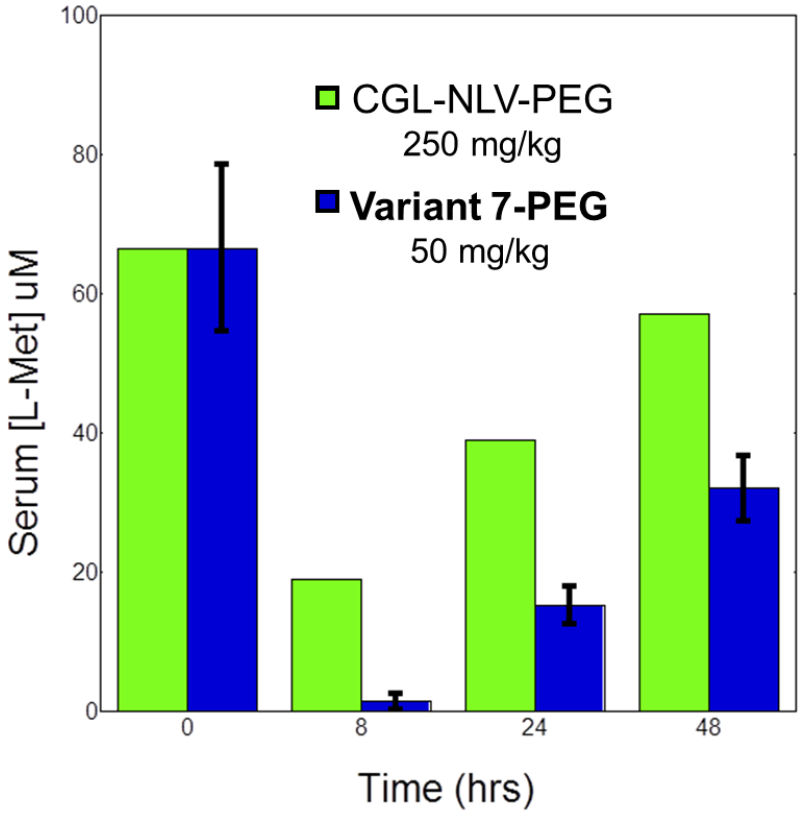

Figure 14: Mouse serum L-Met levels after enzyme treatment at time 0 at the defined doses of CGL-NLV (Variant 2) and Variant 7 as measured by HPLC. The animals were fed a complete diet in both cases.

3.3 Discussion and Summary

Through iterative rounds of phylogenetic analysis, mutagenesis, and selection, we have identified an efficient L-Met-degrading enzyme which, upon administration at a

dose that can be translated to a practical human therapeutic, can reduce serum L-Met to a level that can potentially impact tumor growth. The second generation hMGL enzymes (Variants 7 and 9) developed here display 7-10 fold better L-Met degrading activity than the first generation NLV as well as up to a 36 fold improvement in selectivity over the wild-type substrate cystathionine. We have shown that this enzyme is stable and capable of reducing murine serum L-Met levels to a therapeutically useful range without dietary restriction.

3.3.1 Phylogenetic Analysis

Phylogenetic analysis is a powerful tool to engineer desired characteristics into an enzyme by taking advantage of the observation that during evolution residues that are critical to function are conserved (*104-106*). Since protein paralogs in the same family share a common ancestor, residues that are conserved within their respective sub-families but different between them may point to positions that correspond with enzyme phenotype such as substrate specificity, pH optimum, temperature optimum, etc. (*106, 109-111*). Identifying such positions provides an important route to generating mutations that confer improved or altered protein function.

Phylogeny based mutagenesis and protein engineering offers some important advantages over structure-based mutagenesis . First, many more protein sequences are known than structures currently available. This allows a deeper evaluation at each possible position by permitting the alignment of many more sequences than would be

available for structural analysis. Second, a structure by nature traps an enzyme in one static state (such as bound to inhibitor, substrate or intermediate analog, etc.). Phylogenetic analysis however, can identify residues important in other interactions not observable in the static enzyme, such as those that contribute to protein dynamics. Third, structural analysis is generally limited to a small sphere of residues in the immediate vicinity of the active site. Phylogenetic analysis expands the search to the entire sequence and enables the identification of second shell and even distant positions of importance. Finally, phylogenetic analysis provides an opportunity to substitute residues in a more targeted manner by limiting the mutations to amino acids suggested by the alignment (rather than sampling all 20 amino acids at each position). This allows us to sample multiple positions concurrently and still restrict the library to a manageable size, directly probing possible synergistic effects between positions.

Starting with a scaffold of CGL with three mutations (NLV) we applied phylogenetic analysis as a guide to iterative mutagenesis and screening to generate a more active enzyme. The k_{cat}/K_M of Variant 9 was 5.3 $s^{-1}mM^{-1}$ compared to a k_{cat}/K_M of 0.56 $s^{-1}mM^{-1}$ displayed by the first human methionine-γ-lyase, i.e. the CGL-NLV variant of Chapter 2. This second generation variant satisfied the protein engineering goal of 10 fold improvement in k_{cat}/K_M relative to the NLV variant. Notably, Variant 9 displays a slight increase in k_{cat} (9.8 s^{-1} Variant 9 vs. 7.9 s^{-1} NLV), and thus the main consequence of the protein engineering campaign was to achieve a marked decrease in K_M (1.8 mM Variant 9 vs. 14 mM NLV). The cystathionine degrading activity of the enzyme was also

significantly reduced resulting in a 36 fold improvement in enzyme specificity for L-Met over the wild-type substrate.

These results underscore the power of phylogenetic analysis as an engineering technique and the advantages of what is effectively iterative mutagenesis and screening by evolution to arrive at residues suited for the chemistry of interest. Evolution is not a process with a definitive endpoint, nor can we assume that the enzymes in each sub-family have evolved to their greatest specific substrate degrading potential (particularly since their selection pressures likely involve numerous other factors). Therefore, additional engineering and enzyme improvement should be possible, especially since the MGL residues grafted into CGL now exist in the context of a different environment.

3.3.2 Active Site Residues

It is possible to infer possible explanations for the activity and specificity of a number of the beneficial amino acid substitutions identified in the protein engineering campaign by examination of the alignment of the crystal structures of CGL and Variant 9. For example, the S63L mutation is approximately 4 Å away from the distal end of the substrate and the replacement of the polar serine with the very hydrophobic leucine renders the active site more hydrophobic and favors the binding of L-Met over cystathionine (Figure 7b, see also Chapter 2). The introduction of the leucine at position 63 results in a dramatic reduction of k_{cat}/K_M with cystathionine (from 2.1 $s^{-1}mM^{-1}$ to 0.61 $s^{-1}mM^{-1}$) and an increase of the selectivity of the enzyme for target vs. wild-type substrate

from 0.86 to 3.3. Up to this point in engineering Variants 2-5 the activity with the wild-type substrate had remained relatively unchanged, even as the k_{cat}/K_M for L-Met incrementally improved. Therefore, the addition of just one hydrophobic residue in this section of the binding pocket appears to result in markedly improved exclusion of the highly polar cystathionine.

While the S63L mutation alters the specificity of the enzyme by affecting the relative partitioning of the substrates into the active site, the introduction of L91M corresponds to an increase in activity with all amino acids tested (L-Met, cystathionine, cysteine, and homocysteine). It appears that this mutation increases the enzyme rate of chemistry indiscriminately. Inspection of the structure of the Variant 9 enzyme indicates that the L-Met sulfur may be in a good position to interact with both PLP and the substrate. Since the activity enhancement effect occurs for both gamma elimination and cysteine beta elimination, we hypothesize that the sulfur atom plays a role in positioning the PLP in an improved orientation for faster chemistry (Figure 9 and ref. (*112*)).

The N59I and L119A mutations incrementally increased activity against L-Met and improved selectivity by also diminishing cystathionine activity. In the case of L-Met as substrate, the effect of the N59I substitution was to decrease K_M. This may be due to an increase in the hydrophobicity of the binding pocket effects discussed above. The effect of the L119A mutation was primarily to increase the k_{cat}. In the initial stages of engineering a human L-Met-degrading enzyme, the leucine at position 119 played an important role in modulating hydrophobicity of the binding pocket of NLV. With the

introduction of additional mutations, including those also conferring greater hydrophobicity to the active site (N58I, S63L), the need for a hydrophobic residue at this position diminished (Figure 7b). Instead, we hypothesize that the removal of the bulky leucine side chain improves L-Met reaction kinetics by minimizing steric hindrance and facilitating leaving group escape.

3.3.3 Second Shell I353S

I353S is a second shell residue that is positioned somewhat further from the substrate binding pocket than the 1st shell residues. The introduction of this mutation reduces the K_M and produces a twofold improvement in k_{cat}/K_M of NLV. This residue is part of a flexible loop and based on the solved Variant 9 crystal structure appears to introduce a slight twist that results in a shift in the overall loop orientation and a flip of another serine at the 358 position away from the entrance of the active site (Figure 10). In the wild-type CGL enzyme this S358 is positioned less than 5 angstroms away from the substrate and its repositioning may be significant for the way the substrate approaches and docks into the active site. However a caveat in any structural interpretation of mutational effects is that all crystallographic structures are static whereas enzyme flexible loops in solution are not, by definition.

3.3.4 Long Distance Positions

T311G has the effect of reducing the K_M of the enzyme by 5 fold. While it also affects the k_{cat} with a 2.5 fold reduction, the net effect is a twofold improvement in catalytic turnover of L-Met (k_{cat}/K_M). The activity against cystathionine remains effectively unchanged. The structure of CGL and that of Variant 9 reveal that the 311 position is too far away from the active site and substrate binding pocket to directly participate in static binding interactions or chemistry and must therefore be important for conformational effects (Figure 8). The discovery of this mutation encapsulates the power of the phylogenetic analysis approach since it would not have been identified without the sequence alignment. When combined with the I353S mutation, the resulting modest increase in activity suggests a small degree of synergy between the two positions.

The K268R mutation was shown to reproducibly double the k_{cat}, but to also slightly increase the K_M of the enzyme. Based on structure, this residue is well positioned to participate in the formation of a stronger salt bridge between two monomers and has been implicated in the increase of the thermodynamic stability of the enzyme (Figure 11b, and section 2.2.8, ref. (*113*)). The mechanism by which this distant residue affects the reaction rate remains to be elucidated.

3.4 METHODS

Kinetic analysis using MBTH

Kinetic analyses were performed as described in Chapter 2 to measure ketobutyrate production by reaction with 3-methyl-2-benzothiazolone hydrazine hydrochloride (MBTH) to generate a chromophore with a λmax of ~320 nm. Eppendorf tubes (1.5 ml) containing 220 µL of substrate in a 100 mM sodium phosphate buffer, 1mM EDTA (pH 7.3), and 10 uM PLP were incubated at 37°C in a heat block. Reactions were started by adding 20.3 L of enzyme solution and µ quenched with 26.7 µL of 50% trichloroacetic acid after a set length of time (without shaking). Reactions and blanks were then mixed with 733 µL of MBTH solution (2.2 ml: 1.6 ml of 1M acetate buffer pH 5.0 and 0.6 ml of 0.1% MBTH in same) and incubated at 50°C for 40 minutes. After cooling, the samples were transferred to cuvettes and the A320 nm was determined. The assay was shown to be linear between 0 - 320 µM α-ketobutyrate with a lower detection limit of 15 µM. One unit of MGL activity was defined as the amount of enzyme that produced 1 µmol of α-ketobutyrate per minute at infinite concentration of L-Met.

96-well plate screen

This screen was performed the same way as discussed in Chapter 2. Both MGL and CGL produce α-ketobutyrate from their respective substrates. The aforementioned colorimetric assay was adapted to a 96-well plate scale for screening small libraries and for ranking clones with the greatest L-Met degrading activity. Single colonies of *E. coli* BL21 containing plasmids encoding either wild-type (pMGL or hCGL control) or variant hCGL enzymes were picked into 96-well culture plates containing 75 µL of TB

media/well and 50 μg/ml kanamycin. Cells were grown at 37 °C on a plate shaker to an OD_{600} of ~0.8–1, cooled to 25 °C, whereupon an additional 75 μL of media containing 50 μg/ml kanamycin, and 2 mM IPTG were added and incubation with shaking was continued for 2 hrs at 25 °C. Subsequently, 100 μL of culture/well were transferred to a fresh 96 well plate (assay plate). The assay plates were centrifuged (10 min x 3,500 g) to pellet the cells, the media was removed, and the cells were chemically lysed by addition of 50 μL/well of B-PER protein extraction reagent (Pierce, Rockford IL) and mixing for 5 min on a plate shaker. Then 20 uL of 5 mM L-Met at pH 7.3 was added to the lysates and incubated at 37°C for approximately 12 hours. The α-keto acid reaction product is then derivatized by addition of 146 μL of MBTH solution to 54 μL of reaction and heated for 40 min at 50°C. The absorbance at 320 nm was determined spectrophotometrically using a microtiter plate reader. Variants exhibiting high absorbance values and indicative of production can thus be identified and selected for further characterization.

Site-Directed Mutagenesis

QuickChange Site-Directed Mutagenesis kit (Agilent Technology) was utilized to generate single site-mutated hCGL variants. All oligonucleotides were optimized by the constraints of the kit protocol and ordered from Integrated DNA Technologies. After the PCR thermal cycling, the gene product was treated with Dpn I (New England BioLabs) at 37oC for 1 hour. Finally, 4 ul of reaction was used for heat-shock transformation on BL21(DE3) competent cells.

Combinatorial Library Construction

Phylogenetic analysis was performed as described within the chapter. Geneious analysis software was used for the sequence alignment and the source organisms for the enzyme sequences were as follows: eukaryotic cystathionine-γ-lyases - human, cattle, rat, mouse, zebra, bacterial methionine-γ-lyases - *Ruegeria, Pseudomonas, Ferrimonas, Porphyromonas, Shewanella, Bacillus*. Positions were identified as potentially important to conferring substrate specificity. Overlapping PCR was used to generate combinatorial library containing either the wild-type or MGL residue at each position using "DNAWorks" software-designed oligonucleotides (16 total). These were obtained from Integrated DNA Technologies and were additionally further purified by PAGE gel electrophoresis. After the initial PCR reaction the gene product was amplified by thermal cycling with gene-specific end primers. Following digestion with NcoI and EcoRI restriction enzymes, the randomized genes were ligated into pET28a previously digested with NcoI and EcoRI. After ligation, plasmids were transformed into *E. coli* BL21 and transformants were screened as described above. Clones displaying activity were identified by sequencing, re-transformed into *E. coli* BL21, purified and kinetically characterized.

Circular Dichroism Spectroscopy

A 5 μM sample of enzyme in a 100 mM phosphate buffer, pH 7.3 was analyzed on a Jasco J-815 CD spectrometer. The change in molar ellipticity at 222 nm (θ_{222}) was monitored from 25 – 90°C. The fraction of denatured protein at each temperature was calculated by the ratio of $[\theta_{222}]/[\theta_{222}]_d$ where $[\theta_{222}]_d$ is the molar ellipticity of the completely unfolded protein. The resulting data was fit to a modified logistic equation to determine the thermal transition midpoint.

Serum Stability

Purified enzymes were added to pooled human serum (Innovative, Novi MI) at a concentration of 20 μM and incubated at 37°C. At various time points, aliquots were withdrawn and tested in triplicate for their ability to hydrolyze L-Met (10 mM). Data were plotted as observed reaction rate vs. time and fit to a single exponential equation to calculate $t_{1/2}$ values.

Chapter 4: GFP Reporter Screens for the Engineering of Amino Acid Degrading Enzymes From Libraries Expressed in Bacteria[2]

4.1 Chapter Summary

There is significant interest in engineering human amino acid degrading enzymes as non-immunogenic chemotherapeutic agents. We have designed a high-throughput fluorescence activated cell sorting (FACS) assay for detecting the catalytic activity of amino acid degrading enzymes in bacteria, at the single cell level. This assay relies on coupling the synthesis of the GFP reporter to the catalytic activity of the desired amino acid degrading enzyme in an appropriate *E.coli* genetic background. The method described here allows facile screening of much larger libraries (10^6-10^7) than was previously possible. We demonstrate the application of this technique in the screening of libraries for the catalytic optimization of an engineered human methionine-γ-lyase.

[2] Paley, O., Agnello, G., Cantor, J., Yoo, T. H., Georgiou, G., and Stone, E. (2013) GFP reporter screens for the engineering of amino acid degrading enzymes from libraries expressed in bacteria, *Methods Mol Biol 978*, 31-44.

4.2 INTRODUCTION

The screening of large libraries of enzyme variants for improved or altered catalytic function generally presents a daunting challenge. Unlike the screening of protein libraries for ligand binding, which can be accomplished using the same assay format regardless of the identity of the ligand, enzymes catalyze a plethora of reactions which in turn, necessitates the use of specific individualized activity assays. Many, if not most, enzyme-catalyzed reactions are not easily amenable to high-throughput assays. This in turn limits the size of the sequence space that can be practically sampled in directed evolution experiments (*115*).

As discussed in Chapters 1 and 2, the engineering of desired activity into human enzymes can yield potent therapeutics with low immunogenic response risk to patients. In recent years we have demonstrated the use of protein engineering strategies to develop human enzymes with the requisite properties for cancer therapy (*116-119*). High throughput screens target activities can greatly aid the engineering of therapeutic enzymes by directed evolution of human enzymes that catalyze similar reactions. The development of such screens necessitates the engineering of unique *E. coli* strains that are dependent on a metabolite generated by the chemistry of interest. In this chapter we discuss the example of a human methionine degrading enzyme that rescues an *E. coli* strain engineered to be auxotrophic for L-isoleucine by the enzymatic degradation of L-Met to produce α-ketobutyrate (a metabolite required for synthesis of L-Ile) . In turn, this reaction can complement the auxotrophic strain enabling the synthesis of GFP. Thus a

very active enzyme allows GFP to be translated at levels commensurate with non-selective conditions whereas a less active or inactive enzyme results in reduced GFP expression due to the depleted amino acid pool in the auxotroph. FACS can then be used to isolate individual clones based on their fluorescence profile from large libraries of enzyme variants expressed in *E.coli*. Employing several rounds of FACS sorting we can attain thousands of fold enrichment of clones with desired activity and *then* use a secondary assay method to analyze a handful of clones for the rank ordering of enzyme variants and assessment of kinetics. Figure 1 shows the general scheme and workflow of the method.

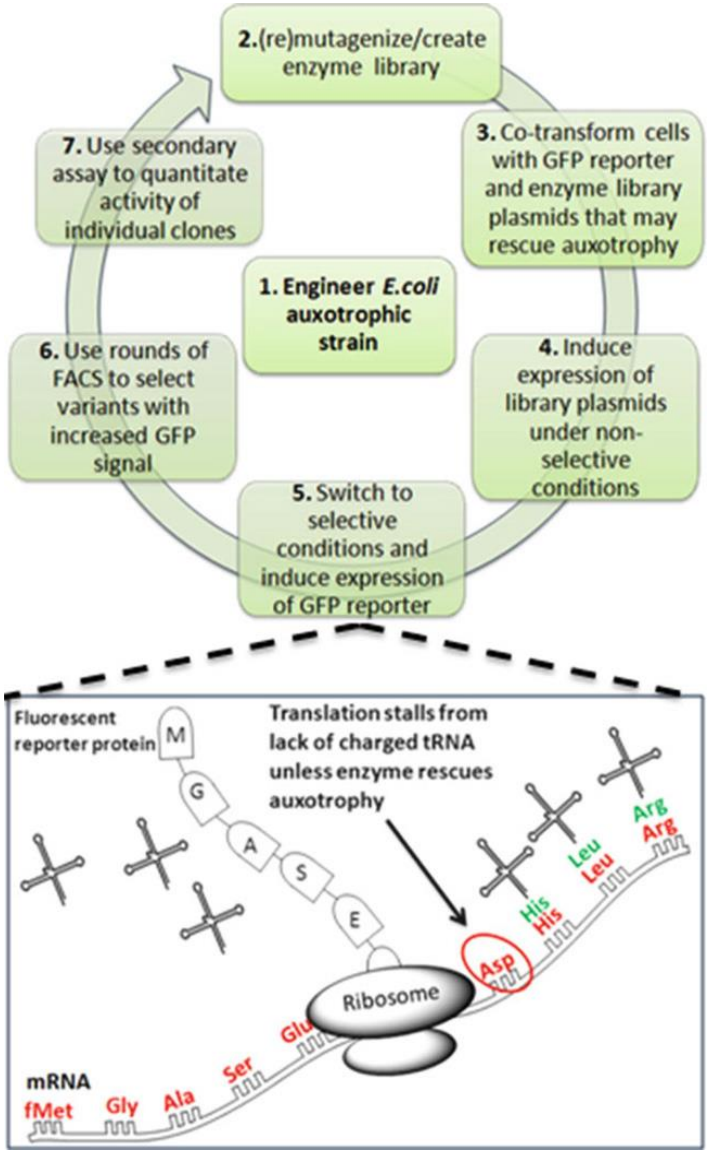

Figure 1: General method 1) Engineer *E.coli* strain that can no longer make a metabolic intermediate needed for growth. 2) Create mutagenized libraries of enzymes that have the potential to make the missing metabolic intermediate. 3) Co-transform auxotrophic strain with library and GFP plasmids that have mutually exclusive promoters. 4) Culture under non-selective conditions and induce expression of enzyme plasmids. 5) Shift culture to selective conditions and induce expression of GFP. If an enzyme variant can rescue the auxotrophy, that cell will express greater levels of GFP. 6) Use rounds of FACS sorting to select cells with high GFP fluorescence. 7) Use secondary screen/assay to rank order clones and if necessary repeat mutagenesis on variants with increased activity.

4.3 Background and Materials Methionine-γ-lyase Screen

The non-mammalian enzyme methionine-γ-lyase (MGL) catalyzes the α,γ-elimination of L-methionine to methanethiol, α-ketobutyrate, and ammonia (Chapter 1). MGL from *P. putida* has shown efficacy in controlling tumor growth in a variety of xenograft models (*30, 32, 33, 37, 46, 65, 67, 68*) but unfortunately has proven to be highly immunogenic in primates (*45*). We employed rational design and scanning saturation mutagenesis to convert the structurally related human enzyme cystathionine-γ-lyase (CGL) into a human L-Methionine γ-lyase (MGL) that catalyzes the α,γ-elimination of L-Methionine to methanethiol, α-ketobutyrate, and ammonia but does not accept L-Met as a substrate. The assay previously available to screen this class of enzymes is a 96-well plate colorimetric assay for α-ketobutyrate production.

4.3.1 Engineering an Isoleucine Auxotroph Rescued by Methionine Lyase Activity

E.coli produces α-ketobutyrate as an intermediate metabolite in the *de novo* production of L-isoleucine (L-Ile) by action of threonine deaminase (ilvA). We thus deleted *ilvA* to create an L-Ile auxotroph that could be rescued by α-ketobutyrate produced from L-Met degradation by MGL (Figure 2a). Additionally, because CGL can also produce α-ketobutyrate from L-cystathionine and L-homocysteine which are metabolites in the *E.coli* pathway for L-Met production, we also deleted the *metA* gene (Figure 2b).

The gene deletions were performed by bacteriophage P1 transduction (*120, 121*). Keio collection donor strains (*122*) were incubated with P1 phage. The resulting lysate contained a small percentage of phage capsids carrying the bacterial chromosome. The DNA was transduced into the host cells and selected for successful gene knockout on plates with the appropriate resistance marker. The antibiotic resistance cassette introduced at the gene site was then removed by site-specific recombination and the resulting scar sequence fragment was confirmed by PCR (*9*). The ilvA gene deletion was performed first, and the resulting BL21(DE3) *ΔilvA* strain was used as the host for the second round of transduction. *E.coli* [BL21(DE3) *ΔilvAΔmetA]* was named <u>*E.coli MI-aux*</u> to reflect its dual L-Met and L-Ile auxotrophies (Figure 2).

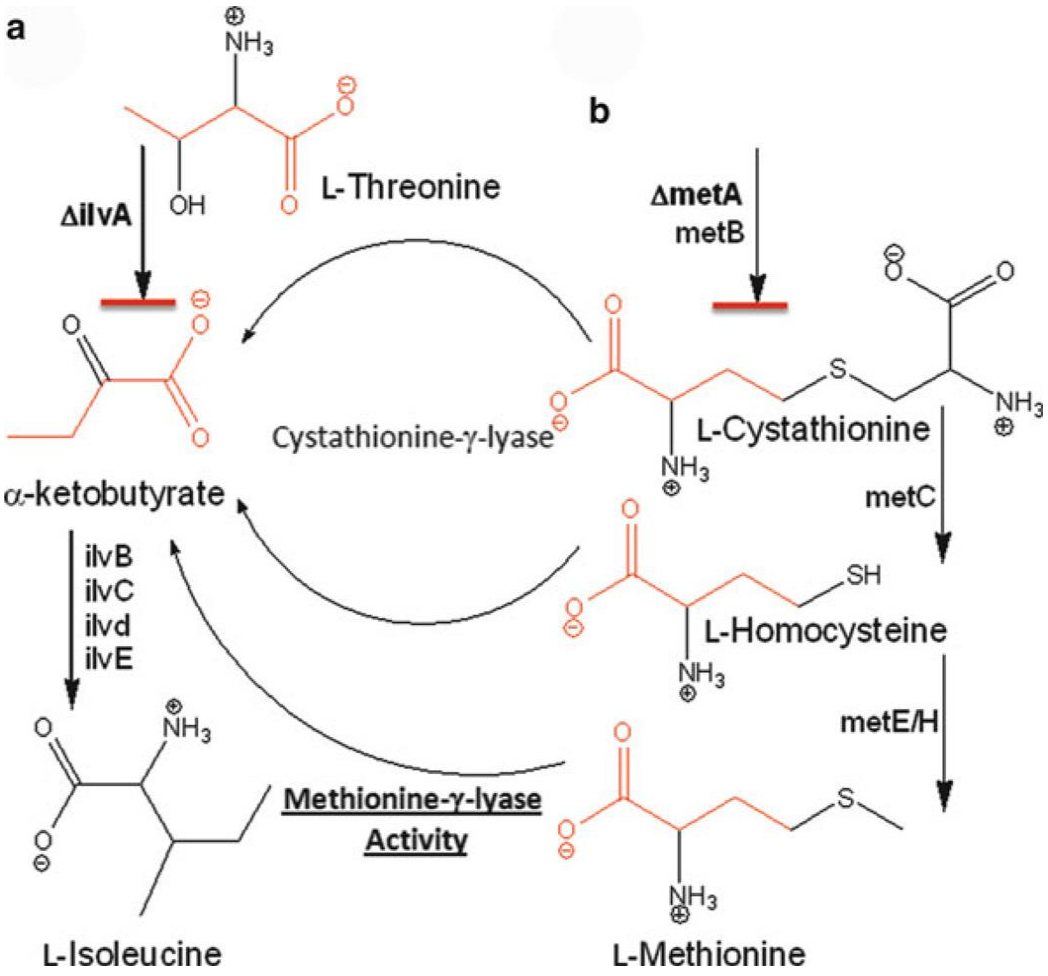

Figure 2: Metabolic pathways a) Summary of the pathway and gene deleted in *E.coli* needed to create an α-ketobutyrate auxotrophic strain that can be rescued by recombinant methionine-γ-lyase activity. b) Summary of the pathway and gene deleted needed to create an L-methionine auxotroph to prevent parental cystathionine-γ-lyase activity from rescuing α-ketobutyrate auxotrophy.

4.3.2 Plasmids

We used the arabinose inducible pBAD-GFP with a chloramphenicol acetyltransferase marker as a reporter plasmid coupled with the IPTG inducible

pET28a with a kanamycin resistance marker as an expression plasmid for parental hCGL and pMGL.

4.3.3 Media/plates/buffer

1. *Non Selective Media:* Enzyme expression media; M9 minimal medium supplemented with 0.4% glucose, 1 mM $MgSO_4$, 0.1 mM $CaCl_2$, 150 μg⁄mL of the amino acids L-Met and L-Ile, 75 μg⁄mL of the remaining amino acids excluding L-Leu and L-Val (see Note 6), 50 μg⁄mL kanamycin, and 34 μg⁄mL chloramphenicol.
2. *Selective Media:* GFP Expression Media; M9 medium supplemented with 0.4% glucose, 1 mM $MgSO_4$, 0.1 mM $CaCl_2$, 150 μg⁄mL of L-Met, 75 μg⁄mL of the remaining amino acids (excluding L-Ile, L-Leu and L-Val), 50 μg⁄mL kanamycin, 34 μg⁄mL chloramphenicol, and 2 % arabinose.
3. *General Media:* LB supplemented with 50 μg/mL kanamycin and 34μg/mL chloramphenicol.
4. *Plates:* 2xYT agar supplemented with 50μg/mL kanamycin and 34μg/mL chloramphenicol.
5. *Competent cells: E.coli MI-aux* harboring pBAD-GFP.
6. *Buffers/reagents:* filter sterilized 0.9% NaCl (4°C), filter sterilized 1X phosphate buffered saline at 4 °C (PBS), filter sterilized solution of L-Ile (250mM) in PBS, filter sterilized solution (1M) of isopropyl-β-D-1-thiogalactopyranoside (IPTG).

7. Culture tubes (5 ml), 1.5 mL Eppendorf tubes, 15 mL Falcon tubes, FACS tubes etc.

4.3.4 Flow cytometric analyses

A FACSAria (BD Biosciences) using a 488-nm solid state laser for the excitation of GFP. A 530/30 band pass filter was used for the detection.

4.4 METHODS METHIONINE-γ-LYASE SCREEN

4.4.1 Cell growth and GFP expression

Use your laboratories favorite methods for library construction, competent cells, transformations etc.

1. Grow an overnight culture (5 mL) of *E.coli* BL21(*MI-aux*) co-transformed with pBAD-GFP and plasmids either a library or a single mutant in 2xYT (see Note 2).
2. Inoculate 1 ml of *Non Selective* Media in a sterile culture tube with *E. coli* BL21(*MI-aux*) cells harboring plasmids of pBAD-GFP reporter and pET28a containing gene of interest to a final OD_{600} of 0.1. The cell source for the inoculation can be previously frozen aliquots or overnight cultures of either a single mutant or a library of variants. Make sure to include tubes for a positive and negative control (1 ml each) for each round if planning to sort a library.

3. Grow cultures with shaking at 250 rpm at 37 °C to an OD_{600} of 0.3-0.4.
4. Add 1M IPTG solution to a final concentration of 1 mM and shift the cultures to 25 °C for 2 hours with shaking at 250 rpm for enzyme expression (See Note 7).
5. Harvest the cells by centrifugation (7,000 rpm, 3 min, 4°C). Wash the cells twice with cold 0.9% NaCl by re-suspending and centrifuging at 7,000 rpm, for 3 min at 4 °C (See Note 8). Use sterile 1.5 ml Eppendorf tubes to harvest the cells and at least 1 ml of the 0.9% NaCl solution for each wash.
6. Re-suspend the washed cells in 1 ml of GFP Expression Media (containing arabinose inducer for GFP expression). Split each 1 ml sample into two small culture tubes (500 μL per tube) and add 250 mM L-Ile solution to a final concentration of 1 mM in one of the two tubes. This will serve as a control for each sample (See Note 9).
7. Continue to grow at 25 °C for an additional 2 hours (shake at 250 rpm).
8. Harvest the cells by centrifugation (7,000 rpm, 3 min) and re-suspend in PBS to a final OD_{600} ~ 0.05–0.1 for flow cytometric analysis and cell sorting.

4.4.2 Cytometric analysis and cell sorting

1. Perform flow cytometric analysis with a FACSAria (BD Biosciences) or an equivalent system. Adjust the throughput rate of cells to 4,000–5,000 events per second.

2. Perform all rounds of sorting in single cell mode, except for the initial sort, which should be in purity mode.
3. Set a gate in the fluorescence channel to recover the 4–5% most highly fluorescent cells. Additionally, set gates based on both the forward- and side-scatter channels to exclude sorting non-single cell events (See Note 10).
4. Sort 10-fold the number of cells expected to cover the diversity for each round.
5. Collect the sorted cells in 0.5 mL of 2xYT medium and plate onto pre-warmed 2xYT medium supplemented with 50 μg⁄mL kanamycin and 34 μg⁄mL chloramphenicol (See Note 11).
6. Following overnight growth at 30 °C, pool the clones and store aliquots in 15% glycerol at −80 °C. At this step, you may also use the pool to inoculate the next round.

4.4.3 Enrichment Experiment with Controls

1. Inoculate two culture tubes of *Non Selective* Media with *E. coli* BL21(*MI-aux*) containing pBAD-GFP/pET28-pMGL for a positive control and pBAD-GFP/pET28-hCGL for a negative controls. Follow the protocols from section **4.4.1** (steps 1-7) keeping the controls separate.
2. After GFP expression, measure the OD_{600} of the cultures and make several 100 μL aliquots of negative controls in 1.5 mL Eppendorf tubes.

3. Through serial dilution of your positive control into your negative control aliquots, generate a pool that contains the negative control in a 10,000-fold excess.
4. Dilute this mixture in PBS to a final OD_{600} ~ 0.05–0.1 for flow cytometric analysis and cell sorting.
5. Follow the remaining steps of the protocol described in section **4.4.2.**
6. Continue additional rounds of sorting until the fluorescence signal of your pool is either: i) equivalent to that of the positive control alone, or ii) no longer changing from one sort round to the next.
7. Sequence at least 20 random clones from the last round plate to verify identity of gene in the pET28a expression plasmid. Alternately, you can perform a *secondary* 96-well plate screen for methionine-γ-lyase activity (*75*) to determine the makeup of the pooled sample.
8. Calculate the fold of enrichment achieved and note the number of sort rounds necessary to achieve the enrichment.
9. A successful Enrichment Test should yield results similar to Figure 3. We achieved a 5,000-fold enrichment within 3 rounds (Additional rounds may be necessary under different conditions) (See Note 12).

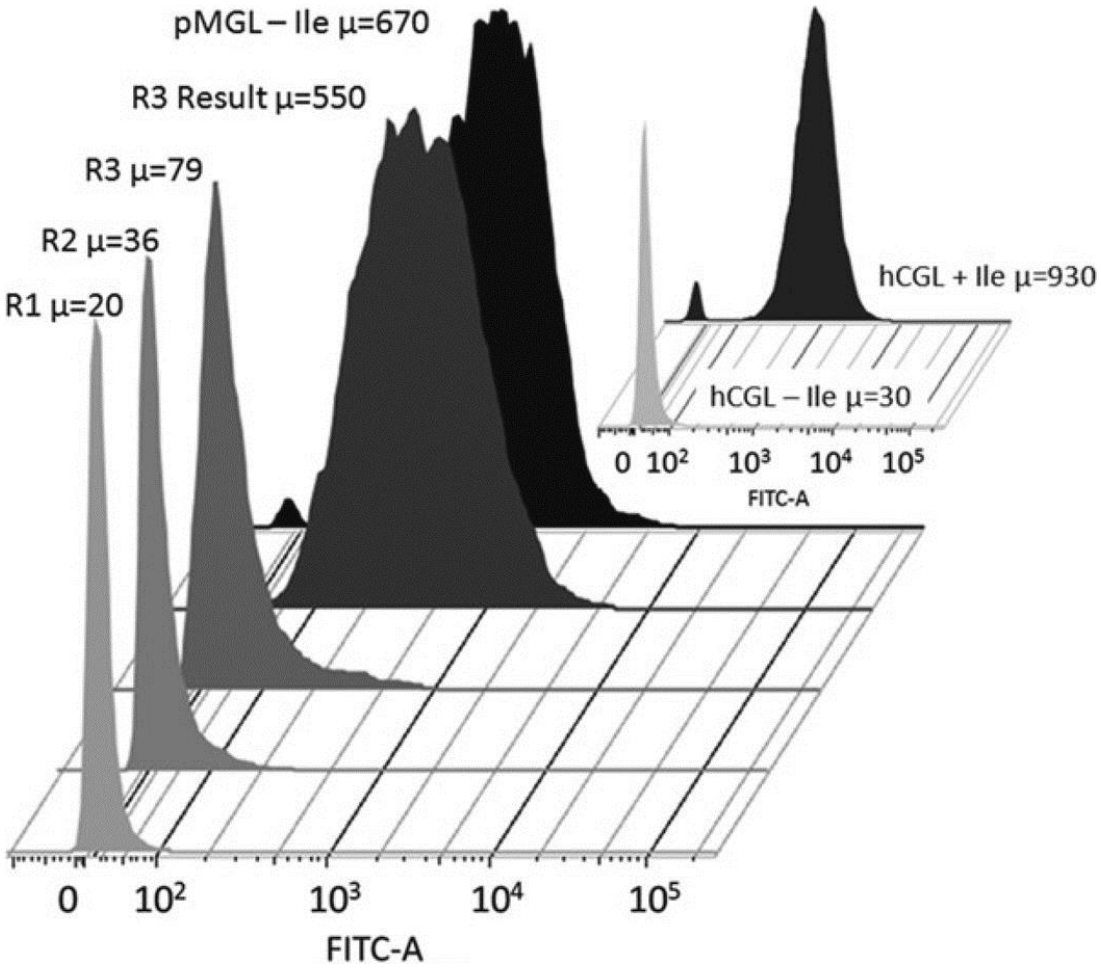

Figure 5. Histogram showing enrichment of positive enzyme control out of a mixed pool of 10,000:1 hCGL to pMGL over the course of four rounds, as well as the signals of a positive enzyme control alone (pMGL -Ile). *Inset*) A histogram of a positive and negative control experiment using hCGL in the presence or absence of L-Ile (+/- Ile).

4. 5 ADDITIONAL NOTES

1. The amount of enzyme required to rescue the auxotrophy depends on the catalytic activity and level of "leaky" expression. In the case of the sufficient parental

enzyme leaky expression, uninduced culture is suitable for the analyses. For a poorly expressed enzyme one can supplement with IPTG.

2. We find it is easiest to prepare competent cells harboring the reporter plasmid pBAD-GFP and then transform with the expression plasmids of interest.
3. The multiple wash steps with PBS ensure removal of the selective expression media for the subsequent cytometric analysis.
4. L-Val and L-Ile are excluded from the Non Selective Growth Media and Selective Growth Media because these branched-chain amino acids are known to inhibit the L-Ile biosynthesis pathway (*123, 124*). The addition of these two amino acids to the Selective Growth Media without L-Ile in our experiments resulted in undetectable GFP expression in all variants tested.
5. Some enzymes express better at lower temperatures thus this parameter can be adjusted on a case by case basis.
6. The multiple wash steps ensure that L-Ile is removed from the media.
7. In the positive control for each sample the expression of GFP will be independent from the enzymatic activity, as the medium is non-selective and supplemented with L-Ile. In the sample the expression of GFP will be dependent on the L-Met degrading activity of the single mutant or of the library, as the medium is selective and deprived of L-Ile.
8. During flow cytometric analysis the applied voltage may be adjusted to improve the signal separation of the controls. A higher voltage will result in higher signals

for both the positive and negative samples, but will also improve the signal to noise ratio when the positive control signal is at the lower end of the optimal dynamic range for the instrument and the negative control is near 0 (FITC-A 0-10,000).

9. When plating cells collected from a round of sorting, optimal recovery is achieved if the agar plate is pre-warmed for 30 minutes to 1 hour at 37°C.

10. Various parameters may be adjusted to optimize the process. Optimization should maximize the fluorescence signal difference between the positive and negative control variants. The expression of enzyme can be tuned by changing the IPTG inducer concentration, altering the expression temperature and time, as well as by choosing a different OD_{600} reading to initiate expression. GFP expression can be similarly controlled by altering the arabinose concentration in the Selective Media and varying expression time and temperature.

4.6 CONCLUSION

We have developed a high throughput FACS- based method of screening libraries of upwards of 10^7 clones for the catalytic optimization of enzymes. By coupling the synthesis of GFP to catalytic activity in a cell line engineered to be dependent on a product of the target chemical reaction, we can selectively enrich for the population

expressing enzymes with greater catalytic activity. In the specific example of a methionine degrading enzyme, we coupled GFP production to the generation of α-ketobutyrate in an isoleucine auxotroph host. Applying this screen, were able to enrich the population expressing positive control pMGL 5,000 fold over the course of only three rounds of screening (1 in 10,000 to 1 in 2).

At the time of protocol development, we also tested this method with a mixed population of 1:1000 Variant 1 NLV to wild-type CGL (Chapter 2), but were unable to see any enrichment after 7 rounds of screening. Variant 1 has a methionine degrading activity (as measured by k_{cat}/K_M) that is only 1% the activity of the bacterial MGL, and we concluded that this rate of α-ketobutyrate production is insufficient to generate detectable (above background) levels of GFP in the absence of isoleucine. A 10 fold faster enzyme (10% of MGL activity) has now been engineered through the application of phylogenetic analysis and iterative lower throughput 96 well plate screens (Chapter 3). Future work will test whether enrichment in the FACS based assay is possible with the improved baseline activity of Variant 9.

Chapter 5: *In vitro* Effects of Enzyme-Mediated L-Met Depletion on the Melanoma and Prostate Carcinoma Cell Lines

5.1 Chapter Summary

Various malignant cells experiencing starvation stress in response to methionine deprivation are known to undergo processes that arrest cell division and ultimately lead to cell death. The study of the mechanisms of the death response and other processes induced by treatment with the engineered human L-Met degrading enzyme serves to aid in the selection of appropriate cancer targets, prediction of effects on other neoplasms and normal tissues, and identification of effective combination therapies. We have shown that treatment with CGL-NLV is correlated with an induction of autophagy and cell death by apoptosis in A375 melanoma cell line. Prostate cancer cell line DU145 treated with Variant 7 also responds by undergoing extensive cell death, though the precise mechanism of the process remains unclear. The mouse prostate model HMVP2 treated with Variant 7 arrests in the G2 phase and experiences a buildup of reactive oxygen species. The newly engineered human enzyme Variant 9 (Chapter 3) is capable of inducing extensive cell killing of a variety of neoplasms at therapeutically useful doses. Finally, we have shown that hMGL is also capable of degrading cystine to operate as a dual amino acid depletion treatment expected to be more potent than methionine depletion alone.

5.2 INTRODUCTION

Melanoma and prostate carcinoma neoplasms have both been shown to have an absolute requirement for methionine and to undergo cell cycle arrest and death upon the degradation of this amino acid by the bacterial pMGL (*62, 125-130*). Melanoma is a highly aggressive malignancy of the pigment producing melanocytes in the skin, and though it is the least common form of skin cancer, is has the greatest rates of mortality (75% of all skin carcinoma deaths) (*131*). The 10 year survival rate for patients whose melanoma has metastasized is less than 10%. The current standard of care for treatment remains highly toxic chemotherapeutic treatment along with surgical interventions and radiation (*132*). Prostate carcinoma is the most common form of sub-cutaneous cancer and the second leading cause of male cancer mortality globally (*World Cancer Report 2014*). Though many prostate neoplasms are slow growing, they are often asymptomatic until later stages of the disease precluding early detection, and other forms of the cancer are significantly more aggressive (*133*). Though prostate cancer generally responds well to traditional therapies (such as androgen deprivation and chemotherapy), a subset of patients will experience a recurrence of the malignancy that is resistant to standard treatment (*134*). The unfavorable outcomes of advanced melanoma and prostate carcinoma as well as the general toxicity associated with chemotherapeutic treatment demonstrate the need for an effective and better-tolerated therapeutic against these neoplasms. Characterization of the mechanism of action of such a therapeutic supports the selection of appropriate models of efficacy, prediction of effects on normal tissues,

and identification of effective combination therapies. We therefore investigated the *in vitro* effects of methionine depletion with our engineered human enzyme.

Since both melanoma and prostate carcinoma are known to be methionine auxotrophs (*125*), we expect treatment to result in extensive cell death. Neoplasm death is a complex group of processes that are initiated by stress to the cell (*135*) and can occur in multiple overlapping forms in a given cell population (*136*). The various processes associated with cell death can be loosely classified into "types", and the three most relevant to our studies were: apoptosis (caspase dependent and independent), necrosis, and autophagic cell death. For simplicity, Figure 1 presents only the key features of each type.

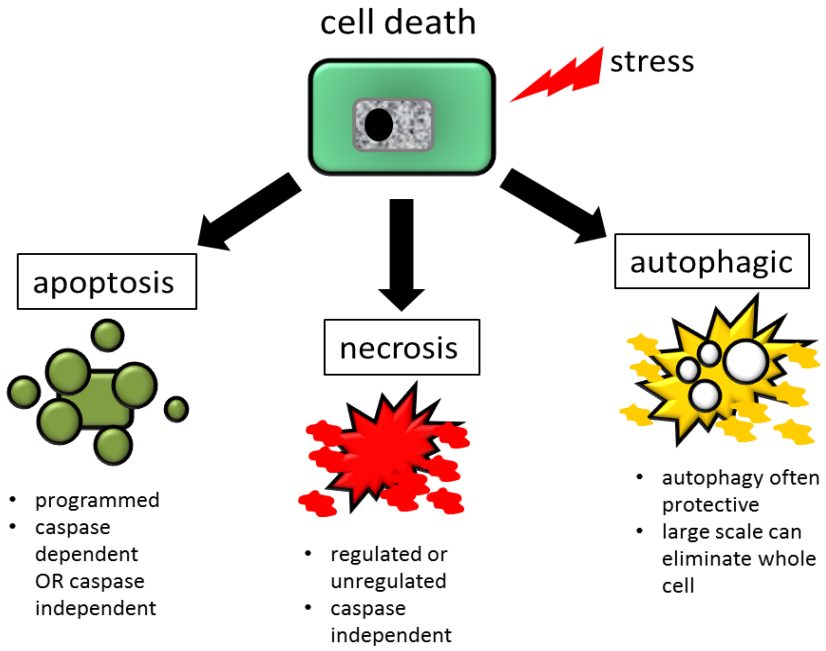

Figure 1: Three mechanisms of cell death considered in melanoma and prostate cancer methionine depletion.

Apoptosis, a process of programmed cell death, has been previously studied as a response to methionine starvation of cancer (*137*). The apoptotic process is generally defined by the presence of activated caspase proteases that participate in a signaling cascade, ultimately resulting in nuclear degradation and the packaging of cellular contents into blebs that can be phagocytosed and degraded by neighboring cells such as macrophages (*138*). Caspases are or cysteine-dependent aspartate-specific proteases that are activated by cleavage and play a central role in the transduction of apoptotic signals and execution of proteolytic degradation within the cell. Apoptosis can be initiated both extrinsically in response to external stress, or intrinsically by internal factors such as DNA damage, oxidative stress, and many others (*135*). Though the vast majority of research has focused on the caspase-dependent process, caspase-independent apoptosis does exist as some cells die with a similar morphology even after caspase proteolysis is irreversibly inhibited (*139*).

Due to the absence of defined morphological traits associated with apoptosis or autophagy, necrosis has traditionally been considered an accidental cell death mechanism that results from external trauma to the cell (*140*). It is now known that necrosis can occur in both a regulated and unregulated manner, and that regulated necrosis can be triggered by intracellular causes (*135*).

Finally, autophagy is a well regulated process that can play dual roles in the survival of a cell. During nutrient deprivation and other stress, autophagy can serve a protective role by catabolically recycling unnecessary proteins and other cell components

to regenerate the raw materials critical to survival (*141*). The general mechanism of autophagy is shown in Figure 2. Autophagosomes initially engulf cytoplasm along with the components to be degraded. The autophagosomes then proceed to fuse with lysosomes carrying hydrolytic enzymes to form autolysosomes in which cellular proteins and organelles are degraded. The recycled raw materials are then transported back into the cytoplasm. Though in most known cases autophagy constitutes a protective response (*135*), large scale autophagy has also previously been shown to result in the elimination of entire cells (*142*).

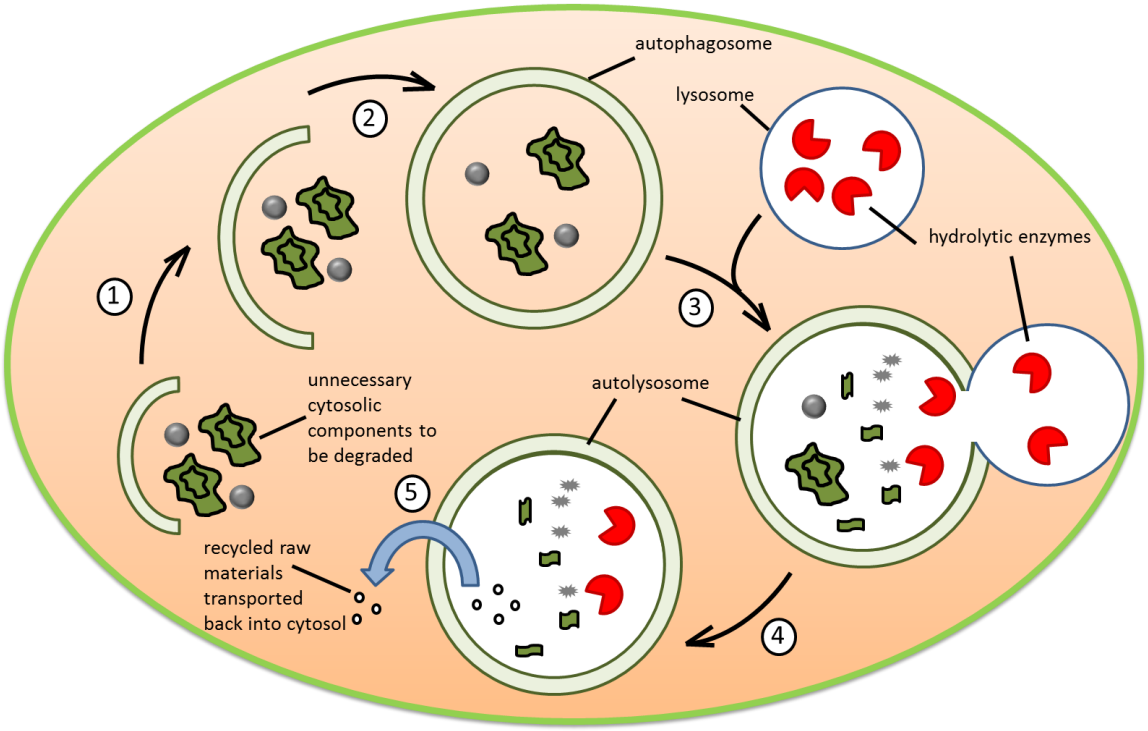

Figure 2: Schematic showing the general process of autophagy 1) an early autophagosome precursor (phagophore) begins to form; 2) the phagophore extends and surrounds the cytosolic material to be degraded 3) the complete autophagosome is formed around target components 4) the autophagosome fuses with a lysosome containing hydrolytic enzymes to form an autolysosome 5) the now degraded contents of the autolysosome are transported back into the cytoplasm and the autolysosome is itself degraded

5.3 Results

The effects of hMGL administration and the ensuing L-Met depletion on cancer cells were studied *in vitro* (i.e. in tissue culture). These studies were conducted while the protein engineering process described in Chapter 3 was ongoing, and hence involved the

use of enzymes at different points along the engineering path. The experiments described below were conducted using NLV, Variant 7 (NLV + 5 additional mutations), or Variant 9 (Variant 7 + N59I, L119A). Though the kinetic details differ between these variants resulting in somewhat different profiles of amino acid degradation, each experiment contributes to the understanding of malignant cell response to treatment with an engineered human methionine degrading therapeutic.

5.3.1 Melanoma Cytotoxicity with MGL, NLV, and Variant 7

Numerous melanoma cell lines have been reported to have a high degree of dependence on methionine and to undergo cell cycle arrest and programmed cell death in its absence(*125-128, 130*). We sought to determine the sensitivity of an A375 melanoma cell line to treatment with NLV (Chapter 2) and Variant 7 (Chapter 3) and to compare the results to treatment with bacterial MGL (Figure 2 and Table 1). Cells were treated for 5 days and their viability was measured by an MTS Cell Proliferation Assay as a percent of untreated control. The MTS assay detects viable cells by their ability to convert a chromogenic substrate with active cellular oxidoreductase enzymes. The calculated EC50 value for the bacterial enzyme was 580 nM. While NLV has a much lower k_{cat}/K_M than pMGL for methionine, its much higher stability in serum and in growth media resulted in an EC50 value that was lower than pMGL (400 nM). Variant 7 kinetic constants with methionine are 7 fold greater than NLV (Table 2, Chapter 3) and the increased activity results in an EC50 of 80 nM, or more than 7 fold better than pMGL. The improved

cytotoxicity of the human variants underscores the importance of their longer half-lives and the benefits of enhancing k_{cat}/K_M through engineering.

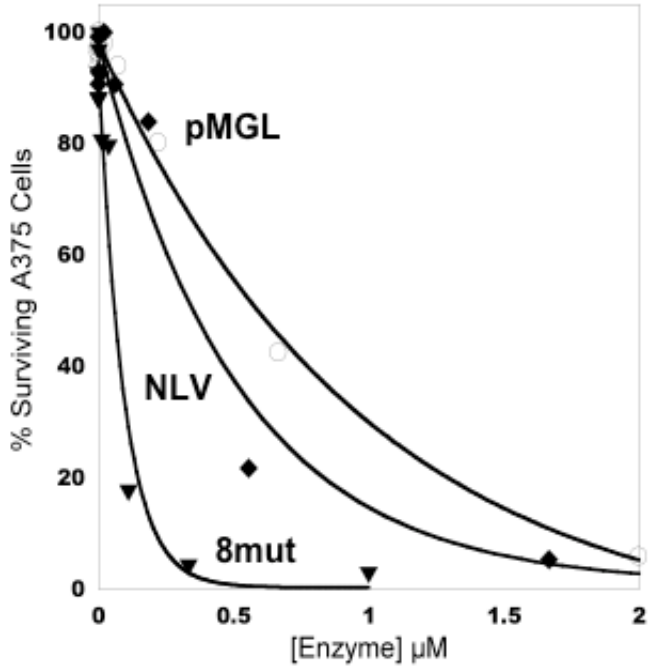

Figure 3: Effect of enzyme engineering on cytotoxicity with A375 melanoma cell line. Bacterial enzyme is denoted "pMGL", Variant 1 "NLV", and Variant 7 "8mut"

	EC_{50} (nM) with A375
pMGL	580
NLV	400
8mut (Variant 7)	80

Table 1: Calculated EC50 values for treatment in Figure 3.

Along with enzyme concentration, the exposure time necessary for a therapeutic to have a desired cytotoxic effect *in vitro* provides important drug potency information that may be extrapolated to future *in vivo* experiments. We therefore determined the time dependence of A375 melanoma cell death in response to Variant 7 treatment over the course of three days (Figure 3). Most of the cell killing effect occurs very rapidly within the first 24 hours, with diminishing drops in viability over the course of the next two days.

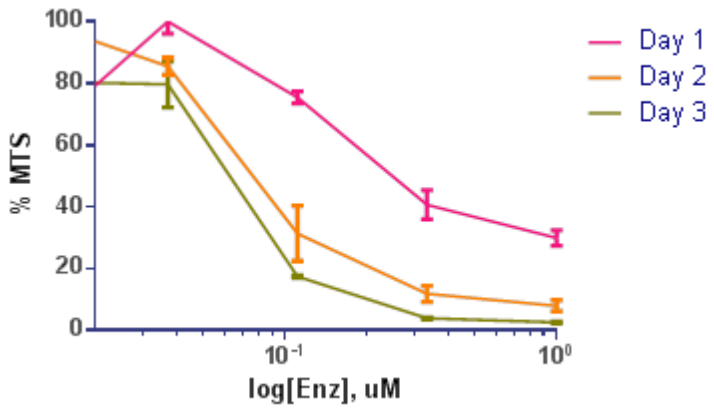

Figure 4: Cytotoxicity time course with Variant 7 (8mut) and A375 melanoma cell line.

5.3.2 Melanoma Apoptosis

Apoptosis is a well-defined process of programmed cell death (*138*) and it is well established that L-Met depletion triggers apoptosis in a variety of cancer cell lines (*8, 57, 126, 128*). One of the key features of apoptosis is the activation of caspases, or cysteine-

dependent aspartate-specific proteases, that are activated by cleavage and play a central role in the transduction of apoptotic signals and execution of proteolytic degradation of intracellular proteins- ultimately resulting in cell death.

In order to understand what role apoptosis plays in the killing of A375 cells by treatment with a human methionine degrading enzyme, we decided to directly probe for the presence of activated caspases within the cell (*135*) using FITC-VAD-FMK, a cell permeable, irreversible pan-caspase inhibitor conjugated to a fluorescein isothiocyanate group (*143*). Cells were seeded on day 0, and on day 1 cultures received either fresh media or fresh media with NLV enzyme at 500 nM or 1000 nM. On day 2, camptothecin was added to a previously untreated culture as a positive control. Camptothecin is a quinoline alkaloid that triggers apoptosis in cells by inhibiting their topoisomerase I DNA enzyme. Finally, on day 3 the cells were collected, washed and incubated with FITC-VAD-FMK as well as propidium iodide, a fluorescent intercalating molecule that is only capable of permeating dead or dying cells that have lost integrity (*144*). The samples were then analyzed by flow cytometry.

The results of the experiment are presented as two-dimensional scatter plots in Figure 5. Cells falling into Q3 correspond to those that are FITC negative and PI negative, which means they do not have detectable activated caspases and thus are alive with full membrane integrity. Cells falling in Q1 quadrant after staining are FITC negative but PI positive indicating they may be necrotic or dying via other caspase activation-independent mechanisms (Introduction, (*136*)). Cells in the second quadrant,

Q2, stain for both FITC and PI, a staining pattern consistent with "dead by apoptosis" in that they have lost integrity in the presence of activated caspase enzymes. Finally, Q4 cells are ones in which apoptosis has been induced and in which active caspases are present, but these cells have not yet become permeable to PI. This population can be expected to shift into Q2 given additional time.

For comparison, cells that were not treated with enzyme were overwhelmingly FITC and PI negative, and almost exclusively contained in the Q3 quadrant. The positive camptothecin-treated control is assumed to be representative of a population of cells in the process of undergoing apoptosis, with 44% of cells FITC and active caspase positive. Additionally, 26% of active caspase positive cells are also positive for PI and are dead or dying. The enzyme treated sample shows a similar distribution of cells. Additionally, a doubling in treatment enzyme concentration results in a slight decrease in the number of live non-apoptotic cells and a slight increase in the FITC positive cell population. For all treatment conditions, Q1 contains 1% or less of total cells. This population can be defined as dead by a non caspase-dependent process. These results imply that the primary response to enzyme treatment for melanoma A375 is to undergo programmed caspase-mediated cell death.

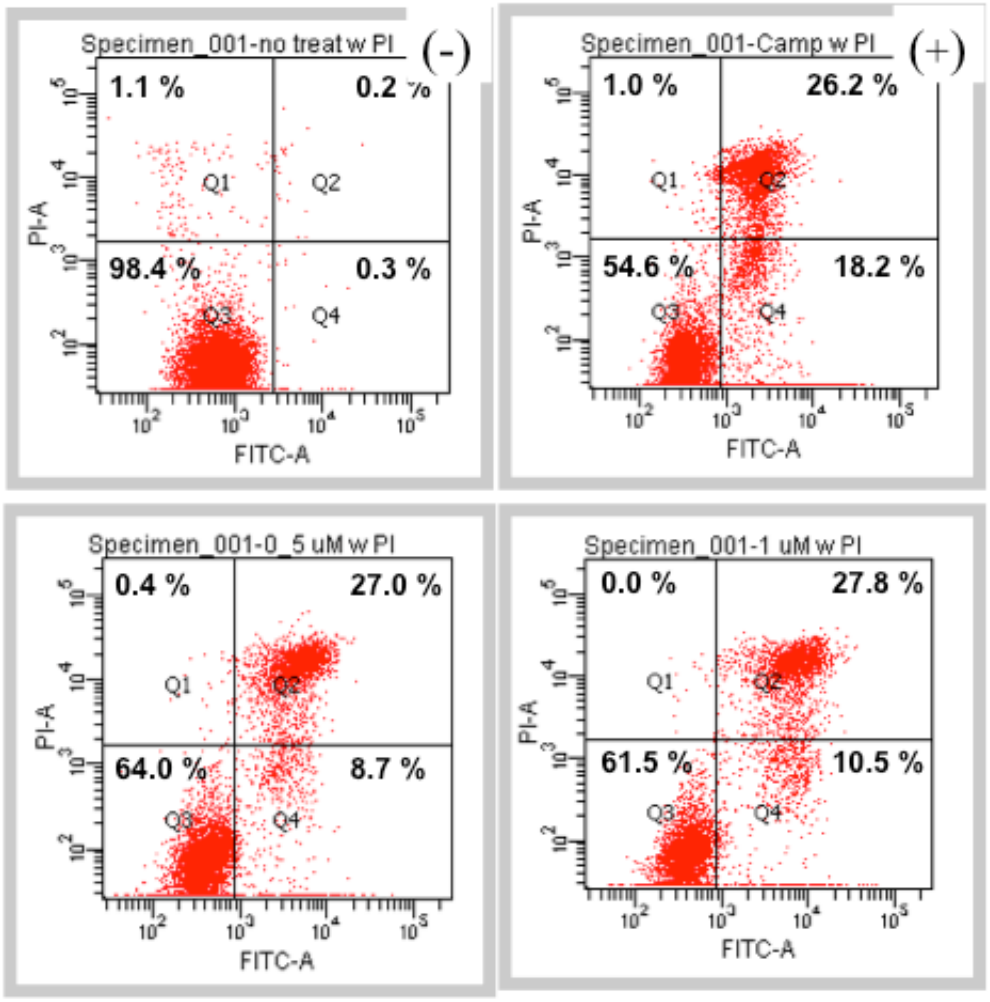

Figure 5: Flow cytometric analyses showing cell integrity and presence of activated caspases. (-) Top left: negative untreated control. (+) Top right: positive control treated with camptothecin. Bottom left: treated with 0.5 µM Variant 1 NLV. Bottom right: treated with 1.0 µM Variant 1 NLV. FITC positive (right two quadrants for each) correspond to presence of activated caspases. PI positive (top two quadrants for each) correspond to dead cells.

Two additional experiments were performed to confirm apoptosis as the mechanism of A375 melanoma cell death in response to treatment with the methionine-depleting enzyme NLV. First, the flow cytometry experiment was repeated in the

presence of the Z-VAD-FMK apoptosis inhibitor. This pan caspase inhibitor irreversibly binds to the catalytic site of initiator caspases and prevents the induction of the signaling cascade that activates effector caspases and results in apoptosis (*145*). Two A375 aliquots were treated with media and enzyme. One of these cultures was also pre-incubated for 30 minutes with Z-VAD-FMK (unlabeled) inhibitor before enzyme was added. In order to assure extensive killing, the cells were treated for a total of 4 days. Results are presented in Figure 6. Untreated cells were alive and stained negative for active caspase while the positive control and cells treated with enzyme without caspase inhibitor show a high percentage of apoptosis. Notably, in the presence of the inhibitor during treatment the percent of apoptotic cells is drastically reduced and the percentage of "live cells" in Q3 approaches that of the untreated control. Since inhibiting the apoptotic cascade modulates cell killing so effectively, we can conclude that apoptosis is indeed the dominant mechanism of cell death in this cell line.

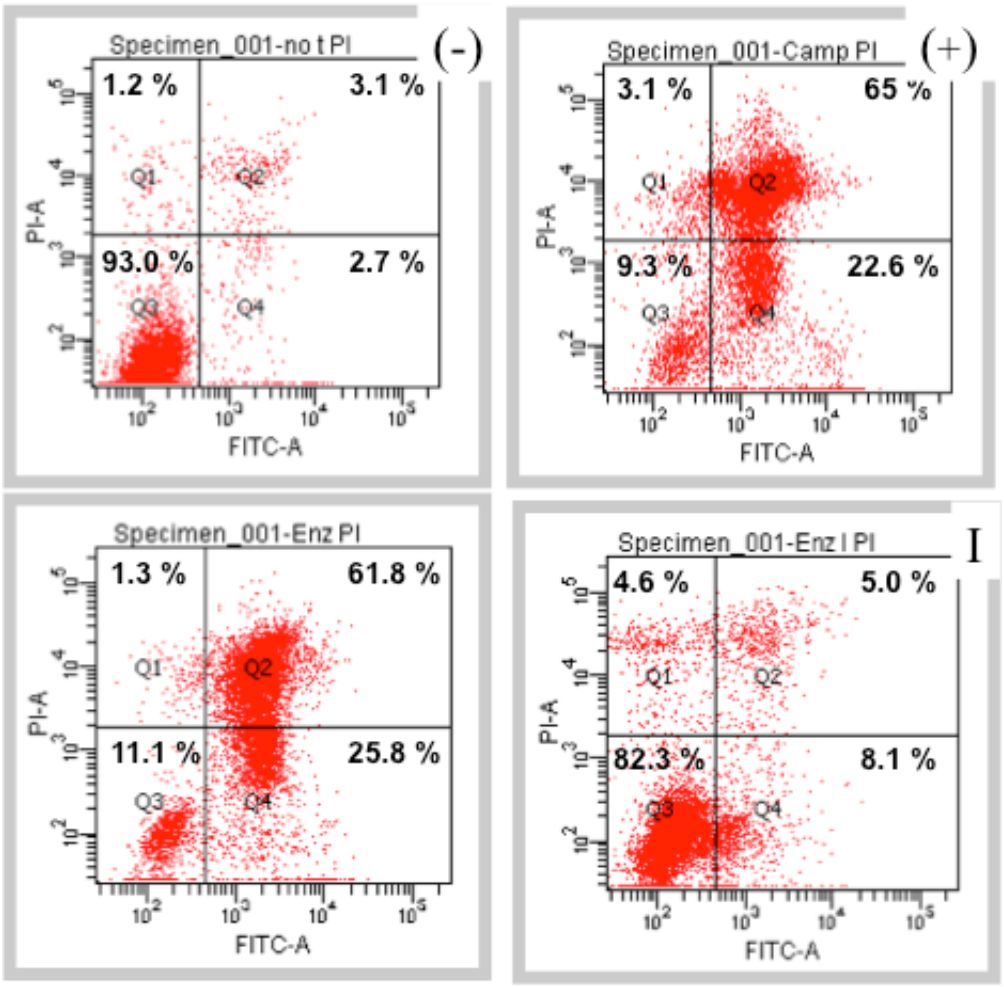

Figure 6: A375 flow cytometric analyses showing cell integrity and presence of activated caspases with apoptosis inhibitor. (-) Top left: negative untreated control. (+) Top right: positive control treated with camptothecin. Bottom left: treated with Variant 1 NLV. (I) Bottom right: pre-treated with apoptosis inhibitor and then treated with Variant 1 NLV. FITC positive (right two quadrants for each) correspond to presence of activated caspases. PI positive (top two quadrants for each) correspond to dead cells.

We also performed a Western Blot for the activated Caspase-3. Caspase-3 is a critical effector caspase associated with the "death cascade" and therefore a specific marker for the initiation of the apoptotic signaling pathway (*139*). Upon initiation of

apoptosis, the inactive protoenzyme of Casp-3 undergoes proteolytic processing to produce two subunits that dimerize to form the active enzyme (*139*). The smaller 17 kDa subunit produced can be detected directly with an antibody specific to the cleaved fragment (*146*). Using this active Casp-3 specific antibody, we detected the active fraction present in the cells after treatment with the apoptosis-inducing positive control camptothecin discussed above, or the NLV enzyme therapeutic. We also included a caspase inhibitor test by pre-incubating one of the samples with another pan caspase inhibitor prior to enzyme treatment (Q-VD-Oph). The treated cells were collected, counted, and diluted to a consistent cell density before being denatured and separated by SDS-PAGE. The GAPDH housekeeping gene was also detected as a loading control since the levels of this protein are not expected to vary with treatment (*147*). In support of the results obtained from flow cytometry, both positive control and uninhibited enzyme yielded detectable cleaved Casp-3 (Figure 7). Addition of the inhibitor also prevented activation. Finally, increase in the enzyme treatment concentration was correlated with decreased survival and a more extensive activation of apoptosis as defined by a brighter cleaved Casp-3 band in the Western Blot (Figure 8).

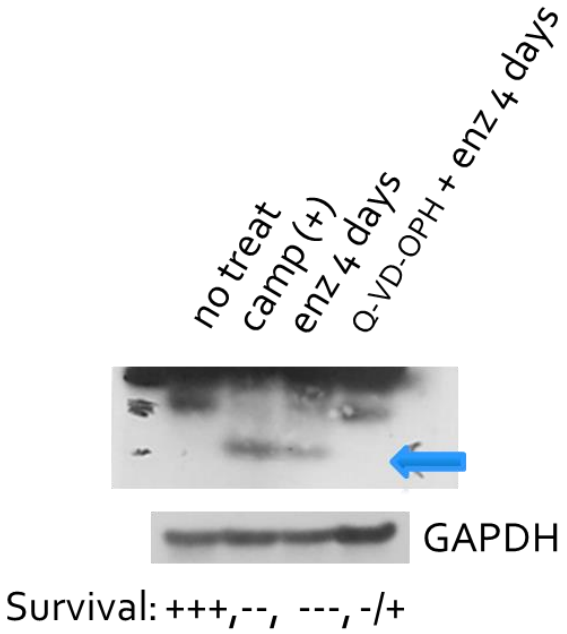

Figure 7: Western Blot for activated caspases (band at blue arrow) for (lanes left to right): untreated, positive control treated with camptothecin, treated with Variant 1 NLV, and pre-incubated with apoptosis inhibitor and then treated with Variant 1 NLV. GAPDH band used as standard for number of loaded cells.

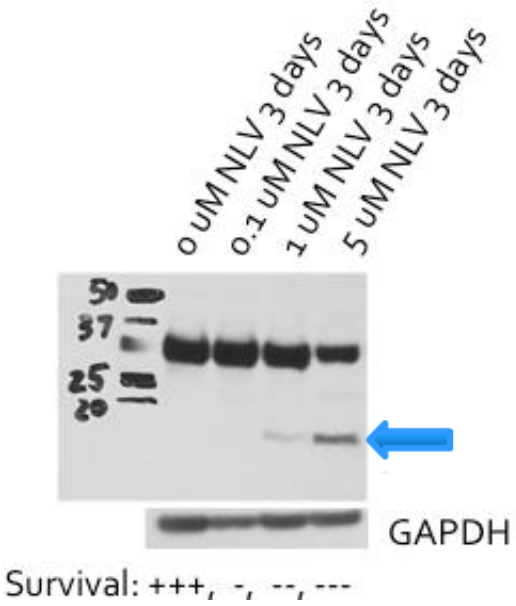

Figure 8: Western Blot for activated caspases (band at blue arrow) for several treatment concentrations of Variant 1 NLV. GAPDH band used as standard for number of loaded cells.

5.3.3 Melanoma Autophagy

Nutritional deprivation based cancer treatment lends itself to the study of the malignancy autophagic response. Autophagy is the catabolic mechanism response to starvation stress that recycles unnecessary components in a cell to regenerate raw materials and funnel them into pathways necessary for survival (*148*). As discussed in the introduction, this mechanism has been implicated as both protective and as a possible mechanism of cell death (*142*). In order to confirm an autophagic response to methionine-degrading enzyme treatment in A375 melanoma, we performed a Western Blot for LC3-II.

Microtubule-associated protein light chain 3 (LC3) is a soluble protein that exists ubiquitously in the cell (*149*). When the autophagic response is triggered, autophagosomes engulf cytoplasm along with its components. The cytosolic form of LC3, LC3-I is conjugated to a phosphatidylethanolamine to form LC3-II. This modified protein is then incorporated into autophagosomal membranes. The autophagosomes proceed to fuse with lysosomes to form autolysosomes in which cellular proteins and organelles are degraded. Therefore, the detection and quantification of LC3-II correlates with the amount of autophagic activity present within the cells (*149*).

The results are presented in Figure 9. Staurosporine is a known activator of autophagy and was used as a positive control (*150*). A375 cells were treated at three different concentrations of NLV for three days. Higher enzyme concentration during

treatment correlates with a greater detectable LC3-II signal, confirming that treatment with NLV induces an autophagic starvation stress response in A375 melanoma cells.

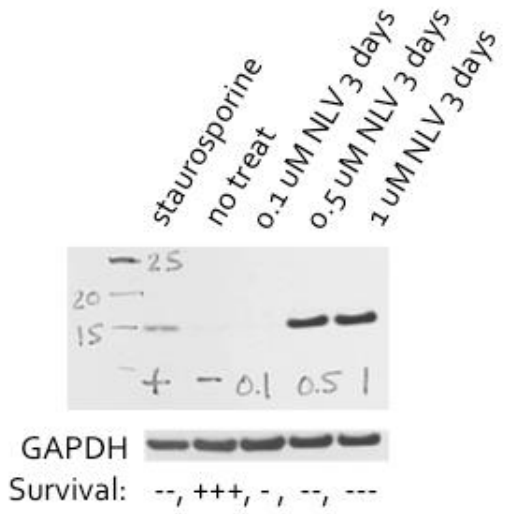

Figure 9: Western Blot for LC3-II (~17 kDa) for positive staurosporine control, negative untreated control, and several treatment concentrations of Variant 1 NLV. GAPDH band used as standard for number of loaded cells.

5.3.4 Normal Cell Cytotoxicity

The effect of enzyme treatment on human skin melanocytes was compared to the response of the A2058 melanoma cell line. An equivalent number of cells were seeded on day 0 and treated for four days in the presence of the specified amount of Variant 7 (Figure 10). At the end of treatment the dead cells were washed away and the remaining adherent living cells were counted. At the end of day 4, treatment resulted in almost

complete killing of the malignant cells. The normal cells treated at the same concentration retained 75% viability. At a lower enzyme concentration the melanocyte viability remained closer to 100%, but monitoring for any adverse effects in normal tissues remains a priority for future *in vivo* experiments.

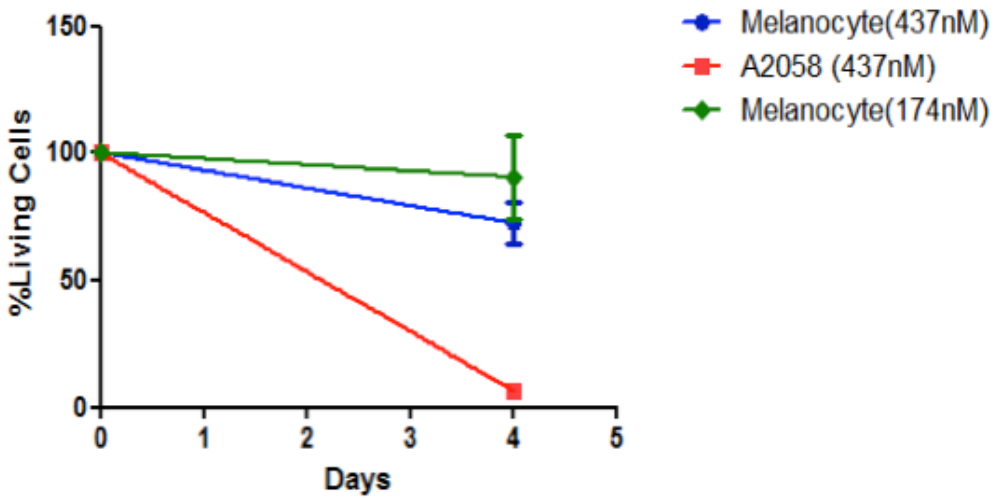

Figure 10: Cytotoxicity of normal melanocytes and melanoma A2058 with Variant 1 NLV as measured by live cell counting.

5.3.5 Prostate Carcinoma Cytotoxicity

Prostate cancer is the second leading cause of death in men and the most common neoplasm outside skin cancer (*World Cancer Report 2014*). DU145 is a "classical" cell line of human prostate cancer with moderate metastatic potential (*151*). To evaluate the therapeutic potency of Variant 7 against this cancer target, we performed a cytotoxicity

time course experiment, evaluating the EC50 daily (Figure 11). DU154 is less sensitive to treatment than A374 melanoma evaluated previously with a somewhat higher EC50 (210 nM vs. 80 nM) and a slower response (more than two days of treatment were necessary for extensive cell killing). Greater than 98% killing is ultimately observed at day 5 with $\geq$ 0.9 μM enzyme.

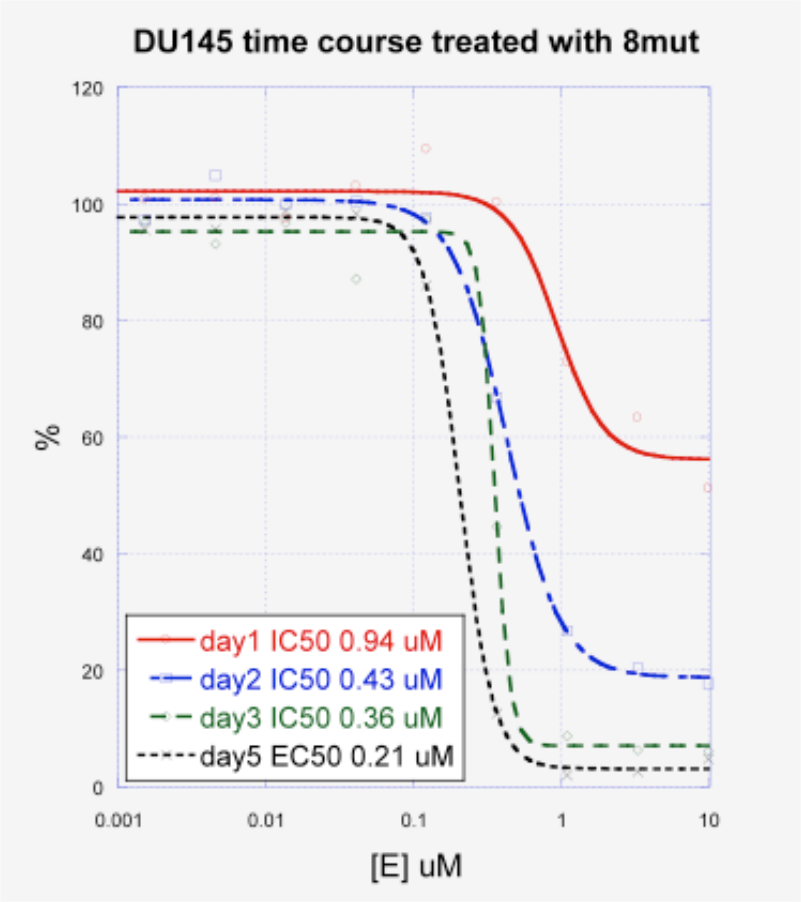

Figure 11: Cytotoxicity time course with Variant 7 (8mut) and DU145 prostate carcinoma cell line. Calculated IC50 values for each day inset.

5.3.6 Prostate Carcinoma Apoptosis

The DU145 cell line was also tested for a caspase-dependent apoptotic response to treatment by flow cytometry and FITC labeling of activated caspases. Experiments were conducted in the same way as described for A375 melanoma and results are presented in Figure 12. The positive control for apoptosis was again camptothecin. The scatter plot for this sample shows that only 14.9% of the total cells are FITC and active caspase positive, and only 1.6% are also permeable to PI. Prostate cancer cells treated with Variant 7 for two days behaved similarly to the positive control with 19.4% FITC and active caspase positive and 1.7% also permeable to PI. Almost all of the PI positive "dead" cells from enzyme and camptothecin treated samples were in Q1 and did not have a detectable FITC active caspase signal. This cell distribution suggests that though a subpopulation of treated cells has activated the apoptotic pathway, the dead cells present are active caspase free and therefore likely died by a mechanism other than caspase dependent apoptosis. It is possible that given additional time the Q4 active caspase positive/PI negative cells would lose their membrane integrity and shift into Q2, but it is notable that even the positive control lacks this population. Possible mechanisms of DU145 killing may therefore be caspase independent apoptosis or necrosis (*135, 152*).

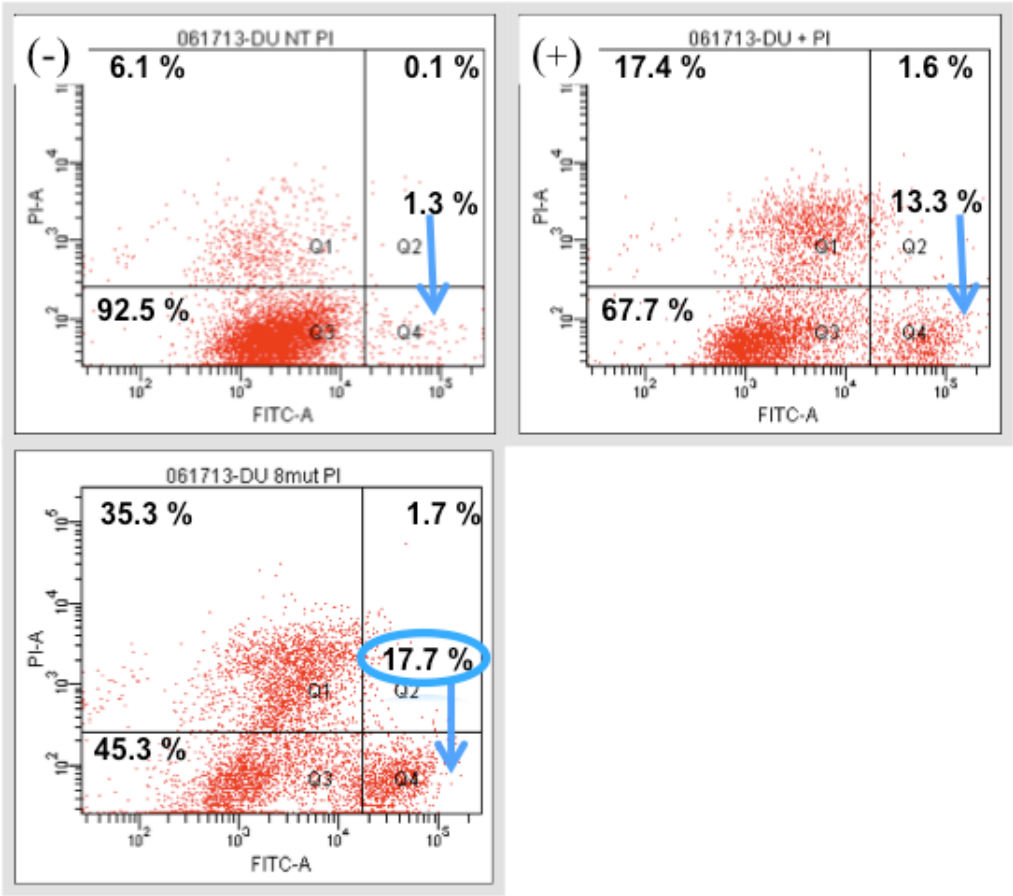

Figure 12: DU145 flow cytometric analyses showing cell integrity and presence of activated caspases. (-) Top left: negative untreated control. (+) Top right: positive control treated with camptothecin. Bottom left: treated with Variant 7 (8mut). FITC positive (right two quadrants for each) correspond to presence of activated caspases. PI positive (top two quadrants for each) correspond to dead cells.

5.3.7 Prostate Carcinoma Cell Cycle Arrest

To further explore the effects of hMGL treatment, we collaborated with Dr. John DiGiovanni from the UT Austin College of Pharmacy and Dr. Stefano Tiziani from the

School of Human Ecology. The DiGiovanni lab has extensive experience with a variety of prostate cancer cell lines, including human and mouse derived prostate carcinomas. The HMVP2 mouse prostate cancer cell line in particular has been previously defined as a valid model of human prostate cancer (*153*). Allograft efficacy experiments in the mouse with HMVP2 neoplasms can be uniquely useful because they are often more representative of the local tumor environment, vascularization, and immune system response than xenografts (*154*).

Many cancer cell types respond to methionine starvation by undergoing cell cycle arrest in the G2 phase (*3*). We tested the effect of treatment at three different concentrations of Variant 7 on the cell cycle parameters of HMVP2 cells by DNA fluorescent labeling and flow cytometry (Figure 13). The 3 day EC50 of these cells with Variant 7 was previously determined to be 100 nM. With increasing enzyme concentration, the malignant cell response becomes more pronounced and the cells cease cell division and accumulate in G2 phase.

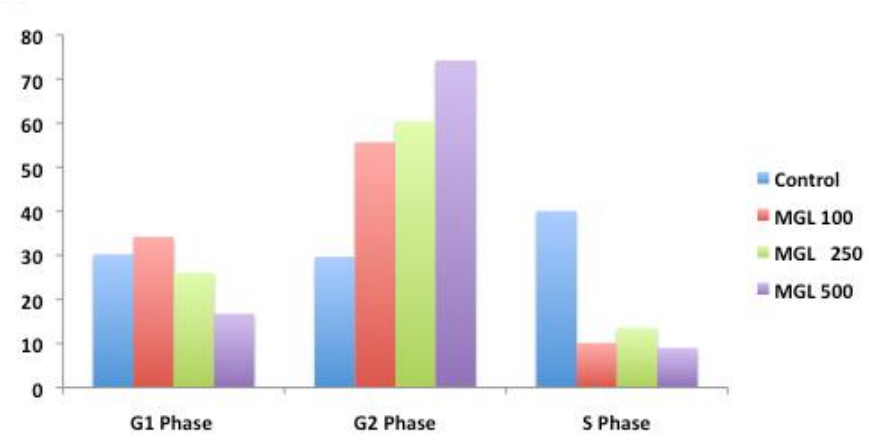

Figure 13: Percent of HMVP2 murine prostate cancer cells in each phase of the cell-division cycle as a function of Variant 7 (MGL) treatment concentration.

5.3.8 Direct Measurement of Amino Acid Levels

In collaboration with Dr. Tiziani, we tested the extracellular and intracellular levels of methionine post treatment with Variant 7. HMVP2 cells were incubated with several concentrations of enzyme and the media and cells were both analyzed by NMR spectroscopy for metabolite content (Figure 14).

Treatment resulted in complete degradation of methionine in the extracellular medium. Intracellularly, the methionine levels decreased with increasing enzyme concentration, confirming that treatment is capable of affecting the levels of the amino acid in the cytoplasm. Since this malignant cell line is expected to be incapable of recycling homocysteine back into methionine (*127*), all methionine present in the cell

must be imported from the medium or derived from autophagic degradation of cell components.

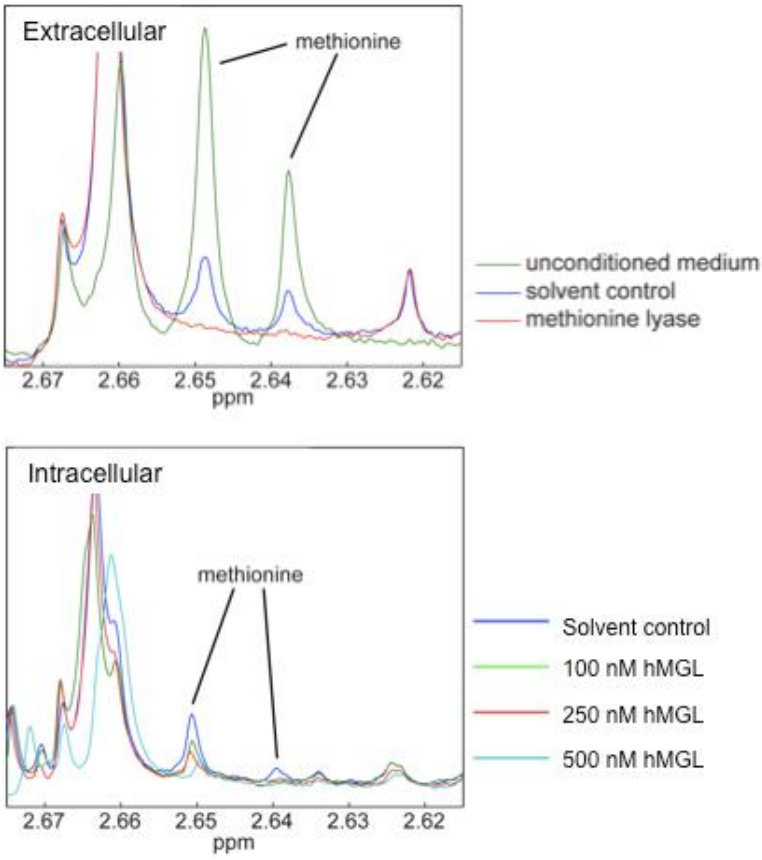

Figure 14: NMR spectroscopy results for extracellular and intracellular methionine content as a function of Variant 7 (MGL) treatment concentration with HMVP2 murine prostate cancer cells. Extracellular methionine was below detection at all concentrations.

We observed that Variant 7 treatment was also associated with a dramatic decrease in the extracellular cystine concentration (Figure 15). Cysteine is a non-essential amino acid that exists predominantly as its oxidized cystine form in serum (*155*). The depletion of cystine was either due to an increased uptake by malignant cells or direct

degradation by the enzyme therapeutic. hMGL is known to have appreciable kinetics with cysteine (Table 6, Chapter 3). We therefore measured the kinetic constants of cystine degradation with Variant 7 and found a k_{cat} and K_M of 0.74 $\pm$ 0.3 s^{-1} and 0.47 $\pm$ 0.4 mM, respectively ($k_{cat}/ K_M \sim 1.6\ s^{-1}\ mM^{-1}$).

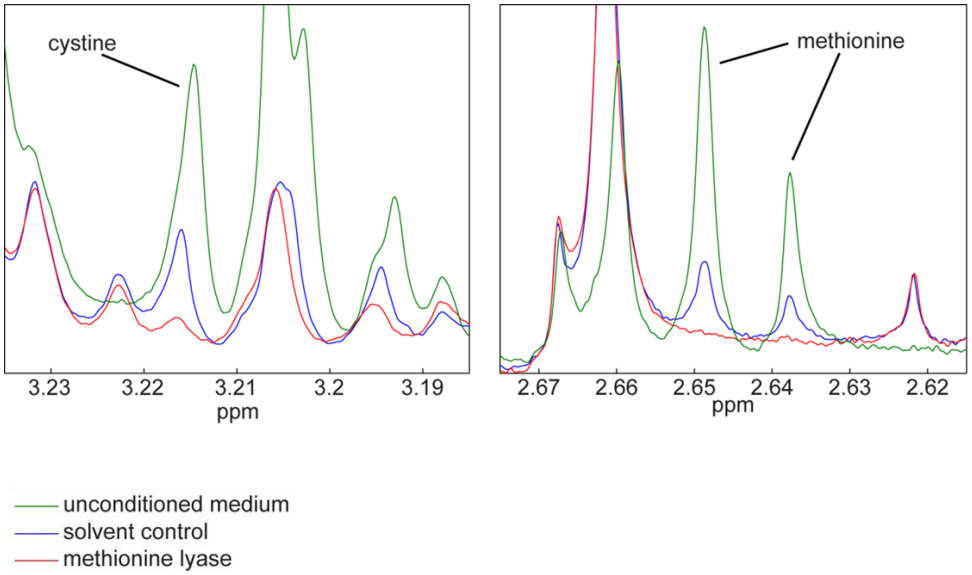

Figure 15: NMR spectroscopy results for extracellular methionine (right) and cystine (left) content in response to Variant 7 (MGL) treatment.

To evaluate the requirement of cystine for cell proliferation in a human prostate carcinoma line and to understand what role cystine degradation by Variant 7 may play in cytotoxicity we incubated DU145 cells with dropout media supplemented with cystine, methionine, or both, as well as full media treated with Variant 7 (Figure 16). Although

the absence of methionine results in ~50% decrease in proliferation as measured by the MTS assay, the absence of cystine with or without methionine ceases all growth.

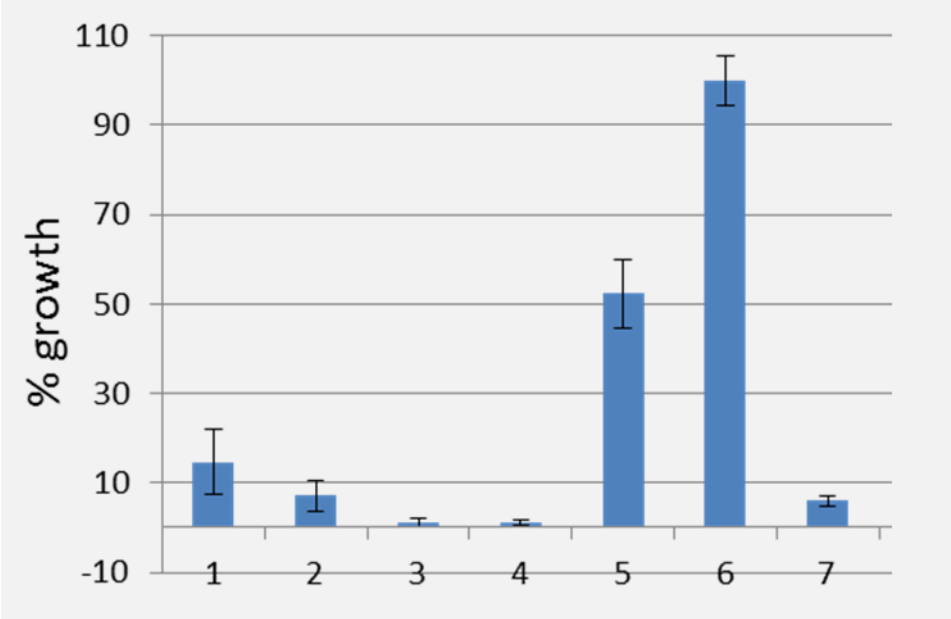

Column	Condition with DU145 cell line
1	cystine (C), methionine (M), glutamine (G) free RPMI media
2	+ FBS (fetal bovine serum)
3	+ FBS and G
4	+ FBS, G, and M
5	+ FBS, G, and C
6	+ FBS, G, M, and C
7	+ FBS, G, M, C, and 3 µM Variant 7

Figure 16: DU145 cell response to dropout media. The composition for each condition (1-7) is listed in the table.

5.3.9 Reactive Oxygen Species in Prostate Carcinoma

Reactive oxygen species (ROS) are byproducts of normal aerobic metabolism and must be neutralized by glutathione, which acts as the main antioxidant within the cell (*156*). Without sufficient glutathione, ROS levels can rise and lead to oxidative damage and cell death (*157*). Many malignant cells are known to have higher glutathione levels than normal tissues, making them less sensitive to oxidative stress (*158*) and prostate cancer specifically has been shown to be associated with a high degree of ROS production that correlates with an aggressive phenotype (*159*). Methionine and cystine are both precursors for glutathione synthesis. We therefore expect that depleted levels of these amino acids in the treatment media will correspond to lowered intracellular glutathione concentrations and a higher level of ROS.

We analyzed the ROS content of HMVP2 cells with and without treatment with Variant 7. The cells were incubated with a cell permeable chemical that reacts with ROS to yield a green fluorescent product detectable by flow cytometry. Results are presented in Figure 17. Enzyme treatment correlates with an increase in ROS levels, suggesting that ROS may be playing a role in treatment-induced cell damage and contributing to the factors that lead to HMVP2 cell death.

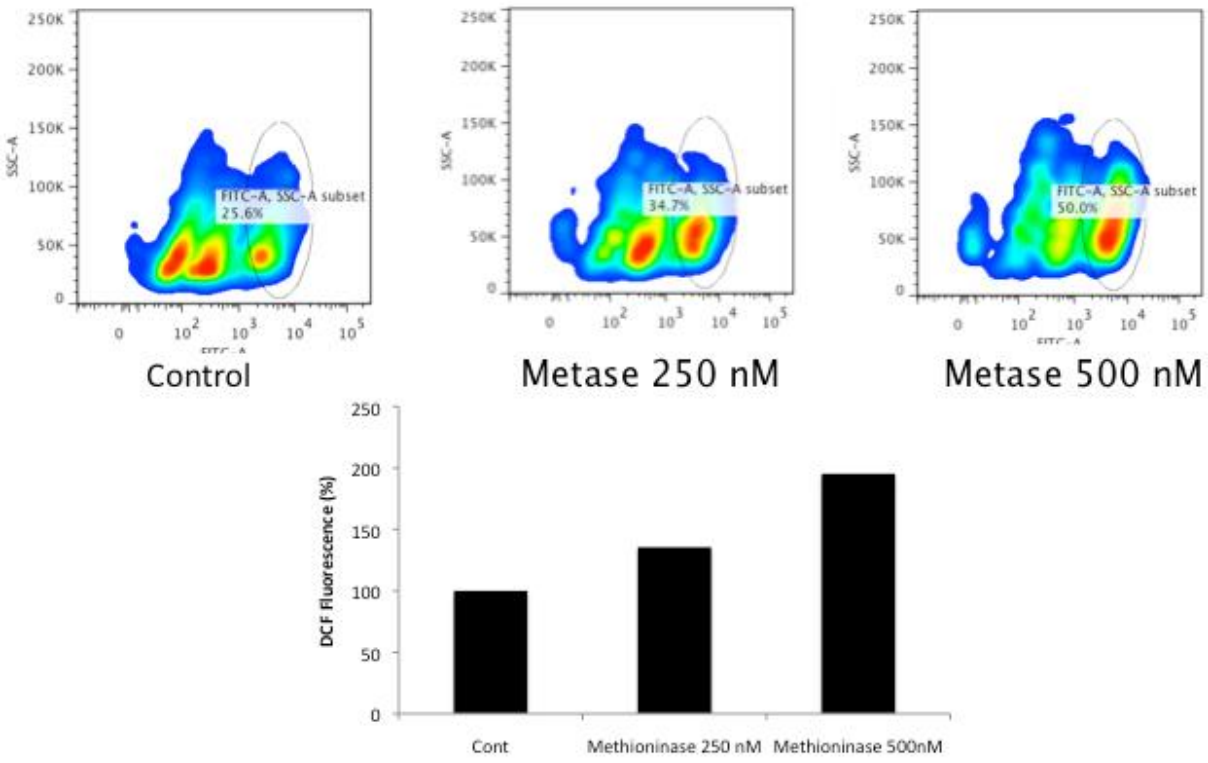

Figure 17: Flow cytometry results measuring the Reactive Oxygen Species (ROS) content of HMVP2 cells at different Variant 7 (Metase) treatment concentrations.

5.3.10 Cancer Cytotoxicity Assays with Variant 9

Finally, we tested the effect of Variant 9 treatment on the survival and proliferation of several cancer cell lines. This enzyme variant has a 10 fold higher methionine k_{cat}/K_M than NLV and is approximately 30% faster than Variant 7 (Table 2, Chapter 3). As discussed in the Introduction to this chapter, melanoma and prostate cancer have both been reported to be sensitive to methionine starvation. In addition, we

examined the effect of enzyme administration on HPAF-II pancreatic cancer cell line and the U138 glioblastoma cell line (*160, 161*). All of these cancers are known to be highly aggressive and have limited treatment option (*132, 133, 162, 163*).

Cells were seeded in a 96 well plate and treated with a range of Variant 9 enzyme concentrations on day 0. On day 3, cells were incubated with fresh enzyme-free media. The cells were allowed to recover for 24 hours and were tested for viability by the MTS assay discussed previously. The EC50 values were calculated and are reported in Table 9 (curves presented in Figure 18).

The EC50 values for Variant 9 treatment are at their lowest at 18 nM with melanoma cell line A2058, and slightly higher at 63 nM with PC3, a highly aggressive line of prostate cancer (*164*). In the case of the pancreatic malignant cell line, it appears that even though the EC50 is a fairly low 38 nM, even the highest enzyme concentration is insufficient to kill > 90% of cells. This response is consistent with a small sub-population with a diminished methionine starvation sensitivity compared to the rest of the population. The evasion of drug treatment induced cell death by a sub-population of cancer cells has previously been attributed to the variability of protein dynamics, with the resistant cells exhibiting protein expression profiles conducive to survival (*165*). The surviving cells can quickly overtake the population and become the new dominant cell in the tumor that is now resistant to the therapeutic (*166*). Drug treatment itself can also induce sub-population resistance by applying stress that can provoke adaptive evolution of the genome (*167*).

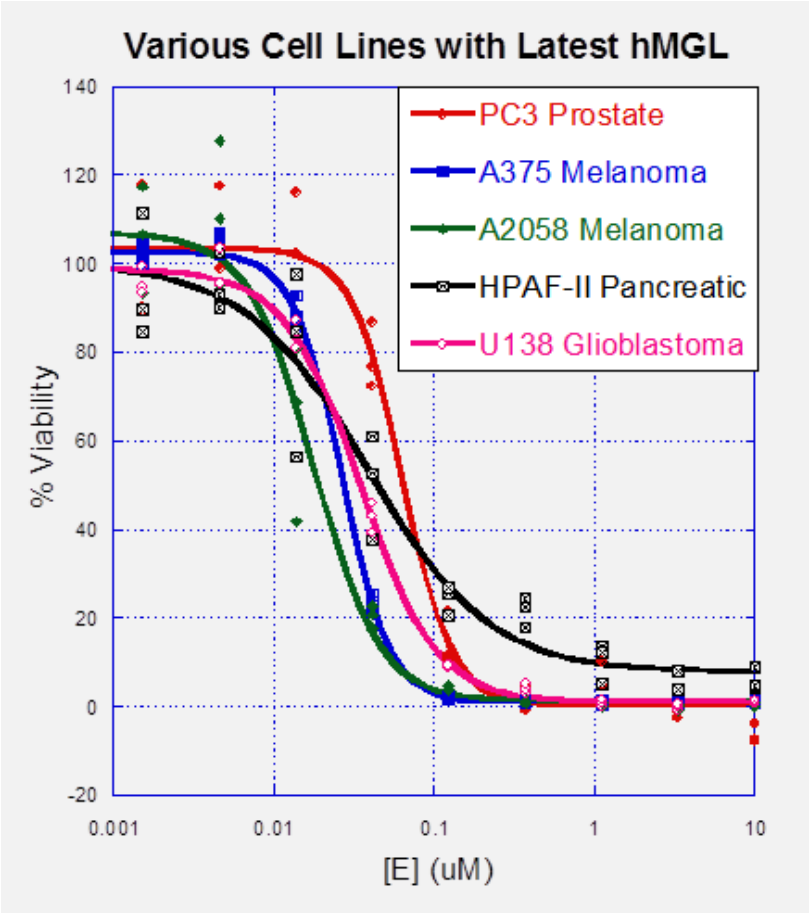

Figure 18: Cytotoxicity dose dependence of a selection of malignant cell lines treated with Variant 9.

Cell Line	Variant 9 EC_{50} (nM)
PC3 Prostate	63
A375 Melanoma	26
A2058 Melanoma	18
HPAF-II Pancreatic	38
U138 Glioblastoma	35

Table 2: Calculated EC50 values for treatment in Figure 18.

5.4 Summary and Discussion

We have shown that an engineered human enzyme that degrades methionine has cytotoxic effects with a wide variety of cancer cell lines. An enhancement of this activity through engineering correlates with improved cytotoxicity profile across all malignancies tested. Variant 9 treatment of melanoma cell lines A2058 and A375 in particular led to rapid and extensive cell killing with an EC50 that was < 26 nM at three days. We investigated the mechanism of cell death of the A375 cell line and concluded that the majority of cells die by caspase-dependent apoptosis. Pretreatment with an inhibitor of apoptosis promotes cell survival and supports this hypothesis. Based on the presence of LC-II in this cell line after treatment with NLV, we know that the cells initiate an autophagic response to starvation stress to recycle the raw materials critical for survival, but that any protective effects of this process are insufficient to prevent cell death.

The prostate cancer cell lines tested (PC3, DU145, HMVP2) were also sensitive to treatment, but had somewhat higher EC50 values that melanoma. DU145 also exhibited a slower response to the drug than A375 cells. Though active caspases could be detected in a subpopulation of DU145 cells, none of the PI permeable dead cells were caspase positive, ruling out caspase dependent apoptosis as the dominant cell death mechanism. Programmed cell death dysregulation is a well-defined causative factor in the development and progression of cancer (*168*), as well as a resistance to the body's own immune responses and a barrier to efficacy of chemotherapeutics (*169*). However, even

in the absence of a caspase mediated programmed death response, the prostate carcinoma cells readily respond to treatment by a yet not well understood mechanism of cell death.

We determined that in addition to catalyzing the hydrolysis of methionine, the engineered enzyme is a potent cystine-lyase. Cysteine (and cystine, its predominant disulfide form in serum) is not considered to be an essential amino acid as many tissues are capable of synthesizing it through the combination of homocysteine and serine in the transsulfuration pathway (*170, 171*). Numerous cancer cells, likely due to their increased rate of protein synthesis and requirement for antioxidants, have been shown to be critically dependent on the serum pool of this amino acid and satisfy their demand through xCT(-) antiporter mediated exchange of glutamine for extracellular cystine (*172*). Cysteine is critical for maintaining the correct redox potential of the cell and its surrounding environment through two mechanisms. Intracellularly, like methionine, cysteine is a precursor in the biosynthesis of glutathione, a potent antioxidant (*156*). Additionally, some tumors may export cysteine back into the extracellular medium as a method of modulating their surrounding redox environment (*187*).

Based on dropout media experiments, DU145 prostate carcinoma cells have an absolute requirement for cystine/cysteine. This has been previously shown by the blocking of the xCT(-) antiporter with sulfosalazine and a resulting 100% inhibition of growth *in vitro* (*173*). It appears that in the case of HVMP2 murine prostate cells, the promiscuous activity of the engineered enzyme against methionine, cystine, and cysteine

works synergistically to arrest the cells in G2 phase, lead to a buildup of intracellular ROS, and ultimately induce cell death.

The understanding of the mechanisms of cell death and other responses to treatment with the human methionine depleting enzyme aids in the selection of appropriate targets for the drug, prediction of effects on normal tissues, and identification of effective combination therapies. We have shown that treatment with NLV, Variant 7, and Variant 9 is correlated with an induction of autophagy and cell death by apoptosis in A375 melanoma cell line. Prostate cancer cell line DU145 also responds to treatment by undergoing extensive cell death, though the mechanism of the process remains unclear. The mouse prostate model HMVP2 displays an arrest in the G2 phase and a buildup of reactive oxygen species upon incubation with hMGL. The novel human enzyme Variant 9 is capable of inducing extensive cell killing of a variety of neoplasms at therapeutically useful doses. Finally, we have shown that hMGL is also capable of degrading cystine to operate as a dual amino acid depletion treatment that is expected to be more potent than methionine depletion alone.

5.5 METHODS

Cell culture

Androgen insensitive human prostate cancer cell lines DU145 and PC-3, Melanoma cell lines A375 and A2058, human normal cell melanocytes, HPAF-II

pancreatic cancer, and U138 glioblastoma cell line were all purchased from ATCC. Cells were maintained in either RPMI-1640 medium or DMEM with 10% FBS. The prostate tumor cell line, HMVP2, was derived from the ventral prostate of a one year old HiMyc mouse (*174*) and cultured in RPMI-1640 medium containing 10% FBS (Blando, J. Saha, A, Kiguchu, K., and DiGiovanni, J., unpublished studies). Cells were cultured in 95% air and 5% CO_2 incubator at 37°C.

Cytotoxicity of hMGL Variants

The *in vitro* cytotoxicity of hCGL-NLV, pMGL, Variant 7, and Variant 9 was compared in the a variety of cell lines. Typically cells seeded at ~3000 cells/well were incubated in 96-well plates and varying amounts of enzyme were added 24 hours later. After 3-5 days exposure, proliferation was measured by MTS assay and plotted to calculate apparent IC_{50} values (*175*). For melanocyte cytotoxicity, cells were counted visually with a hemocytometer.

Cell cycle analysis

HMVP2 cells were treated with various concentrations of hMGL for 24 h. After that cells were harvested and washed twice with phosphate buffered saline (PBS) and then fixed in ice cold 70% ethanol overnight at 20 °C (PMID 20686221). Following fixation, cells were washed and resuspended in PBS containing RNase (250m g/ml) and

incubated for 30 min at 37 °C. Cells were then treated with PI (50m g/ml) solution, incubated for 30 min in the dark, and distribution of different phase of cell-cycle was analyzed by Guava-based flow cytometry (Millipore)

Apoptosis assay

The percentage of apoptotic cells was determined using CaspACE™ FITC-VAD-FMK In Situ Marker (Promega) with the pan Caspase (active) FITC Staining Kit (abcam) apoptosis detection kit following the recommended protocol. Active caspase positive and PI positive cells were detected by a BD LSRFortessa cell analyzer.

Measurement of Reactive Oxygen Species

The intracellular reactive oxygen species (ROS) was measured by using DCFDA fluorescence. Briefly, HMVP2 cells were treated with indicated concentrations of hMGL for 24h. After the indicated time point, the cells were washed with PBS twice and then stained by H_2DCFDA (20 μmol/L, Invitrogen) at 37ºC for 30 min. After washing with PBS, fluorescence intensity was measured using a flow cytometer (Guava, Millipore).

Western Blotting

Cells were treated with indicated concentrations of enzyme or control substance for the designated time. After incubation, both adherent (live) and floating (dead) cells

were collected, resuspended in PBS, and lysed by incubating them at 95°C for 10 minutes. Proteins were separated by 12% SDS-PAGE gel and transferred to nitrocellulose membrane. After blocking in 5% BSA for 1h, the membranes were probed with specific primary antibodies for overnight at 4°C. Following secondary antibody incubation, the membranes were visualized using commercial chemiluminescent detection kit (Pierce Biotechnology).

NMR acquisition

Frozen extracellular media were thawed on ice and then separated from protein by ultrafiltration (Nanosep 3K OMEGA, Pall Corporation, MI) at 4°C (*176, 177*). An aliquot of 160 μL of filtered media was placed in 3 mm MRS tube (Norell, Landisville, NJ, USA) containing 40 μL of phosphate buffer (final concentration 100 mM, pH 7.0), sodium 3-(trimethylsilyl)propionate-2,2,3,3-d4 (TMSP, 0.1 mM final concentration; Cambridge Isotope Laboratories, Andover MA), 0.75% (w/v) sodium azide and 10% D_2O (final concentration; Cambridge Isotope Laboratories).

Extraction of intracellular metabolites was performed as described previously (*178*). Briefly, extraction of intracellular metabolites from cell pellets was performed using a modified Bligh-Dyer procedure (*179*). Samples were dried using a refrigerated centrifugal vacuum concentrator CentriVap (Labconco, Kansas City, MO). The dried polar extracts were redissolved in 90% H_2O/10% D_2O (99.8 atom%; Cambridge Isotopes

Laboratories, Andover MA) prepared as 100 mM phosphate buffer (pH 7.0), containing 0.1 mM sodium 3-(trimethylsilyl)propionate-2,2,3,3-d4 (TMSP, Cambridge Isotope Laboratories, Andover MA) as internal reference.

One dimensional ^{1}H-MRS spectra were acquired on the extra and intracellular metabolite fractions using a 700-MHz Bruker Avance spectrometer equipped with a TCI cryoprobe and SampleXpress high-throughput robotics. (Bruker BioSpin Corp., MA, USA). Each sample was allowed to equilibrate for 5 min inside the probe before starting data acquisition. The acquisition parameters for 1D spectra were a 90° flip angle, 6 kHz spectral width, 1 s relaxation delay, 32,000 data points, 8 dummy scans, and 6 kHz spectral width. Excitation sculpting pulse sequence was implemented to suppress the water signal (*180*). All the MRS datasets were processed using MetaboLab (*181*) in the MATLAB programming environment (MathWorks, Inc., Natick, MA). MRS resonances were assigned and the metabolites quantified using the Chenomx NMR Suite and other available libraries (*182-185*).

Chapter 6: Major Findings and Future Recommendations

6.1 Major Findings

It has been known for nearly half a century that many cancers have an absolute requirement for the amino acid methionine (L-Met). Studies have shown that in the absence of L-Met, sensitive neoplasms experience cell cycle arrest and perish. Without the metabolic deviations that characterize L-Met auxotrophs, normal cells are able to grow on precursors such as homocysteine and tolerate L-Met starvation. The differential requirement for this amino acid between normal and tumor cells has been exploited through enzymatic serum degradation of L-Met by a bacterial methionine-γ-lyase. Though MGL was able to deplete L-Met to therapeutically useful levels in animal models and exert a significant cytotoxic effect on malignant cell lines *in vitro* and on tumor xenografts *in vivo*, the clinical implementation of this enzyme is hampered by its short serum half-life and potential for catastrophic immune response.

We have circumvented the limitations of the bacterial MGL by re-engineering its human structural homologue cystathionine-γ-lyase to accept L-Met as a substrate. The introduction of three critical mutations to the CGL scaffold by the process of rational design, saturation mutagenesis, and screening yielded a novel human L-Met degrading enzyme CGL-NLV. Due to its human origin, CGL-NLV is unlikely to elicit adverse immunological responses in the patient and displays a 15 fold longer serum half-life than

bacterial MGL. Furthermore, the human enzyme cytotoxicity against a variety of neuroblastoma cell lines was similar to MGL and administration of CGL-NLV in athymic mouse Lan-1 neuroblastoma xenografts resulted in complete retardation of tumor growth.

In order to decrease the dosage requirement for our therapeutic, we have applied the technique of phylogenetic analysis to perform additional enzyme engineering. Sequence alignments of paralogs within the gamma lyase family identified positions of importance for activity and specificity. Iterative rounds of mutagenesis and screening yielded next generation enzymes with up to 10 fold better L-Met degrading activity than CGL-NLV (Variant 9). The additional mutations were shown to not negatively impact serum stability and an improved variant (Variant 7) was capable of reducing serum L-Met to target levels in a mouse model at a clinically useful dose.

We tested human L-Met degrading enzymes against a variety of cancer cell lines including neuroblastoma, pancreatic carcinoma, glioblastoma, melanoma, and prostate carcinoma. In all cases, treatment led to extensive cell killing. Second-generation enzymes with faster L-Met-degradation kinetics displayed EC50 values in the nM range with all lines tested. We also studied the treatment response of melanoma and prostate carcinoma in more detail. The melanoma cell line A375 undergoes rapid and extensive apoptosis in spite of initiating an (assumed to be protective) autophagic response to stress. Prostate cancer was shown to undergo non apoptotic cell death and to experience G2 phase cell cycle arrest and a buildup of intracellular reactive oxygen species. Variant 7 hMGL was also found to have an appreciable activity against cystine that may function

synergistically to deprive cancer cells of multiple required sulfur-containing amino acids and enhance the potency of the drug. Finally, since the mode of action of hMGL is systemic and does not require breaching the blood-brain barrier, we believe this enzyme may be particularly well suited for the treatment of sensitive tumors that arise from or metastasize to the central nervous system- a target that has historically been limited in treatment options.

We have designed a high-throughput fluorescence activated cell sorting (FACS) assay for detecting the catalytic activity of amino acid degrading enzymes in bacteria, at the single cell level. This assay relies on coupling the catalytic activity to the synthesis of a GFP reporter in an appropriate *E.coli* genetic background. To demonstrate the utility of the assay in the case of methionine-γ-lyase engineering, we generated a strain auxotrophic for isoleucine that can be rescued by α-ketobutyrate, a product of the L-Met degradation reaction. We were able to enrich a 1:10,000 population of MGL:CGL expressing clones 5,000 fold in only three rounds of sorting.

6.2 Proposals for Future Work

Further improvement in enzyme kinetic parameters should be possible through additional engineering. The positions of interest identified by phylogenetic analysis can be reengineered through saturation mutagenesis to select residues that afford enhanced activity in the context of the human enzyme active site and the other mutations. Synergy of various positions can be investigated by generating larger libraries and selecting for

clones with the greatest activities by the high throughput GFP reporter screen presented in Chapter 4. The screen conditions should be re-optimized for the latest variants by adjusting parameters such as expression time, temperature, IPTG inducer concentration, and others. We also plan to investigate the potential benefits of using homocysteine in place of, or in conjunction with, methionine to achieve necessary rates of α-ketobutyrate production. The gamma elimination of homocysteine also produces α-ketobutyrate and we have previously reported that for a given enzyme variant, homocysteine hydrolysis activity correlates with methionine and is generally significantly higher (Chapters 1 & 3). Further exploration of the reaction chemistry and mechanism of different variants through the analysis of steady and non-steady state reaction kinetics will be performed and should yield important information for both scientific understanding and future engineering.

Forthcoming experiments with numerous cancer cell lines will examine the general importance of cystine degradation as a complement to methionine depletion for enzyme cytotoxicity and efficacy. Additional studies will be performed to better understand the exact mechanism of cell killing of prostate carcinoma and other neoplasms that do not die by readily defined caspase-dependent apoptosis. We will also investigate the benefits of combining our enzyme therapeutic with other anti-cancer drugs. Combination therapies are a powerful tool in the treatment of cancer and we plan to identify those drugs that synergize well with the engineered methionine/cystine degrading enzyme. We will conduct cytotoxicity experiments with a variety of cancer

cell lines in combination with the chemotherapeutic drugs most commonly used as the standard of care such as: carmustine(BCNU), cisplatin, cyclophosphamide, etoposide, methotrexate, temozolomide, thiotepa and vinblastine/vincristine as well as autophagy inhibitors and inducers such as chloroquine and rapamycin. Those combinations that show a high degree of synergy as defined by their combination index (CI) will be tested for toxicity with "normal" human cell lines and efficacy *in vivo (186)*.

References

1. Shen, L.-J., Beloussow, K., and Shen, W.-C. (2006) Modulation of arginine metabolic pathways as the potential anti-tumor mechanism of recombinant arginine deiminase, *Cancer Lett 231*, 30-35.
2. Wetzler, M., Sanford, B. L., Kurtzberg, J., DeOliveira, D., Frankel, S. R., Powell, B. L., Kolitz, J. E., Bloomfield, C. D., and Larson, R. A. (2007) Effective asparagine depletion with pegylated asparaginase results in improved outcomes in adult acute lymphoblastic leukemia: Cancer and Leukemia Group B Study 9511, *Blood 109*, 4164.
3. Cellarier, E., Durando, X., Vasson, M. P., Farges, M. C., Demiden, A., Maurizis, J. C., Madelmont, J. C., and Chollet, P. (2003) Methionine dependency and cancer treatment, *Cancer treatment reviews 29*, 489-499.
4. Dinndorf, P. A., Gootenberg, J., Cohen, M. H., Keegan, P., and Pazdur, R. (2007) FDA drug approval summary: pegaspargase (oncaspar) for the first-line treatment of children with acute lymphoblastic leukemia (ALL), *Oncologist 12*, 991-998.
5. Pui, C. H. (2009) Toward a total cure for acute lymphoblastic leukemia, *J Clin Oncol 27*, 5121-5123.
6. Pieters, R., Hunger, S. P., Boos, J., Rizzari, C., Silverman, L., Baruchel, A., Goekbuget, N., Schrappe, M., and Pui, C. H. (2011) L-asparaginase treatment in acute lymphoblastic leukemia: a focus on Erwinia asparaginase, *Cancer 117*, 238-249.
7. Avramis, V. I., and Panosyan, E. H. (2005) Pharmacokinetic/pharmacodynamic relationships of asparaginase formulations: the past, the present and recommendations for the future, *Clin Pharmacokinet 44*, 367-393.
8. Breillout, F., Antoine, E., and Poupon, M. F. (1990) Methionine dependency of malignant tumors: a possible approach for therapy, *J Natl Cancer Inst 82*, 1628-1632.
9. Datsenko, K. A., and Wanner, B. L. (2000) One-step inactivation of chromosomal genes in Escherichia coli K-12 using PCR products, *Proc Natl Acad Sci U S A 97*, 6640-6645.
10. Durando, X., Thivat, E., Farges, M., Cellarier, E., D Incan, M., Demidem, A., Vasson, M., Barthomeuf, C., and Chollet, P. (2008) Optimal methionine-free diet duration for nitrourea treatment: a Phase I clinical trial, *Nutrition and cancer 60*, 23-30.
11. Halpern, B., Clark, B., Hardy, D., Halpern, R., and Smith, R. (1974) The effect of replacement of methionine by homocystine on survival of malignant and normal adult mammalian cells in culture, *Proceedings of the National Academy of Sciences of the United States of America 71*, 1133.
12. Kokkinakis, D. M., Schold, S. C., Hori, H., and Nobori, T. (1997) Effect of long-term depletion of plasma methionine on the growth and survival of human brain tumor xenografts in athymic mice, *Nutrition and cancer 29*, 195-204.
13. Kreis, W. (1979) Tumor therapy by deprivation of L-methionine: rationale and results, *Cancer treatment reports 63*, 1069.
14. Kreis, W., Baker, A., Ryan, V., and Bertasso, A. (1980) Effect of nutritional and enzymatic methionine deprivation upon human normal and malignant cells in tissue culture, *Cancer research 40*, 634.

15. Kreis, W., and Goodenow, M. (1978) Methionine requirement and replacement by homocysteine in tissue cultures of selected rodent and human malignant and normal cells, *Cancer research 38*, 2259.
16. Thomas, T., and Thomas, T. J. (2003) Polyamine metabolism and cancer, *J Cell Mol Med 7*, 113-126.
17. Megosh, L., Gilmour, S. K., Rosson, D., Soler, A. P., Blessing, M., Sawicki, J. A., and O'Brien, T. G. (1995) Increased frequency of spontaneous skin tumors in transgenic mice which overexpress ornithine decarboxylase, *Cancer Res 55*, 4205-4209.
18. Auvinen, M., Paasinen, A., Andersson, L. C., and Holtta, E. (1992) Ornithine decarboxylase activity is critical for cell transformation, *Nature 360*, 355-358.
19. Frau, M., Feo, F., and Pascale, R. M. (2013) Pleiotropic effects of methionine adenosyltransferases deregulation as determinants of liver cancer progression and prognosis, *J Hepatol 59*, 830-841.
20. Bertino, J. R., Lubin, M., Johnson-Farley, N., Chan, W. C., Goodell, L., and Bhagavathi, S. (2012) Lack of expression of MTAP in uncommon T-cell lymphomas, *Clin Lymphoma Myeloma Leuk 12*, 306-309.
21. Ashe, H., Clark, B. R., Chu, F., Hardy, D. N., Halpern, B. C., Halpern, R. M., and Smith, R. A. (1974) N5-methyltetrahydrofolate: homocysteine methyltransferase activity in extracts from normal, malignant and embryonic tissue culture cells, *Biochemical and biophysical research communications 57*, 417.
22. Halpern, B. C., Clark, B. R., Hardy, D. N., Halpern, R. M., and Smith, R. A. (1974) The effect of replacement of methionine by homocystine on survival of malignant and normal adult mammalian cells in culture, *Proceedings of the National Academy of Sciences 71*, 1133-1136.
23. Poirier, L. A., and Wilson, M. J. (1980) The elevated requirement for methionine by transformed rat liver epithelial cells in vitro, *Annals of the New York Academy of Sciences 349*, 283-293.
24. Kenyon, S. H., Waterfield, C. J., Timbrell, J. A., and Nicolaou, A. (2002) Methionine synthase activity and sulphur amino acid levels in the rat liver tumour cells HTC and Phi-1, *Biochemical pharmacology 63*, 381-391.
25. Stabler, S. P., Marcell, P. D., Podell, E. R., and Allen, R. H. (1987) Quantitation of total homocysteine, total cysteine, and methionine in normal serum and urine using capillary gas chromatography-mass spectrometry, *Anal Biochem 162*, 185-196.
26. Kokkinakis, D. M., Schold, S. C., Hori, H., and Nobori, T. (1997) Effect of long-term depletion of plasma methionine on the growth and survival of human brain tumor xenografts in athymic mice, *Nutr Cancer 29*, 195-204.
27. Goseki, N., Yamazaki, S., Shimojyu, K., Kando, F., Maruyama, M., Endo, M., Koike, M., and Takahashi, H. (1995) Synergistic effect of methionine-depleting total parenteral nutrition with 5-fluorouracil on human gastric cancer: a randomized, prospective clinical trial, *Jpn J Cancer Res 86*, 484-489.
28. Epner, D. E. (2001) Can dietary methionine restriction increase the effectiveness of chemotherapy in treatment of advanced cancer?, *J Am Coll Nutr 20*, 449.

29. Xiao, H., Cao, W., Yin, H., Lin, Y., and Ye, S. (2001) Influence of L-methionine-deprived total parenteral nutrition with 5-fluorouracil on gastric cancer and host metabolism, *WORLD JOURNAL OF GASTROENTEROLOGY 7*, 698-701.
30. Tan, Y., Xu, M., Tan, X., Wang, X., Saikawa, Y., Nagahama, T., Sun, X., Lenz, M., and Hoffman, R. M. (1997) Overexpression and large-scale production of recombinant L-methionine-a-deamino-g-mercaptomethane-lyase for novel anticancer therapy, *Protein Expression and Purification 9*, 233-245.
31. Tan, Y., Zavala, J. S. R., Xu, M., Zavala, J. J. R., and Hoffman, R. M. (1996) Serum methionine depletion without side effects by methioninase in metastatic breast cancer patients, *Anticancer research 16*, 3937-3942.
32. Lishko, V. K., Lishko, O. V., and Hoffman, R. M. Depletion of serum methionine by methioninase in mice, *Anticancer research 13*, 1465.
33. Tan, Y., Xu, M., Guo, H., Sun, X., Kubota, T., and Hoffman, R. M. (1996) Anticancer efficacy of methioninase in vivo, *Anticancer research 16*, 3931-3936.
34. Yoshioka, T., Wada, T., Uchida, N., Maki, H., Yoshida, H., Ide, N., Kasai, H., Hojo, K., Shono, K., and Maekawa, R. (1998) Anticancer efficacy in vivo and in vitro, synergy with 5-fluorouracil, and safety of recombinant methioninase, *Cancer Research 58*, 2583-2587.
35. Yang, Z., Wang, J., Lu, Q., Xu, J., Kobayashi, Y., Takakura, T., Takimoto, A., Yoshioka, T., Lian, C., and Chen, C. (2004) PEGylation confers greatly extended half-life and attenuated immunogenicity to recombinant methioninase in primates, pp 6673-6678, AACR.
36. Yang, Z., Wang, J., Yoshioka, T., Li, B., Lu, Q., Li, S., Sun, X., Tan, Y., Yagi, S., and Frenkel, E. P. (2004) Pharmacokinetics, methionine depletion, and antigenicity of recombinant methioninase in primates, pp 2131-2138, AACR.
37. Tan, Y., Zavala, J. S. R., Han, Q., Xu, M., Sun, X., Tan, X., Magana, R., Geller, J., and Hoffman, R. M. (1997) Recombinant methioninase infusion reduces the biochemical endpoint of serum methionine with minimal toxicity in high-stage cancer patients, *Anticancer research 17*, 3857-3860.
38. Sridhar, V., Xu, M., Han, Q., Sun, X., Tan, Y., Hoffman, R. M., and Prasad, G. S. (2000) Crystallization and preliminary crystallographic characterization of recombinant L-methionine--deamino--mercaptomethane lyase (methioninase), *Acta Crystallographica Section D: Biological Crystallography 56*, 1665-1667.
39. Nakamura, T., Esaki, N., Sugiem, K., Beresov, T., Tanaka, H., and Soda, K. (1984) Purification of bacterial L-methionine-lyase, *Anal. Biochem 138*, 421–424.
40. Hori, H., Takabayashi, K., Orvis, L., Carson, D. A., and Nobori, T. (1996) Gene cloning and characterization of Pseudomonas putida L-methionine-alpha-deamino-gamma-mercaptomethane-lyase, *Cancer Research 56*, 2116-2122.
41. Esaki, N., and Soda, K. (1987) L-methionine gamma-lyase from Pseudomonas putida and Aeromonas, *Methods in enzymology 143*, 459.
42. Ito, S., Nakamura, T., and Eguchi, Y. (1976) Purification and characterization of methioninase from Pseudomonas putida, *Journal of Biochemistry 79*, 1263.
43. Kudou, D., Misaki, S., Yamashita, M., Tamura, T., Takakura, T., Yoshioka, T., Yagi, S., Hoffman, R. M., Takimoto, A., and Esaki, N. (2007) Structure of the Antitumour Enzyme

L-Methionine {gamma}-Lyase from Pseudomonas putida at 1.8 A Resolution, *Journal of Biochemistry 141*, 535.

44. Takakura, T., Takimoto, A., Notsu, Y., Yoshida, H., Ito, T., Nagatome, H., Ohno, M., Kobayashi, Y., Yoshioka, T., and Inagaki, K. (2006) Physicochemical and pharmacokinetic characterization of highly potent recombinant L-methionine -lyase conjugated with polyethylene glycol as an antitumor agent, *Cancer Research 66*, 2807.
45. Yang, Z., Wang, J., Lu, Q., Xu, J., Kobayashi, Y., Takakura, T., Takimoto, A., Yoshioka, T., Lian, C., Chen, C., Zhang, D., Zhang, Y., Li, S., Sun, X., Tan, Y., Yagi, S., Frenkel, E. P., and Hoffman, R. M. (2004) PEGylation confers greatly extended half-life and attenuated immunogenicity to recombinant methioninase in primates, *Cancer Res 64*, 6673-6678.
46. Hu, J., and Cheung, N. K. (2009) Methionine depletion with recombinant methioninase: in vitro and in vivo efficacy against neuroblastoma and its synergism with chemotherapeutic drugs, *International journal of cancer 124*, 1700-1706.
47. Rose, W. C., Coon, M. J., Lockhart, H. B., and Lambert, G. F. (1955) The amino acid requirements of man. XI. The threonine and methionine requirements, *J Biol Chem 215*, 101-110.
48. Rose, W. C., and Wixom, R. L. (1955) The amino acid requirements of man. XIII. The sparing effect of cystine on the methionine requirement, *J Biol Chem 216*, 753-773.
49. Inoue, H., Inagaki, K., Sugimoto, M., Esaki, N., Soda, K., and Tanaka, H. (1995) Structural analysis of the L-methionine {gamma}-lyase gene from Pseudomonas putida, *Journal of Biochemistry 117*, 1120.
50. Steegborn, C., Clausen, T., Sondermann, P., Jacob, U., Worbs, M., Marinkovic, S., Huber, R., and Wahl, M. C. (1999) Kinetics and Inhibition of Recombinant Human Cystathionine ?-Lyase TOWARD THE RATIONAL CONTROL OF TRANSSULFURATION, *Journal of Biological Chemistry 274*, 12675-12684.
51. Sun, Q., Collins, R., Huang, S., Holmberg-Schiavone, L., Anand, G. S., and Tan, C. H. (2009) Structural Basis for the Inhibition Mechanism of Human Cystathionine {gamma}-Lyase, an Enzyme Responsible for the Production of H2S, *Journal of Biological Chemistry 284*, 3076.
52. Messerschmidt, A., Worbs, M., Steegborn, C., Wahl, M. C., Huber, R., Laber, B., and Clausen, T. (2003) Determinants of enzymatic specificity in the Cys-Met-metabolism PLP-dependent enzymes family: crystal structure of cystathionine gamma-lyase from yeast and intrafamiliar structure comparison, *Biol Chem 384*, 373-386.
53. Stone, E., Paley, O., Hu, J., Ekerdt, B., Cheung, N. K., and Georgiou, G. (2012) De novo engineering of a human cystathionine-gamma-lyase for systemic (L)-Methionine depletion cancer therapy, *ACS Chem Biol 7*, 1822-1829.
54. Breillout, F., Antoine, E., and Poupon, M. F. (1990) Methionine dependency of malignant tumors: a possible approach for therapy, pp 1628-1632, © Oxford University Press.
55. Halpern, B. C., Clark, B. R., Hardy, D. N., Halpern, R. M., and Smith, R. A. (1974) The effect of replacement of methionine by homocystine on survival of malignant and normal adult mammalian cells in culture, *Proceedings of the National Academy of Sciences 71*, 1133.

56. Poirson-Bichat, F., Goncalves, R. A., Miccoli, L., Dutrillaux, B., and Poupon, M. F. (2000) Methionine depletion enhances the antitumoral efficacy of cytotoxic agents in drug-resistant human tumor xenografts, *Clin Cancer Res 6*, 643-653.
57. Hu, J., and Cheung, N.-K. V. (2009) Methionine depletion with recombinant methioninase: in vitro and in vivo efficacy against neuroblastoma and its synergism with chemotherapeutic drugs, *Int J Cancer 124*, 1700-1706.
58. D'Souza, M. M., Sharma, R., Jaimini, A., Panwar, P., Saw, S., Kaur, P., Mondal, A., Mishra, A., and Tripathi, R. P. (2014) 11C-MET PET/CT and Advanced MRI in the Evaluation of Tumor Recurrence in High-Grade Gliomas, *Clin Nucl Med 17*, 17.
59. Thomas, T., and Thomas, T. J. (2003) Polyamine metabolism and cancer, *Journal of Cellular and Molecular Medicine 7*, 113-126.
60. Megosh, L., Gilmour, S. K., Rosson, D., Soler, A. P., Blessing, M., Sawicki, J. A., and O'Brien, T. G. (1995) Increased frequency of spontaneous skin tumors in transgenic mice which overexpress ornithine decarboxylase, *Cancer research 55*, 4205-4209.
61. Auvinen, M., Paasinen, A., Andersson, L. C., and Hölttä, E. (1992) Ornithine decarboxylase activity is critical for cell transformation.
62. Lu, S., and Epner, D. E. (2000) Molecular mechanisms of cell cycle block by methionine restriction in human prostate cancer cells, *Nutrition and cancer 38*, 123-130.
63. Stabler, S. P., Marcell, P. D., Podell, E. R., and Allen, R. H. (1987) Quantitation of total homocysteine, total cysteine, and methionine in normal serum and urine using capillary gas chromatography-mass spectrometry, *Analytical biochemistry 162*, 185-196.
64. Kokkinakis, D. M., Von Wronski, M. A., Vuong, T. H., Brent, T. P., and Schold Jr, S. C. (1997) Regulation of O6-methylguanine-DNA methyltransferase by methionine in human tumour cells, *British journal of cancer 75*, 779.
65. Yang, Z., Wang, J., Lu, Q., Xu, J., Kobayashi, Y., Takakura, T., Takimoto, A., Yoshioka, T., Lian, C., Chen, C., Zhang, D., Zhang, Y., Li, S., Sun, X., Tan, Y., Yagi, S., Frenkel, E. P., and Hoffman, R. M. (2004) PEGylation confers greatly extended half-life and attenuated immunogenicity to recombinant methioninase in primates, pp 6673-6678, Cancer Research.
66. Lishko, V. K., Lishko, O. V., and Hoffman, R. M. (1993) Depletion of serum methionine by methioninase in mice, *Anticancer research 13*, 1465.
67. Yang, Z., Wang, J., Yoshioka, T., Li, B., Lu, Q., Li, S., Sun, X., Tan, Y., Yagi, S., Frenkel, E. P., and Hoffman, R. M. (2004) Pharmacokinetics, methionine depletion, and antigenicity of recombinant methioninase in primates, *Clinical Cancer Research 10*, 2131-2138.
68. Yoshioka, T., Wada, T., Uchida, N., Maki, H., Yoshida, H., Ide, N., Kasai, H., Hojo, K., Shono, K., Maekawa, R., Yagi, S., Hoffman, R. M., and Sugita, K. (1998) Anticancer efficacy in vivo and in vitro, synergy with 5-fluorouracil, and safety of recombinant methioninase, *Cancer research 58*, 2583-2587.
69. Sun, X., Yang, Z., Li, S., Tan, Y., Zhang, N., Wang, X., Yagi, S., Yoshioka, T., Takimoto, A., and Mitsushima, K. (2003) In vivo efficacy of recombinant methioninase is enhanced by the combination of polyethylene glycol conjugation and pyridoxal 5'-phosphate supplementation, pp 8377-8383, AACR.

70. Yang, Z., Sun, X., Li, S., Tan, Y., Wang, X., Zhang, N., Yagi, S., Takakura, T., Kobayashi, Y., Takimoto, A., Yoshioka, T., Suginaka, A., Frenkel, E. P., and Hoffman, R. M. (2004) Circulating half-life of PEGylated recombinant methioninase holoenzyme is highly dose dependent on cofactor pyridoxal-5'-phosphate, *Cancer research 64*, 5775.
71. Hwang, W. Y. K., and Foote, J. (2005) Immunogenicity of engineered antibodies, *Methods 36*, 3-10.
72. Magdelaine-Beuzelin, C., Vermeire, S., Goodall, M., Baert, F., Noman, M., Assche, G. V., Ohresser, M., Degenne, D., Dugoujon, J. M., and Jefferis, R. (2009) IgG1 heavy chain-coding gene polymorphism (G1m allotypes) and development of antibodies-to-infliximab, *Pharmacogenetics and genomics 19*, 383.
73. Steegborn, C., Clausen, T., Sondermann, P., Jacob, U., Worbs, M., Marinkovic, S., Huber, R., and Wahl, M. C. (1999) Kinetics and inhibition of recombinant human cystathionine gamma-lyase. Toward the rational control of transsulfuration, *J Biol Chem 274*, 12675-12684.
74. Khersonsky, O., and Tawfik, D. S. (2010) Enzyme promiscuity: a mechanistic and evolutionary perspective, *Annu Rev Biochem 79*, 471-505.
75. Takakura, T., Mitsushima, K., Yagi, S., Inagaki, K., Tanaka, H., Esaki, N., Soda, K., and Takimoto, A. (2004) Assay method for antitumor L-methionine -lyase: comprehensive kinetic analysis of the complex reaction with L-methionine, *Analytical biochemistry 327*, 233-240.
76. Ditscheid, B., Fünfstück, R., Busch, M., Schubert, R., Gerth, J., and Jahreis, G. (2005) Effect of L-methionine supplementation on plasma homocysteine and other free amino acids: a placebo-controlled double-blind cross-over study, *European journal of clinical nutrition 59*, 768-775.
77. Araki, A., and Sako, Y. (1987) Determination of free and total homocysteine in human plasma by high-performance liquid chromatography with fluorescence detection, *Journal of Chromatography: Biomedical Applications 422*, 43-52.
78. Serjeant, E. P., and Dempsey, B. (1979) Ionization constants of organic acids in solution, IUPAC Chemical Data Series No. 23, Oxford (UK): Pergamon Press.
79. Huang, S., Chua, J. H., Yew, W. S., Sivaraman, J., Moore, P. K., Tan, C. H., and Deng, L. W. (2010) Site-Directed Mutagenesis on Human Cystathionine-[gamma]-Lyase Reveals Insights into the Modulation of H2S Production, *Journal of molecular biology 396*, 708-718.
80. Southwood, S., Sidney, J., Kondo, A., del Guercio, M. F., Appella, E., Hoffman, S., Kubo, R. T., Chesnut, R. W., Grey, H. M., and Sette, A. (1998) Several common HLA-DR types share largely overlapping peptide binding repertoires, *The Journal of Immunology 160*, 3363.
81. Purswani, M. U., Eckert, S. J., Arora, H. K., and Noel, G. J. (2002) Effect of ciprofloxacin on lethal and sublethal challenge with endotoxin and on early cytokine responses in a murine in vivo model, *Journal of Antimicrobial Chemotherapy 50*, 51-58.
82. Deb, K., Chaturvedi, M. M., and Jaiswal, Y. K. (2005) Gram-negative bacterial LPS induced poor uterine receptivity and implantation failure in mouse: Alterations in IL-1b

expression in the preimplantation embryo and uterine horns, *Infectious diseases in Obstetrics and Gynecology 13*, 125-134.

83. Seeger, R. C., Brodeur, G. M., Sather, H., Dalton, A., Siegel, S. E., Wong, K. Y., and Hammond, D. (1985) Association of multiple copies of the N-myc oncogene with rapid progression of neuroblastomas, *The New England journal of medicine 313*, 1111-1116.
84. Azarova, A. M., Gautam, G., and George, R. E. (2011) Emerging importance of ALK in neuroblastoma, *Seminars in cancer biology 21*, 267-275.
85. Cheung, N. K., Zhang, J., Lu, C., Parker, M., Bahrami, A., Tickoo, S. K., Heguy, A., Pappo, A. S., Federico, S., Dalton, J., Cheung, I. Y., Ding, L., Fulton, R., Wang, J., Chen, X., Becksfort, J., Wu, J., Billups, C. A., Ellison, D., Mardis, E. R., Wilson, R. K., Downing, J. R., Dyer, M. A., and St Jude Children's Research Hospital-Washington University Pediatric Cancer Genome, P. (2012) Association of age at diagnosis and genetic mutations in patients with neuroblastoma, *JAMA : the journal of the American Medical Association 307*, 1062-1071.
86. Takakura, T., Takimoto, A., Notsu, Y., Yoshida, H., Ito, T., Nagatome, H., Ohno, M., Kobayashi, Y., Yoshioka, T., Inagaki, K., Yagi, S., Hoffman, R. M., and Esaki, N. (2006) Physicochemical and pharmacokinetic characterization of highly potent recombinant L-methionine gamma-lyase conjugated with polyethylene glycol as an antitumor agent, *Cancer research 66*, 2807.
87. Epner, D. E. (2001) Can dietary methionine restriction increase the effectiveness of chemotherapy in treatment of advanced cancer?, *Journal of the American College of Nutrition 20*, 443.
88. Cao, H., Lin, H., and Ye, S. H. (2001) Influence of L-methionine-deprived total parenteral nutrition with 5-fluorouracil on gastric cancer and host metabolism, *( ) 7*.
89. Durando, X., Thivat, E., Farges, M. C., Cellarier, E., D'Incan, M., Demidem, A., Vasson, M. P., Barthomeuf, C., and Chollet, P. (2008) Optimal methionine-free diet duration for nitrourea treatment: a Phase I clinical trial, *Nutrition and cancer 60*, 23.
90. Tan, Y., Sun, X., Xu, M., Tan, X., Sasson, A., Rashidi, B., Han, Q., Wang, X., An, Z., Sun, F., and Hoffman, R. M. (1999) Efficacy of recombinant methioninase in combination with cisplatin on human colon tumors in nude mice, *Clinical Cancer Research 5*, 2157-2163.
91. Kokkinakis, D. M., Wick, J. B., and Zhou, Q. X. (2002) Metabolic response of normal and malignant tissue to acute and chronic methionine stress in athymic mice bearing human glial tumor xenografts, *Chemical research in toxicology 15*, 1472-1479.
92. Kokkinakis, D. M., Hoffman, R. M., Frenkel, E. P., Wick, J. B., Han, Q., Xu, M., Tan, Y., and Schold, S. C. (2001) Synergy between methionine stress and chemotherapy in the treatment of brain tumor xenografts in athymic mice, *Cancer research 61*, 4017.
93. Glazer, E. S., Piccirillo, M., Albino, V., Di Giacomo, R., Palaia, R., Mastro, A. A., Beneduce, G., Castello, G., De Rosa, V., Petrillo, A., Ascierto, P. A., Curley, S. A., and Izzo, F. (2010) Phase II study of pegylated arginine deiminase for nonresectable and metastatic hepatocellular carcinoma, *Journal of Clinical Oncology 28*, 2220.
94. Reinders, M. K., and Tim, L. (2010) New advances in the treatment of gout: review of pegloticase, *Therapeutics and Clinical Risk Management 6*, 543.

95. Hoover, D. M., Boulegue, C., Yang, D., Oppenheim, J. J., Tucker, K., Lu, W., and Lubkowski, J. (2002) The structure of human macrophage inflammatory protein-3alpha /CCL20. Linking antimicrobial and CC chemokine receptor-6-binding activities with human beta-defensins, *J Biol Chem 277*, 37647-37654.
96. Gill, S. C., and von Hippel, P. H. (1989) Calculation of protein extinction coefficients from amino acid sequence data, *Anal Biochem 182*, 319-326.
97. Wang, P., Sidney, J., Dow, C., Mothé, B., Sette, A., and Peters, B. (2008) A systematic assessment of MHC class II peptide binding predictions and evaluation of a consensus approach, *PLoS Comput Biol 4*, e1000048.
98. Cantor, J. R., Yoo, T. H., Dixit, A., Iverson, B. L., Forsthuber, T. G., and Georgiou, G. (2011) Therapeutic enzyme deimmunization by combinatorial T-cell epitope removal using neutral drift, *Proc Natl Acad Sci U S A 108*, 1272-1277.
99. Sun, X., Tan, Y., Yang, Z., Li, S., and Hoffman, R. M. (2005) A rapid HPLC method for the measurement of ultra-low plasma methionine concentrations applicable to methionine depletion therapy, *Anticancer Res 25*, 59-62.
100. MarvinSketch. (2011) 5.5.0.1 edn., ChemAxon.
101. Hirata, H., Kawanishi, M., Iwata, Y., Sakaki, K., and Yanagishita, H. (2007) Kinetic studies on lipase-catalyzed acetylation of 2-alkanol with vinyl acetate in organic solvent, *Journal of Oleo Science 56*, 309-317.
102. Cheung, N. K. V., Guo, H. F., Modak, S., and Cheung, I. Y. (2003) Anti-idiotypic antibody facilitates scFv chimeric immune receptor gene transduction and clonal expansion of human lymphocytes for tumor therapy, *Hybridoma and hybridomics 22*, 209-218.
103. Sanceau, J., Poupon, M. F., Delattre, O., Sastre-Garau, X., and Wietzerbin, J. (2002) Strong inhibition of Ewing tumor xenograft growth by combination of human interferon-alpha or interferon-beta with ifosfamide, *Oncogene 21*, 7700-7709.
104. Benner, S. A., and Gaucher, E. A. (2001) Evolution, language and analogy in functional genomics, *Trends Genet 17*, 414-418.
105. Skovgaard, M., Kodra, J. T., Gram, D. X., Knudsen, S. M., Madsen, D., and Liberles, D. A. (2006) Using evolutionary information and ancestral sequences to understand the sequence-function relationship in GLP-1 agonists, *J Mol Biol 363*, 977-988.
106. Yamashiro, K., Yokobori, S., Koikeda, S., and Yamagishi, A. (2010) Improvement of Bacillus circulans beta-amylase activity attained using the ancestral mutation method, *Protein Eng Des Sel 23*, 519-528.
107. Sokalingam, S., Raghunathan, G., Soundrarajan, N., and Lee, S. G. (2012) A study on the effect of surface lysine to arginine mutagenesis on protein stability and structure using green fluorescent protein, *PLoS ONE 7*, 9.
108. Takakura, T., Takimoto, A., Notsu, Y., Yoshida, H., Ito, T., Nagatome, H., Ohno, M., Kobayashi, Y., Yoshioka, T., Inagaki, K., Yagi, S., Hoffman, R. M., and Esaki, N. (2006) Physicochemical and pharmacokinetic characterization of highly potent recombinant L-methionine gamma-lyase conjugated with polyethylene glycol as an antitumor agent, *Cancer Res 66*, 2807-2814.

109. Gaucher, E. A., Miyamoto, M. M., and Benner, S. A. (2003) Evolutionary, structural and biochemical evidence for a new interaction site of the leptin obesity protein, *Genetics 163*, 1549-1553.
110. Perez-Jimenez, R., Li, J., Kosuri, P., Sanchez-Romero, I., Wiita, A. P., Rodriguez-Larrea, D., Chueca, A., Holmgren, A., Miranda-Vizuete, A., Becker, K., Cho, S. H., Beckwith, J., Gelhaye, E., Jacquot, J. P., Gaucher, E. A., Sanchez-Ruiz, J. M., Berne, B. J., and Fernandez, J. M. (2009) Diversity of chemical mechanisms in thioredoxin catalysis revealed by single-molecule force spectroscopy, *Nat Struct Mol Biol 16*, 890-896.
111. Yuen, C. M., and Liu, D. R. (2007) Dissecting protein structure and function using directed evolution, *Nat Methods 4*, 995-997.
112. Pal, D., and Chakrabarti, P. (2001) Non-hydrogen bond interactions involving the methionine sulfur atom, *J Biomol Struct Dyn 19*, 115-128.
113. Borders, C. L., Jr., Broadwater, J. A., Bekeny, P. A., Salmon, J. E., Lee, A. S., Eldridge, A. M., and Pett, V. B. (1994) A structural role for arginine in proteins: multiple hydrogen bonds to backbone carbonyl oxygens, *Protein Sci 3*, 541-548.
114. Paley, O., Agnello, G., Cantor, J., Yoo, T. H., Georgiou, G., and Stone, E. (2013) GFP reporter screens for the engineering of amino acid degrading enzymes from libraries expressed in bacteria, *Methods Mol Biol 978*, 31-44.
115. Farinas, E. T. (2006) Fluorescence activated cell sorting for enzymatic activity, *Combinatorial Chemistry &# 38; High Throughput Screening 9*, 321-328.
116. Agrawal, V., Woo, J. H., Mauldin, J. P., Jo, C., Stone, E. M., Georgiou, G., and Frankel, A. E. (2012) Cytotoxicity of human recombinant arginase I (Co)-PEG5000 in the presence of supplemental L-citrulline is dependent on decreased argininosuccinate synthetase expression in human cells, *Anti-Cancer Drugs 23*, 51.
117. Cantor, J. R., Panayiotou, V., Agnello, G., Georgiou, G., and Stone, E. M. (2012) Engineering Reduced-Immunogenicity Enzymes for Amino Acid Depletion Therapy in Cancer, *Protein Engineering for Therapeutics 502*, 291.
118. Stone, E., Chantranupong, L., Gonzalez, C., O'Neal, J., Rani, M., VanDenBerg, C., and Georgiou, G. (2011) Strategies for Optimizing the Serum Persistence of Engineered Human Arginase I for Cancer Therapy, *Journal of Controlled Release*.
119. Stone, E. M., Glazer, E. S., Chantranupong, L., Cherukuri, P., Breece, R. M., Tierney, D. L., Curley, S. A., Iverson, B. L., and Georgiou, G. (2010) Replacing Mn2+ with Co2+ in human arginase I enhances cytotoxicity toward l-arginine auxotrophic cancer cell lines, *ACS chemical biology 5*, 333-342.
120. Donath, M. J., 2nd, Dominguez, M. A., and Withers, S. T., 3rd. (2011) Development of an automated platform for high-throughput P1-phage transduction of Escherichia coli, *J Lab Autom 16*, 141-147.
121. Barrick, J. E., Yu, D. S., Yoon, S. H., Jeong, H., Oh, T. K., Schneider, D., Lenski, R. E., and Kim, J. F. (2009) Genome evolution and adaptation in a long-term experiment with Escherichia coli, *Nature 461*, 1243-1247.
122. Baba, T., Ara, T., Hasegawa, M., Takai, Y., Okumura, Y., Baba, M., Datsenko, K. A., Tomita, M., Wanner, B. L., and Mori, H. (2006) Construction of Escherichia coli K-12 in-frame, single-gene knockout mutants: the Keio collection, *Mol Syst Biol 2*, 21.

123. Leavitt, R. I., and Umbarger, H. (1962) ISOLEUCINE AND VALINE METABOLISM IN ESCHERICHIA COLI XI. K-12: Valine Inhibition of the Growth of Escherichia coli Strain, *Journal of bacteriology 83*, 624.
124. Gollop, N., Chipman, D. M., and Barak, Z. (1983) Inhibition of acetohydroxy acid synthase by leucine, *Biochimica et Biophysica Acta (BBA)-Protein Structure and Molecular Enzymology 748*, 34-39.
125. Guo, H. Y., Herrera, H., Groce, A., and Hoffman, R. M. (1993) Expression of the biochemical defect of methionine dependence in fresh patient tumors in primary histoculture, *Cancer Res 53*, 2479-2483.
126. Morvan, D., Demidem, A., Guenin, S., and Madelmont, J. C. (2006) Methionine-dependence phenotype of tumors: metabolite profiling in a melanoma model using L-[methyl-13C]methionine and high-resolution magic angle spinning 1H-13C nuclear magnetic resonance spectroscopy, *Magn Reson Med 55*, 984-996.
127. Pavillard, V., Drbal, A. A., Swaine, D. J., Phillips, R. M., Double, J. A., and Nicolaou, A. (2004) Analysis of cell-cycle kinetics and sulfur amino acid metabolism in methionine-dependent tumor cell lines; the effect of homocysteine supplementation, *Biochem Pharmacol 67*, 1587-1599.
128. Tan, Y., Xu, M., and Hoffman, R. M. (2010) Broad selective efficacy of recombinant methioninase and polyethylene glycol-modified recombinant methioninase on cancer cells In Vitro, *Anticancer Res 30*, 1041-1046.
129. Tan, Y., Xu, M., Tan, X., Wang, X., Saikawa, Y., Nagahama, T., Sun, X., Lenz, M., and Hoffman, R. M. (1997) Overexpression and large-scale production of recombinant L-methionine-alpha-deamino-gamma-mercaptomethane-lyase for novel anticancer therapy, *Protein Expr Purif 9*, 233-245.
130. Watkins, D. (1998) Cobalamin metabolism in methionine-dependent human tumour and leukemia cell lines, *Clin Invest Med 21*, 151-158.
131. Jerant, A. F., Johnson, J. T., Sheridan, C. D., and Caffrey, T. J. (2000) Early detection and treatment of skin cancer, *Am Fam Physician 62*, 357-368.
132. Bhatia, S., Tykodi, S. S., and Thompson, J. A. (2009) Treatment of metastatic melanoma: an overview, *Oncology 23*, 488-496.
133. Miller, D. C., Hafez, K. S., Stewart, A., Montie, J. E., and Wei, J. T. (2003) Prostate carcinoma presentation, diagnosis, and staging: an update form the National Cancer Data Base, *Cancer 98*, 1169-1178.
134. Li, S., Kennedy, M., Payne, S., Kennedy, K., Seewaldt, V. L., Pizzo, S. V., and Bachelder, R. E. (2014) Model of tumor dormancy/recurrence after short-term chemotherapy, *PLoS ONE 9*.
135. Galluzzi, L., Vitale, I., Abrams, J. M., Alnemri, E. S., Baehrecke, E. H., Blagosklonny, M. V., Dawson, T. M., Dawson, V. L., El-Deiry, W. S., Fulda, S., Gottlieb, E., Green, D. R., Hengartner, M. O., Kepp, O., Knight, R. A., Kumar, S., Lipton, S. A., Lu, X., Madeo, F., Malorni, W., Mehlen, P., Nunez, G., Peter, M. E., Piacentini, M., Rubinsztein, D. C., Shi, Y., Simon, H. U., Vandenabeele, P., White, E., Yuan, J., Zhivotovsky, B., Melino, G., and Kroemer, G. (2012) Molecular definitions of cell death subroutines: recommendations of the Nomenclature Committee on Cell Death 2012, *Cell Death Differ 19*, 107-120.

136. Stevens, J. B., Abdallah, B. Y., Liu, G., Horne, S. D., Bremer, S. W., Ye, K. J., Huang, J. Y., Kurkinen, M., Ye, C. J., and Heng, H. H. (2013) Heterogeneity of cell death, *Cytogenet Genome Res 139*, 164-173.
137. Kokkinakis, D. M., Brickner, A. G., Kirkwood, J. M., Liu, X., Goldwasser, J. E., Kastrama, A., Sander, C., Bocangel, D., and Chada, S. (2006) Mitotic arrest, apoptosis, and sensitization to chemotherapy of melanomas by methionine deprivation stress, *Mol Cancer Res 4*, 575-589.
138. Elmore, S. (2007) Apoptosis: a review of programmed cell death, *Toxicol Pathol 35*, 495-516.
139. van Loo, G., Saelens, X., van Gurp, M., MacFarlane, M., Martin, S. J., and Vandenabeele, P. (2002) The role of mitochondrial factors in apoptosis: a Russian roulette with more than one bullet, *Cell Death Differ 9*, 1031-1042.
140. Kroemer, G., Galluzzi, L., Vandenabeele, P., Abrams, J., Alnemri, E. S., Baehrecke, E. H., Blagosklonny, M. V., El-Deiry, W. S., Golstein, P., Green, D. R., Hengartner, M., Knight, R. A., Kumar, S., Lipton, S. A., Malorni, W., Nunez, G., Peter, M. E., Tschopp, J., Yuan, J., Piacentini, M., Zhivotovsky, B., and Melino, G. (2009) Classification of cell death: recommendations of the Nomenclature Committee on Cell Death 2009, *Cell Death Differ 16*, 3-11.
141. Sheen, J. H., Zoncu, R., Kim, D., and Sabatini, D. M. (2011) Defective regulation of autophagy upon leucine deprivation reveals a targetable liability of human melanoma cells in vitro and in vivo, *Cancer Cell 19*, 613-628.
142. Eisenberg-Lerner, A., and Kimchi, A. (2009) The paradox of autophagy and its implication in cancer etiology and therapy, *Apoptosis 14*, 376-391.
143. Jayaraman, S. (2003) Intracellular determination of activated caspases (IDAC) by flow cytometry using a pancaspase inhibitor labeled with FITC, *Cytometry A 56*, 104-112.
144. al-Rubeai, M., Emery, A. N., and Chalder, S. (1991) Flow cytometric study of cultured mammalian cells, *J Biotechnol 19*, 67-81.
145. Cain, K., Inayat-Hussain, S. H., Couet, C., and Cohen, G. M. (1996) A cleavage-site-directed inhibitor of interleukin-1 beta-converting enzyme-like proteases inhibits apoptosis in primary cultures of rat hepatocytes, *Biochem J 314*, 27-32.
146. Unglaub, F., Thomas, S. B., Kroeber, M. W., Dragu, A., Fellenberg, J., Wolf, M. B., and Horch, R. E. (2009) Apoptotic pathways in degenerative disk lesions in the wrist, *Arthroscopy 25*, 1380-1386.
147. Barber, R. D., Harmer, D. W., Coleman, R. A., and Clark, B. J. (2005) GAPDH as a housekeeping gene: analysis of GAPDH mRNA expression in a panel of 72 human tissues, *Physiol Genomics 21*, 389-395.
148. Kirkegaard, K., Taylor, M. P., and Jackson, W. T. (2004) Cellular autophagy: surrender, avoidance and subversion by microorganisms, *Nat Rev Microbiol 2*, 301-314.
149. Tanida, I., Ueno, T., and Kominami, E. (2008) LC3 and Autophagy, *Methods Mol Biol 445*, 77-88.
150. Ha, J. Y., Kim, J. S., Kim, S. E., and Son, J. H. (2014) Simultaneous activation of mitophagy and autophagy by staurosporine protects against dopaminergic neuronal cell death, *Neurosci Lett 561*, 101-106.

151. Alimirah, F., Chen, J., Basrawala, Z., Xin, H., and Choubey, D. (2006) DU-145 and PC-3 human prostate cancer cell lines express androgen receptor: implications for the androgen receptor functions and regulation, *FEBS Lett 580*, 2294-2300.
152. de Bruin, E. C., and Medema, J. P. (2008) Apoptosis and non-apoptotic deaths in cancer development and treatment response, *Cancer Treat Rev 34*, 737-749.
153. Saha, A., Blando, J., Silver, E., Beltran, L., Sessler, J., and DiGiovanni, J. (2014) 6-Shogaol from dried ginger inhibits growth of prostate cancer cells both in vitro and in vivo through inhibition of STAT3 and NF-kappaB signaling, *Cancer Prev Res 7*, 627-638.
154. Teicher, B. A. (2006) Tumor models for efficacy determination, *Mol Cancer Ther 5*, 2435-2443.
155. Psychogios, N., Hau, D. D., Peng, J., Guo, A. C., Mandal, R., Bouatra, S., Sinelnikov, I., Krishnamurthy, R., Eisner, R., Gautam, B., Young, N., Xia, J., Knox, C., Dong, E., Huang, P., Hollander, Z., Pedersen, T. L., Smith, S. R., Bamforth, F., Greiner, R., McManus, B., Newman, J. W., Goodfriend, T., and Wishart, D. S. (2011) The human serum metabolome, *PLoS ONE 6*, 0016957.
156. Meister, A., and Anderson, M. E. (1983) Glutathione, *Annu Rev Biochem 52*, 711-760.
157. Pompella, A., Visvikis, A., Paolicchi, A., De Tata, V., and Casini, A. F. (2003) The changing faces of glutathione, a cellular protagonist, *Biochem Pharmacol 66*, 1499-1503.
158. Hanigan, M. H. (2014) Gamma-glutamyl transpeptidase: redox regulation and drug resistance, *Adv Cancer Res 122*, 103-141.
159. Kumar, B., Koul, S., Khandrika, L., Meacham, R. B., and Koul, H. K. (2008) Oxidative stress is inherent in prostate cancer cells and is required for aggressive phenotype, *Cancer Res 68*, 1777-1785.
160. Rajasekaran, S. A., Gopal, J., Espineda, C., Ryazantsev, S., Schneeberger, E. E., and Rajasekaran, A. K. (2004) HPAF-II, a cell culture model to study pancreatic epithelial cell structure and function, *Pancreas 29*, e77-83.
161. Mahe, C., Bernhard, M., Bobirnac, I., Keser, C., Loetscher, E., Feuerbach, D., Dev, K. K., and Schoeffter, P. (2004) Functional expression of the serotonin 5-HT7 receptor in human glioblastoma cell lines, *Br J Pharmacol 143*, 404-410.
162. Xie, Q., Mittal, S., and Berens, M. E. *Targeting adaptive glioblastoma: an overview of proliferation and invasion*, Neuro Oncol. 2014 Jul 30. pii: nou147.
163. Arslan, C., and Yalcin, S. (2014) Current and future systemic treatment options in metastatic pancreatic cancer, *J Gastrointest Oncol 5*, 280-295.
164. Kaighn, M. E., Narayan, K. S., Ohnuki, Y., Lechner, J. F., and Jones, L. W. (1979) Establishment and characterization of a human prostatic carcinoma cell line (PC-3), *Invest Urol 17*, 16-23.
165. Cohen, A. A., Geva-Zatorsky, N., Eden, E., Frenkel-Morgenstern, M., Issaeva, I., Sigal, A., Milo, R., Cohen-Saidon, C., Liron, Y., Kam, Z., Cohen, L., Danon, T., Perzov, N., and Alon, U. (2008) Dynamic proteomics of individual cancer cells in response to a drug, *Science 322*, 1511-1516.
166. Heng, H. H., Liu, G., Stevens, J. B., Bremer, S. W., Ye, K. J., and Ye, C. J. (2010) Genetic and epigenetic heterogeneity in cancer: the ultimate challenge for drug therapy, *Curr Drug Targets 11*, 1304-1316.

167. Heng, H. H., Stevens, J. B., Liu, G., Bremer, S. W., Ye, K. J., Reddy, P. V., Wu, G. S., Wang, Y. A., Tainsky, M. A., and Ye, C. J. (2006) Stochastic cancer progression driven by non-clonal chromosome aberrations, *J Cell Physiol 208*, 461-472.
168. Reed, J. C. (1999) Dysregulation of apoptosis in cancer, *J Clin Oncol 17*, 2941-2953.
169. Hanahan, D., and Weinberg, R. A. (2000) The hallmarks of cancer, *Cell 100*, 57-70.
170. McBean, G. J. (2012) The transsulfuration pathway: a source of cysteine for glutathione in astrocytes, *Amino Acids 42*, 199-205.
171. Deplancke, B., and Gaskins, H. R. (2002) Redox control of the transsulfuration and glutathione biosynthesis pathways, *Curr Opin Clin Nutr Metab Care 5*, 85-92.
172. Conrad, M., and Sato, H. (2012) The oxidative stress-inducible cystine/glutamate antiporter, system x (c) (-) : cystine supplier and beyond, *Amino Acids 42*, 231-246.
173. Doxsee, D. W., Gout, P. W., Kurita, T., Lo, M., Buckley, A. R., Wang, Y., Xue, H., Karp, C. M., Cutz, J. C., Cunha, G. R., and Wang, Y. Z. (2007) Sulfasalazine-induced cystine starvation: potential use for prostate cancer therapy, *Prostate 67*, 162-171.
174. Ellwood-Yen, K., Graeber, T. G., Wongvipat, J., Iruela-Arispe, M. L., Zhang, J., Matusik, R., Thomas, G. V., and Sawyers, C. L. (2003) Myc-driven murine prostate cancer shares molecular features with human prostate tumors, *Cancer cell 4*, 223-238.
175. Hu, J., and Cheung, N. K. V. (2009) Methionine depletion with recombinant methioninase: In vitro and in vivo efficacy against neuroblastoma and its synergism with chemotherapeutic drugs, *International journal of cancer 124*.
176. Tiziani, S., Einwas, A. H., Lodi, A., Ludwig, C., Bunce, C. M., Viant, M. R., and Gunther, U. L. (2008) Optimized metabolite extraction from blood serum for 1H nuclear magnetic resonance spectroscopy, *Analytical Biochemistry 377*, 16-23.
177. Tiziani, S., Kang, Y., Harjanto, R., Axelrod, J., Piermarocchi, C., Roberts, W., and Paternostro, G. (2013) Metabolomics of the tumor microenvironment in pediatric acute lymphoblastic leukemia, *PloS one 8*, e82859.
178. Lodi, A., Tiziani, S., Khanim, F. L., Drayson, M. T., Gunther, U. L., Bunce, C. M., and Viant, M. R. (2011) Hypoxia triggers major metabolic changes in AML cells without altering indomethacin-induced TCA cycle deregulation, *ACS Chem. Biol. 6*, 169-175.
179. Tiziani, S., Lodi, A., Khanim, F. L., Viant, M. R., Bunce, C. M., and Gunther, U. L. (2009) Metabolomic Profiling of Drug Responses in Acute Myeloid Leukaemia Cell Lines, *Plos One 4, e4251*.
180. Hwang, T. L., and Shaka, A. J. (1995) Water suppression that works - Excitation sculpting using arbitrary wave-forms and pulsed-field gradients, *Journal of Magnetic Resonance Series A 112*, 275-279.
181. Ludwig, C., and Günther, U. L. (2011) MetaboLab - advanced NMR data processing and analysis for metabolomics, *BMC bioinformatics 12*, 366.
182. Psychogios, N., Hau, D. D., Peng, J., Guo, A. C., Mandal, R., Bouatra, S., Sinelnikov, I., Krishnamurthy, R., Eisner, R., Gautam, B., Young, N., Xia, J. G., Knox, C., Dong, E., Huang, P., Hollander, Z., Pedersen, T. L., Smith, S. R., Bamforth, F., Greiner, R., McManus, B., Newman, J. W., Goodfriend, T., and Wishart, D. S. (2011) The Human Serum Metabolome, *Plos One 6*.

183. Quehenberger, O., Armando, A. M., Brown, A. H., Milne, S. B., Myers, D. S., Merrill, A. H., Bandyopadhyay, S., Jones, K. N., Kelly, S., Shaner, R. L., Sullards, C. M., Wang, E., Murphy, R. C., Barkley, R. M., Leiker, T. J., Raetz, C. R. H., Guan, Z. Q., Laird, G. M., Six, D. A., Russell, D. W., McDonald, J. G., Subramaniam, S., Fahy, E., and Dennis, E. A. (2010) Lipidomics reveals a remarkable diversity of lipids in human plasma, *Journal of Lipid Research 51*, 3299-3305.
184. Wishart, D. S., Jewison, T., Guo, A. C., Wilson, M., Knox, C., Liu, Y., Djoumbou, Y., Mandal, R., Aziat, F., and Dong, E. (2013) HMDB 3.0—The Human Metabolome Database in 2013, *Nucleic Acids Research 41*, D801-D807.
185. Ludwig, C., Easton, J. M., Lodi, A., Tiziani, S., Manzoor, S. E., Southam, A. D., Byrne, J. J., Bishop, L. M., He, S., and Arvanitis, T. N. (2012) Birmingham metabolite library: A publicly accessible database of 1-D 1H and 2-D 1H J-resolved NMR spectra of authentic metabolite standards (BML-NMR), *Metabolomics 8*, 8-18.
186. Chou, T. C. (2006) Theoretical basis, experimental design, and computerized simulation of synergism and antagonism in drug combination studies, *Pharmacol Rev 58*, 621-681.
187. Ungard R, Singh G. Oxidative stress and glutamate release in glioma. *In:* Ghosh A, editor. *Glioma - Exploring Its Biology and Practical Relevance*.Rijeka: Intech; 2011. p. 451-65